UNIVERSITY OF STIRLING

The Role of Non-Linearities in Visual Perception studied with a Computational Model of the Vertebrate Retina

by

Matthias Helge Hennig

A thesis submitted in partial fulfillment for the
degree of Doctor of Philosophy

in the
Faculty of Human Sciences
Department of Psychology

12th December 2005

UNIVERSITY OF STIRLING

ABSTRACT

FACULTY OF HUMAN SCIENCES
DEPARTMENT OF PSYCHOLOGY

Doctor of Philosophy

by Matthias Helge Hennig

Processing of visual stimuli in the vertebrate retina is complex and diverse. The retinal output to the higher centres of the nervous system, mediated by ganglion cells, consists of several different channels. Neurons in these channels can have very distinct response properties, which originate in different retinal pathways. In this work, the retinal origins and possible functional implications of the segregation of visual pathways will be investigated with a detailed, biologically realistic computational model of the retina. This investigation will focus on the two main retino-cortical pathways in the mammalian retina, the parvocellular and magnocellular systems, which are crucial for conscious visual perception.

These pathways differ in two important aspects. The parvocellular system has a high spatial, but low temporal resolution. Conversely, the magnocellular system has a high temporal fidelity, spatial sampling however is less dense than for parvocellular cells. Additionally, the responses of magnocellular ganglion cells can show pronounced nonlinearities, while the parvocellular system is essentially linear. The origin of magnocellular nonlinearities is unknown and will be investigated in the first part of this work. As their main source, the results suggest specific properties of the photoreceptor response and a specialised amacrine cell circuit in the inner retina. The results further show that their effect combines in a multiplicative way.

The model is then used to examine the influence of nonlinearities on the responses of ganglion cells in the presence of involuntary fixational eye movements. Two different stimulus conditions will be considered: visual hyperacuity and motion induced illusions. In both cases, it is possible to directly compare properties of the ganglion cell population response with psychophysical data, which allows for an analysis of the influence of different components of the retinal circuitry. The simulation results suggest an important role for nonlinearities in the magnocellular stream for visual perception in both cases. First, it will be shown how nonlinearities, triggered by fixational eye

movements, can strongly enhance the spatial precision of magnocellular ganglion cells. As a result, their performance in a hyperacuity task can be equal to or even surpass that of the parvocellular system. Second, the simulations imply that the origin of some of the illusory percepts elicited by fixational eye movements could be traced back to the nonlinear properties of magnocellular ganglion cells. As these activity patterns strongly differ from those in the parvocellular system, it appears that the magnocellular system can strongly dominate visual perception in certain conditions.

Taken together, the results of this theoretical study suggest that retinal nonlinearities may be important for and strongly influence visual perception. The model makes several experimentally verifiable predictions to further test and quantify these findings. Furthermore, models investigating higher visual processing stages may benefit from this work, which could provide the basis to produce realistic afferent input.

Contents

Acknowledgements

It's been a long way, and I am very grateful to the many people who have helped me during this time. My supervisor Florentin Wörgötter was the driving force behind this work, and I have to thank him for his help and guidance. He was always available for discussions and open to new ideas, and provided me with enough computers to perform the large-scale simulations for this work[1]. I am equally grateful to my co-supervisor, Peter Hanckock, who especially helped a lot with the psychophysics for Chapter 8.

Many thanks to all current and former members of the (former) Computational Neuroscience group st Stirling for their support and the nice atmosphere: Markus Dahlem, Tao Geng, Sinan Kalkan, Norbert Krüger, Tomas Kulvicius, Bernd Porr, Nicolas Pugeault, Ausra Saudargiene, Kevin Swingler and Minija Tamosiunaite. The Department of Psychology in Stirling was a great place to work, and I would like to thank everyone there. In particular, I have to thank Paul Dudchenko, who carefully read one of our manuscripts, Ranald Macdonald, who helped me with statistical issues, and Bill Phillips and Roger Watt, who provided valuable comments on this work at various stages. Thanks also to everyone else from the CCCN for feedback in our seminars. For their help with all those organisational and administrative issues and their patience with me, I am grateful to Kay Faichney, Kerry Fairbairns, Peter Hucker, Bruce Sutherland, Claire Wilson and Ursula Wörgötter.

Thanks to Klaus Funke and Nicolas Kerscher, who contributed substantially to this work, especially with their experimental work on fixational eye movements. For the many fruitful discussions and help with a paper, I would like to thank Martin Greschner. Thanks also to Hans Ekkehard Plesser for discussions and the matlab code to plot ganglion cell activity on hexagonal grids. Furher, many thanks to Harriet Nevill for carefully reading parts of this thesis.

Most importantly, thanks to my family: to my parents for their support and to Stephanie and little Jonas & Joshua for all the nice time away from science.

[1] A rough lower estimate of the computing time required to simulate the data presented in Chapters 7 and 8 yields $20 \cdot 10^{15}$ instructions. This estimate is based on a total of 11300 simulations, each running for an average of 30 minutes. As a mean processor speed, 1000MIPS (million instructions per second) for an 1GHz Pentium III was assumed.

Declaration

Publications based upon the work contained in this thesis:

Hennig MH, Kerscher NJ, Funke K, Wörgötter F (2002) Stochastic resonance in visual cortical neurons: does the eye-tremor actually improve visual acuity? *Neurocomputing* 44:115–120.

Hennig MH, Kerscher NJ, Funke K, Wörgötter F (2002) Noise in the visual system: high-frequency eye tremor improves responsivity and visual acuity in cortical neurons. *Perception* 31:177, Suppl. S 2002.

Hennig MH, Funke K, Wörgötter F (2002) The influence of different retinal subcircuits on the nonlinearity of ganglion cell behavior. *J Neurosci* 22:8726–8738.

Hennig MH, Wörgötter F (2003) Eye micromovements improve hyperacuity in extra-foveal ganglion cells. In *Proc. Society for Neuroscience Annual Meeting (SFN'03)*.

Hennig MH, Wörgötter F (2004) Eye micro-movements improve stimulus detection beyond the Nyquist limit in the peripheral retina. In *Advances in Neural Information Processing Systems* 16. MIT Press.

Chapter 1

Introduction

Processing of visual information begins in the retina. Its task is to transform light into electrical activity and to create neural representations of visual stimuli, which are then sent to various structures in the central nervous system. To solve this task, retinal processing employs three distinct mechanisms. First, a transduction mechanism converts light into electrical activity in photoreceptors. Second, photoreceptor activity is transmitted via bipolar cells to ganglion cells, the output neurons of the retina. Third, retinal neurons are laterally interconnected by various interneurons, which alter the feedforward transmission of visual information.

The overall structural organisation of the retina reflects this basic functional layout, but the retinal network turns out to be a complex structure, comprising about 70-80 different cell types, each with a distinctive morphology, chemistry and connectivity (Masland, 2001a). Experimental work has shown that this diversity provides the basis for the segregation of visual information into several parallel, functionally distinct retinal pathways (Roska and Werblin, 2001). The detailed analysis of the retinal circuitry has further revealed that functional segregation is obtained by modifications originating in *functional circuits*, which usually involve different cell types and specific connectivity patterns (reviewed by Sterling and Demb, 2004).

Functional segregation is not only a feature of the retina, but is also found in the higher visual system, in particular in the visual cortex (Merigan and Maunsell, 1993). Anatomical studies have established that the retinal segregation is partially preserved in the cortex, where the projections of different pathways innervate distinct layers. Hence, it appears that the breakdown of visual information in the retina into different sub-aspects may be used in the higher visual systems for specific tasks (Schiller and Logothetis, 1990).

This study investigates functional segregation at the level of the retina. This is important because visual perception relies on the output of the retina, hence the properties of different retinal ganglion cell types determine the way visual information is processed in the brain. Here, responses of two broad ganglion cell classes will be compared, the parvocellular stream (PC-cells or X-like cells) with low temporal, but high spatial resolution and the magnocellular stream (MC-cells or Y-like cells) with high temporal fidelity, but reduced spatial resultion. It will be shown that these classes differ strongly with regard to the linearity of their responses, and that this segregation can have several important functional consequences.

1.1 Linear and Nonlinear Ganglion Cells

An important distinction between different ganglion cell types is based on their temporal dynamics. Typically, a substantial proportion of ganglion cells shows either linear temporal responses (X-like cells) or behaves strongly nonlinear (Y-like cells) (Enroth-Cugell and Robson, 1966; Demb et al., 1999; Kaplan and Benardete, 2001). The nonlinearities investigated in this work enable Y-like cells to detect temporal stimulus modulations on a much smaller scale than the extent of their receptive fields and lead to a spatio-temporal inseparability of their receptive fields. X-like cells, which typically have smaller receptive field than Y-like cells, do not show this phenomenon and their spatio-temporal receptive field is separable.

These extensively studied ganglion cell types are the basis for the aforementioned functional segregation: X-like cells provide high spatial and Y-like cells high temporal acuity. So far, comparably little is known about the factors leading to this difference, and the role of this different behaviour in visual perception is still debated (Kaplan and Benardete, 2001).

In this work, the responses of ganglion cells with linear and nonlinear temporal dynamics will be investigated using computational modelling of the retinal circuitry. A major goal of this work was to establish which physiological and anatomical factors account for the differences in ganglion cell response nonlinearities. This question was addressed by conducting a detailed analysis of physiological factors and selected aspects of the neural circuitry that contribute to the response properties of linear X-cells and nonlinear Y-cells in the cat retina. To allow for comparison with experimental data, the model contains a high level of biological realism.

The differences between X- and Y-like cells were first discovered in the cat retina (Enroth-

Cugell and Robson, 1966), but have since been described in many species (goldfish, Bilotta and Abramov, 1989; cat, Enroth-Cugell and Robson, 1966; rabbit, Caldwell and Daw, 1978; mouse, Stone and Pinto, 1993; guinea pig, Demb et al., 1999 and nonhuman primate, de Monasterio, 1978). In this work, mainly data from the cat, guinea pig and primate retina will be considered, as most experimental work was carried out in these species. In particular, the model developed here aims towards a reproduction of experimental data from the cat and guinea pig, where detailed experimental data is available for comparison. A comparison of the experimental data indeed shows strong similarities between X- and Y-like (i.e. linear and nonlinear) cells in different species (Kaplan and Benardete, 2001). Therefore, a modified version, which in particular takes into account the differences in anatomy, is then used to test responses of the primate retina.

1.2 Ganglion Cell Nonlinearities and Visual Perception

The process of visual perception is initiated by the responses of large populations of neurons in the the retina. Their activity is integrated and processed in higher visual areas to facilitate the correct interpretation of a stimulus. Hence, usually individual response properties of a given neuron class are rarely directly rediscovered at the perceptual level, instead they disappear due to convergence, integration and other mechanisms.

This is not the case for some of the basic limitations of visual perception, which are imposed by the properties of retinal neurons. Typical examples are the detection threshold for absolute luminance, which is based on the sensitivity of photoreceptors, or visual acuity, which is limited by spatial sampling in the retina. On the other hand, the consequences of the segregation of retinal processing into linear and nonlinear ganglion cells are not directly visible, and have to be indirectly inferred by comparing psychophysical performance to known properties of these neurons.

This work attempts to bridge this gap by investigating simulated population responses of ganglion cells under conditions where their performance can be directly compared to psychophysical measures. To this end, in a second step the model was adapted to reflect the properties of the primate (human) retina, and ganglion cell responses were recorded and analysed under conditions similar to those in typical psychophysical experiments.

1.2.1 Fixational Eye Movements

A “typical” psychophysical experimental setting involves freely viewing participants who are often asked to fixate a target in order to minimise effects of eye movements. Nevertheless, due to centrally generated fixational eye movements, the eyes are never completely at rest (Ratliff and Riggs, 1950). Fixational eye movements are generated when the direction of gaze is maintained stable and differ substantially from saccades and pursuit movements, which are produced to shift the direction of gaze: Their amplitude is small compared to saccades, only in the range of a few minutes of arc or less, and their direction is typically random (Martinez-Conde et al., 2004).

Experimental evidence suggested that fixational eye movements can in fact help to improve visual performance by means of nonlinear processing (Hennig et al., 2002; K. Funke, N.J. Kerscher and F. Wörgötter, unpublished data). These results motivated an investigation of the effects of fixational eye movements on ganglion cell responses. It was expected that the influence of fixational eye movements should be very different for linear and nonlinear ganglion cells, because of their known different motion sensitivity. Therefore, in this study the combined influence retinal nonlinearities and fixational eye movements on ganglion cell responses was investigated. Two different stimulus conditions were chosen which will be introduced in the following.

1.2.2 Visual Hyperacuity

Visual hyperacuity refers to the phenomenon that the visual system can discriminate tiny offsets in a visual stimulus, which can be substantially smaller than the distance between two photoreceptors (Westheimer, 1979). This effect is based on the blurring of the stimulus introduced by the ocular optics, which leads to small response differences of photoreceptors for small displacements in the spatial stimulus configuration. Hence, hyperacuity is essentially constrained by the noise present on the neural activity, which may obscure the response differences to the stimulus.

Hyperacuity represents a situation where a high spatial accuracy of ganglion cell responses is required, a feature commonly ascribed to linear, densely distributed X-like cells (Kaplan and Benardete, 2001). However, some experimental studies suggested that nonlinearities could dramatically improve spatial precision of sparsely distributed Y-like cells (Lee et al., 1993; Rüttiger et al., 2002). Furthermore, even 80 years ago it was suggested that fixational eye movements might improve hyperacuity (Averill and Weymouth, 1925).

To test these hypotheses, ganglion cell responses to a typical hyperacuity stimulus were investigated using the model of primate linear and nonlinear ganglion cells. From the simulated ganglion cell activity, psychophysical hyperacuity thresholds were estimated and compared to published data. The results of this investigation suggest that both retinal nonlinearities and fixational eye movements have distinct effects on hyperacuity, and that their combination can the improve psychophysical performance in this task considerably.

1.2.3 Motion Induced Illusions

Visual illusions sometimes provide a valuable insight into the structure and function of the visual system. The retinal motion caused by fixational eye movements is known to induce a number of powerful visual illusions (as reviewed by Wade, 2003). In this study, a subgroup of these motion-induced illusions will be studied, both using the model retina and psychophysical experiments.

The starting point for the investigation of motion-induced illusions was the question how fixational eye movements and retinal nonlinearities interact under natural viewing conditions, away from threshold conditions such as hyperacuity. Rather unexpectedly, the simulations suggested a retinal origin for these illusions, and led to testable experimental predictions.

1.3 Modelling the Retina

In this study, a computer model of the vertebrate retina was developed and tested by comparing modelled responses to experimental data. The model is a detailed implementation of single neurons and their known physiology and connectivity. It is heavily based on experimental anatomical and physiological data, an approach that has become feasible recently due to the large body of available experimental data.

The main advantage of the detailed model used here is that it is easy to introduce modifications in order to simulate pharmacological manipulations or to introduce unphysiological modifications. Both allow for a very detailed testing of various hypotheses, which is often difficult in experimental studies due to technical constraints. Furthermore, the simulated neural responses and pharmacological manipulations can lead to specific, quantitative predictions for experiments.

A further advantage is that the model allows for the simultaneous analysis of the responses of a large number of neurons for a given stimulus condition. This is experimentally difficult to achieve, because here the population response typically has to be inferred from many single cell recordings. While it is in principle also possible to record retinal activity simultaneously from multiple units (using multielectrode arrays), this method is restricted to ganglion cell activity. Therefore, a model can augment these techniques by providing the population response of all retinal neurons, and can thereby help to explain experimental observations.

1.4 Organisation of this Work

The following chapters are broadly organised into three parts. First, the biological background and the model are described (Chapters 2, 3 and 4). This is followed by four chapters, where the findings of this study are presented and discussed (Chapters 5-8). The final chapter (Chapter 9) then provides a more general discussion of the results.

Chapter 2 introduces the structure and relevant functional aspects of the vertebrate retina which provided the biological basis for the model. The chapter begins with an introduction of the influence of the ocular optics on retinal image formation. Then, an overview of the main retinal neuron classes and their basic connectivity is given. This is followed by a review of neural sampling of visual stimuli by the retina and an introduction of retinal receptive fields. Finally, the nonlinearities in ganglion cell responses are introduced, which will be investigated in this work.

To allow for a discussion of the results of this study in the context of visual perception, the following Chapter 3 provides a brief review of the higher visual system. This chapter focuses on the pathways of visual information to the visual cortex and their functional segregation and on receptive fields in the primary visual cortex.

Chapter 4 then describes the model implementation. This is accompanied by an extensive review of the experimental literature to explain and discuss the specifics of the model.

The following four chapters contain a detailed description of the results of this study. In each chapter, first the problem and methods are introduced, which is followed by the description of the results. Each chapter closes with a summary and discussion of the main results.

Chapter 5 explores the origin of response nonlinearities in Y-cells of the cat retina and

contrasts their properties to those of X-cells. It will be shown that response nonlinearities are of multiple origin: they are based on asymmetries in the photoreceptor response and amplified by a specific neural circuit in the inner retina which generates transient responses in Y-cells. This study is based on a concise investigation of different factors and involves various manipulations of the model to isolate the relative contribution of these factors.

Chapter 6 introduces fixational eye movements and explores their influence on primate ganglion cell responses. It will be shown that they exhibit a distinct influence on the responses of MC-cells, which is a result of the nonlinearities identified in Chapter 5.

The influence of fixational eye movements combined with nonlinear processing on visual perception is the topic of the following two chapters. In Chapter 7, the phenomenon of hyperacuity will be studied at the level of ganglion cell responses. The results indicate that dynamic nonlinearities, triggered by fixational eye movements, could significantly enhance the performance of these neurons in a hyperacuity task. These results are consistent with psychophysical data and could resolve the old conflict as to whether eye movements contribute to improve spatial vision. Chapter 8 finally considers the population response of ganglion cells when stimulated with a stimulus that elicits strong motion-induced illusions. The results indicate that the perceptual correlate of this illusion can be traced back to the level of retinal ganglion cells and is a consequence of MC-cell nonlinearities.

The work concludes with a discussion of all results in the context of visual perception in Chapter 9.

Chapter 2

The Vertebrate Retina

The retina is a sheet of neural tissue, about $200\mu m$ thick, that lines the back of the eyes. It develops from the neural tube during embryonic development and is thus a part of the brain, amounting about 0.3% of the total brain tissue. The task of the retinal neuronal network is the processing of visual information. This chapter provides a review of these processes.

A central aim of this chapter is to explain and motivate the model implementation of the vertebrate retina. As this study concentrates on the cat and primate (human) retina, most of the following discussion will focus on these species. First, optical and neural image formation will be discussed, which constrains spatial visual resolution. Then, the different neuron classes and their functional connectivity will be introduced. Finally, the receptive field organisation of retinal ganglion cells will be described, and nonlinear receptive fields will be introduced.

2.1 Formation of the Retinal Image

The main task of the optic apparatus of the eye is to provide a sharp image of the visual world to the photoreceptors. The optical quality of the eye however is poor compared to that of man-made instruments[1]. This fact is not so surprising if one considers that it is made of living tissue and not of glass.

[1]This is best illustrated by a quote of Hermann Helmholtz: "Now it is not too much to say that if an optician wanted to sell me an instrument which had all these defects, I should think myself quite justified in blaming his carelessness in the strongest terms, and giving him back his instrument." (Kline, 1962).

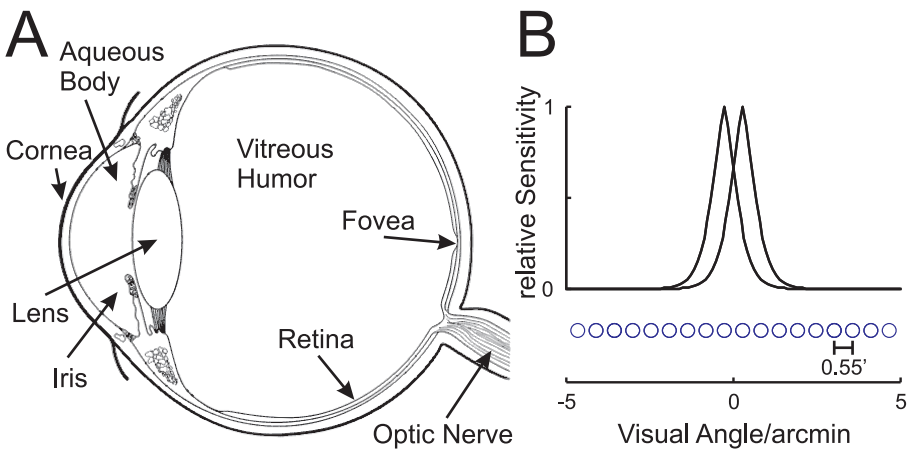

FIGURE 2.1: Optical factors affecting the retinal image. A, Simplified anatomy of the human eye. B, Point spread function describing the optical blurring of the eye. The relative amount of light for two small spots of light reaching plotted as function of the visual angle on the retina surface (after Westheimer, 1986). Individual photoreceptors are shown as circles.

Sources of optical errors are numerous and include diffraction at the pupil, aberration and light scatter. Before light is absorbed by photoreceptors in the retina, it traverses the cornea, the aqueous fluid, the lens and the vitreous body (Figure 2.1A). The cornea makes the strongest contribution to the refractive power of the eye, with about 40 diopters. The refractive power of the other components is low, as they are primarily composed of water. The lens can add up to about 15 diopters and accommodation to a lower focal length is achieved by adjusting its curvature with the ciliary muscles. The iris functions as an aperture and can assist accommodation by increasing the depth of focus.

Helmholtz (1896) was the first to develop a comprehensive model of the human eye, where he also considered optical errors. Much later, double-pass imaging of the retina was developed to assess the optical quality of the living eye (Westheimer and Campbell, 1962; Williams et al., 1994). This led to the characterisation of optical blurring by a point spread function (PSF), which describes the spatial blur of a point light source.

The second task of the eye is to regulate the amount of light that hits the retina. This is necessary since photoreceptors only respond to a limited dynamic range of light stimulation and is achieved by a change of the diameter of the iris from about 2mm to 8mm. This leads to a hundredfold change of the light passing to the retina, which however is still small compared to the 15 orders of magnitude over which the human visual system is responsive. Thus, the main load of adaptation to luminance is carried out on the neural level in the retina. For this purpose, all vertebrate retinas contain at least two types of photoreceptors, the rods and cones. Rod photoreceptors are responsible for detection

of light at very low intensities, particularly at night or in the presence of little ambient light (scotopic conditions). They are extremely sensitive and as a consequence the human visual system is capable of detecting only a few quanta of light (Teich et al., 1982). At normal daylight (above about $0.03cd/m^2$, photopic conditions), rods are saturated and cone photoreceptors mediate vision.

In most mammals, including humans, rods greatly outnumber cones (in humans by a factor of about 19; Osterberg, 1935). The distribution of photoreceptors in many mammals, including primates, is such that a central region on the retina, where images are focused during fixation, is cone-dominated. Called *area centralis* in cats and *fovea* in primates, it is the region with the highest cell density in the retina and provides the highest visual acuity. The retinal periphery is strongly dominated by rods. Both the density of cones and rods decreases with increasing eccentricity, which leads to a strong reduction of peripheral visual acuity. Primates have developed a *duplex retina*, where the fovea exclusively contains cones. As a consequence, the fovea has a high visual acuity for daylight-vision, whereas in the periphery, detection of the faintest sources of light at night is possible[2].

Vertebrate retinas are usually equipped with a variety of different cone types which absorb light at different wavelengths, thereby providing the basis for colour vision. There is a considerable variability of photoreceptor types among different species, which may reflect the adaptation to different visual environments. Many retinas of cold-blooded vertebrates have up to five types of cones, providing them with good colour vision. Most mammals have two types, and primates typically three types.

In this study, models of the cat and primate retina will be examined. In both cases, only responses to achromatic stimuli under photopic conditions were considered. Hence, only cone photoreceptors were considered, and no distinction was made between different wavelength sensitivities. The ocular mechanism for light adaptation was also not included, therefore the model represents a retina for a fixed iris opening[3].

2.2 Main Cell Classes, Connectivity and Function

Photoreceptor signals are processed by about 70-80 different morphological distinguishable types of neurons (Masland, 2001a; MacNeil and Masland, 1998). Despite this

[2] If one tries to fixate a faint star at night with the fovea, it is no longer visible due to the lack of rods there.

[3] A change of the size of the aperture regulated by the iris would also change the amount of diffraction and thus the quality of the retinal image.

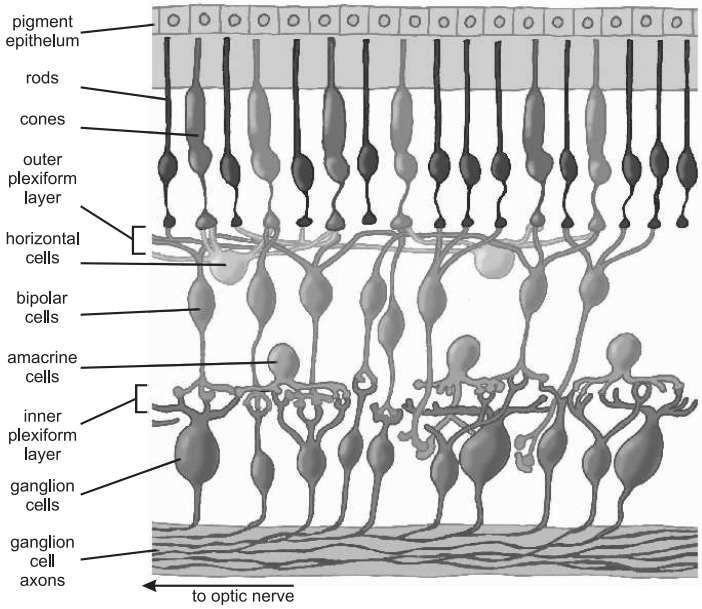

FIGURE 2.2: Simplified anatomy of the vertebrate retina (modified from Kolb, 2003).

considerable variety of cells, the retina shows a high degree of structural organisation. For many cell types, specific functional roles for the processing of visual information have been identified, and numerous *functional circuits* have been identified (reviewed by Sterling, 2003). This functional segregation appears to be the basis for the organisation of visual information in several parallel channels, each transmitting specific information about the visual world to the higher visual areas of the brain (Roska and Werblin, 2001).

The functional neural connectivity of the vertebrate retina can broadly be separated into a feed-forward pathway and two sites of lateral interaction. Anatomically, it is divided into three layers of cell bodies (*nuclear layers*) and two layers containing synapses (*plexiform layers*). Lateral interaction takes place in the two plexiform layers, and each of these two sites has specific functions in the processing of the visual signals.

Figure 2.2 shows a simplified diagram of the main cell classes and their fundamental connectivity. After traversing the ocular optics and the largely transparent retinal network, light is absorbed by photoreceptors, which are arranged on a regular two-dimensional mosaic. They are embedded in the pigment epithelium and their cell bodies form the *outer nuclear layer*. In the *outer plexiform layer* (OPL), photoreceptors make synaptic contacts to horizontal and bipolar cells. Together with amacrine cells, the bipolar cell bodies comprise the *inner nuclear layer*. Horizontal and amacrine cells mediate lateral interaction horizontal to the retinal surface and bipolar cells transmit signals in a feed-forward fashion vertically to amacrine and ganglion cells. Synaptic contacts from bipolar to ganglion cells, along with synapses of some amacrine cell types, are located

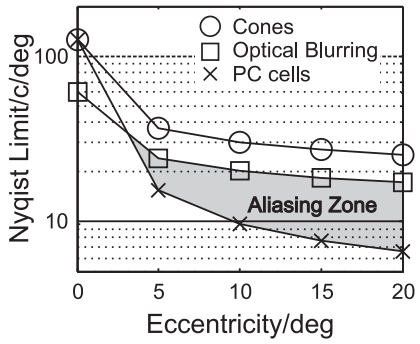

FIGURE 2.3: Spatial sampling limits in the human retina imposed by the photoreceptors (circles), the optical point spread function (squares) and ganglion cells (crosses) as a function of eccentricity. The shaded region indicates where aliasing occurs due to neural undersampling (see text). The data was compiled from Thibos et al. (1987); Dacey and Petersen (1992); Goodchild et al. (1996); Thibos et al. (1996); Sjöstrand et al. (1999).

in the *inner plexiform layer* (IPL). Ganglion cells and displaced amacrine cells are located in the *ganglion cell layer* (GCL). The axons of the ganglion cells finally form the *optic nerve* which transmits retinal output to higher structures of the brain.

2.3 Spatial Sampling in the Retina

As outlined in Section 2.1, the retinal mosaic of mammals is not homogeneous, but contains a region with a high density of cone photoreceptors and ganglion cells providing high spatial acuity. In the primate fovea, the distance between two cones in the fovea is about $0.55'$ (Osterberg, 1935; Curcio et al., 1987; Sjöstrand et al., 1999). Midget ganglion cells receive input from a single cone via a "private-line" cone bipolar cell (Boycott and Wässle, 1991; Wässle and Boycott, 1991; Dacey, 1993). In the area centralis of the cat retina, one cone bipolar cell collects signals from about seven photoreceptors and the convergence of cones onto beta cells is about 30 to 40 (Cohen and Sterling, 1991; Kolb and Nelson, 1993).

Towards the retinal periphery, the density of both cones and ganglion cells decreases steadily. This is accompanied by an increase of the size of the dendritic fields of midget ganglion cells in the primate (Dacey and Petersen, 1992) or beta cells in the cat (Boycott and Wässle, 1974). A general feature of the different ganglion cell populations is a constant coverage of the retina at all eccentricities (Peichl and Wässle, 1979; Cleland et al., 1979).

A consequence of this design is that the spatial resolution of the retina declines rapidly

with increasing eccentricity. The term *resolution* here refers to the highest spatial frequency, or the *Nyquist frequency*, that is detectable according to the sampling theorem. As already formulated by Helmholtz (1896), the detection of a stimulus is only possible if the spatial sampling rate of the neurons (i.e. the inverse of their density) exceeds the spatial frequency of this stimulus by at least by a factor of two. In contrast to the central region, in the retinal periphery an increasing number of cones converge onto one ganglion cell. Hence the retinal Nyquist limit is, depending on the eccentricity, determined by either the cone or ganglion cell density. Additionally, the blurring of the image by the ocular optics (see Section 2.1) also imposes an upper limit on spatial acuity. The resulting Nyquist frequencies for different eccentricities for the human retina are summarised in Figure 2.3.

In the primate fovea, spatial sampling by photoreceptors imposes a limit of about 120 cycles per degree (cpd). Psychophysical detection thresholds are in the range of 60 cpd (De Valois and De Valois, 1988), which results from the additional optical blurring. Using laser interferometry, it became possible to directly project interference fringes onto the retina while bypassing the ocular optical system. These experiments demonstrated that it is possible to detect foveal stimuli with spatial frequencies above the Nyquist limit (Williams, 1985), which then appear as distorted moiré patterns. This effect is a consequence of aliasing and normally prevented by optical blurring.

In the retinal periphery, the Nyquist limit is set by the ganglion cell density, as it decreases more rapidly than the cone density. The optical quality of the eye also decreases due to off-axis refractive errors (Williams et al., 1996), but less rapidly than the neural sampling density, which leads to aliasing from about 5 degrees eccentricity in the human retina (shaded region in Figure 2.3).

2.4 On- and Off-Center Cells

The first electrical recordings from retinal ganglion cells revealed that some cells respond to the onset (*On-cells*) and some to the offset (*Off-cells*) of light, and some respond both to the onset and offset (*On-Off cells*) (Fig. 2.4A, Hartline, 1938; Barlow, 1953; Kuffler, 1953). Subsequently, it was shown that bipolar cells can also be separated into On- and Off-center bipolar cells (Werblin and Dowling, 1969). Furthermore, a subdivision into On-, Off- and On-Off cells is also found within the amacrine cell population (Werblin and Dowling, 1969). This segregation is also reflected by the anatomy of the inner plexiform layer. Here the axon terminals of different bipolar cell types stratify at different levels: On-cells are located in the proximal half (sublima B) and

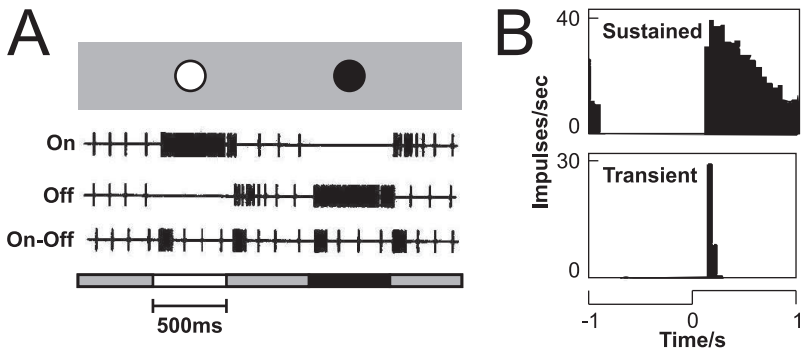

FIGURE 2.4: A, Responses of On-center, Off-center and On-Off ganglion cells to stimulation of the center of their receptive field (modified from Hartline, 1938). Individual spikes of the responses to a light increase and decrease are shown (stimulus time course is shown at the bottom). B, Response of a sustained (top) and transient (bottom) ganglion cell in the mouse retina (modified from Nirenberg and Meister, 1997) Shown are responses of two On-center ganglion cells to a step change in illumination (indicated at the bottom).

Off-cells in the distal half (sublima A, Nelson et al., 1978). Hence in the retina visual information is split into at least two fundamental channels, the On- and Off-pathways, which separately encode the brighter or dimmer half of the total contrast range.

2.5 Center-Surround Receptive Field Organisation

The concept of the *receptive field* was first introduced by Hartline (1938), who defined it as the area in the visual field on which a response can be produced by light-stimulation. Early findings indicated that the sensitivity of a retinal ganglion cell depends on the stimulus position, and further experiments revealed that the receptive field of a ganglion cell typically consists of two regions. In *On-cells* (or On-center cells), a central, circular region exists where stimulation with a small spot of light leads to an increased response. This region is surrounded by a wider region where stimulation leads to suppression of the response (Figure 2.5A). The same organisation, only in reverse, is found in *Off-cells* (Off-center cells). It has been shown that this arrangement is well approximated by two overlapping Gaussian profiles, one with a positive and the other with a negative sign (Rodieck and Stone, 1965; Enroth-Cugell and Robson, 1966). The response $R(\vec{x})$ to a two-dimensional ($\vec{x} = [x, y]$) spatial stimulus configuration $S(\vec{x})$ can be written as convolution of the stimulus with Gaussian profiles:

$$R(\vec{x}) = S(\vec{x}) * \left(A_c e^{-\frac{x^2+y^2}{2\sigma_c^2}} - A_s e^{-\frac{x^2+y^2}{2\sigma_s^2}} \right), \tag{2.1}$$

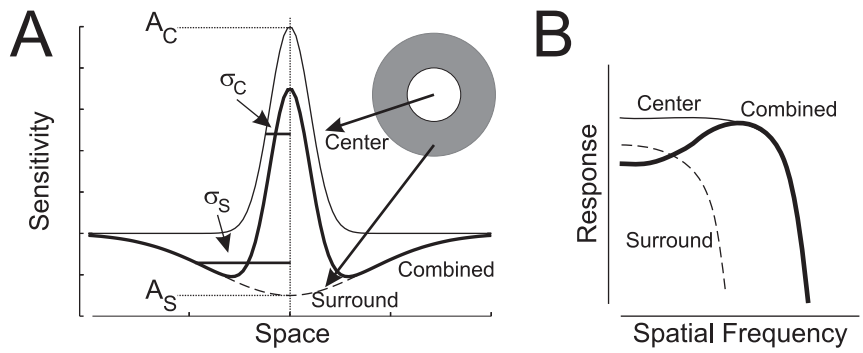

FIGURE 2.5: Spatial structure of ganglion cell receptive fields. A, Ganglion cells receive input from an excitatory center region (straight thin line) and an inhibitory surround (dashed line). The receptive field is obtained by adding these two components (thick line). B, The isolated center and surround components are spatial low-pass filters (straight thin and dashed line, respectively). Their combination leads to a spatial band-pass filter characteristic (thick line).

where A_c and A_s are the amplitude and σ_c and σ_s the width of center and surround, respectively (Figure 2.5A). This model is usually referred to as the "*Difference of Gaussians*"-model. As a consequence, retinal ganglion cells act as spatial bandpass filters (Figure 2.5B).

2.5.1 Receptive Field Center

The basis of the center of the ganglion cell receptive field is excitatory input from bipolar cells. On-center cells receive input from On bipolar cells, and Off-center cells from Off bipolar cells (Nelson et al., 1978; Kolb, 1979; Nelson and Kolb, 1983; Kolb and Nelson, 1993). Anatomically this is established by dendritic stratification in different layers of the IPL. The width of the center input of the receptive field is determined by the width of the dendritic field of the ganglion cell (Peichl and Wässle, 1979; Freed and Sterling, 1988). The amount of dendritic membrane across the dendritic field available for bipolar cell synapses decreases from the center, and as a consequence distal input from bipolar cells is weaker than that to the center of the dendritic tree (Kier et al., 1995). This confirms the notion of separate Gaussian-shaped center and surround inputs to ganglion cells, as defined by Equation 2.1 (Rodieck and Stone, 1965).

Typically, the electrophysiological investigation of the receptive field dimensions suggests wider receptive fields for ganglion cells than the anatomical extend of the dendrites would predict. The main reason for this is that optical blurring already increases the area of the visual field, on which a single photoreceptor can be stimulated. This automatically increases the width of the receptive fields of subsequent neurons (Cohen

and Sterling, 1991) and limits the amount of spatial detail the visual system is able to detect (see also Section 2.3). Consequently, a model for the ganglion cell receptive field must also incorporate optical blurring.

2.5.2 Receptive Field Surround

It is generally accepted that bipolar cells only release the excitatory neurotransmitter glutamate (Wilson, 2003), thus they can not be directly responsible for the inhibition that leads to the receptive field surround of ganglion cells. Recent data indicates that the surround-response is created by a combination of lateral inhibition in the outer and inner plexiform layer. Horizontal cells, located in the outer retina, have wide receptive fields and antagonise bipolar cells. As a consequence, the receptive field of bipolar cells already shows a centre-surround organisation both in the non-mammalian and mammalian retina (Mangel, 1991; Burkhardt, 1993; Dacey et al., 2000). In the inner retina, GABAergic amacrine cells form inhibitory synapses with ganglion cells that leads to additional center-surround antagonism (Flores-Herr et al., 2001).

2.6 Spatiotemporal Nonlinearities in Ganglion Cells

Often, the simple model introduced by Equation 2.1 in the previous section provides an adequate description of the receptive field of ganglion cells. In a similar fashion, a description of the temporal response of a ganglion cell can be obtained, which is typically a linear band-pass filter. Combined, this approach allows the description of the *spatiotemporal* response of a ganglion cell and can be employed to characterise X-cells in the cat retina and PC-cells in the primate (Enroth-Cugell et al., 1983; Benardete and Kaplan, 1997, 1999).

A limitation of this model is the assumption of spatial and temporal linearity and separability, which is not appropriate in all cases. The responses of some ganglion cell types show pronounced nonlinearities, as first shown for Y-cells in the cat (Enroth-Cugell and Robson, 1966) and later also for primate MC-cells (Kaplan and Shapley, 1982; Benardete et al., 1992). This response nonlinearity is particularly visible when Y-like cells are stimulated with contrast-reversed sine gratings. Centering the sine grating at its $0°$ or $180°$-phase (*null-phase*, see Fig. 2.6, right) over the receptive field of a ganglion cell creates a situation where contrast-reversal causes no net stimulation, as both sides of the grating cancel each other. However, Y-like cells typically respond with

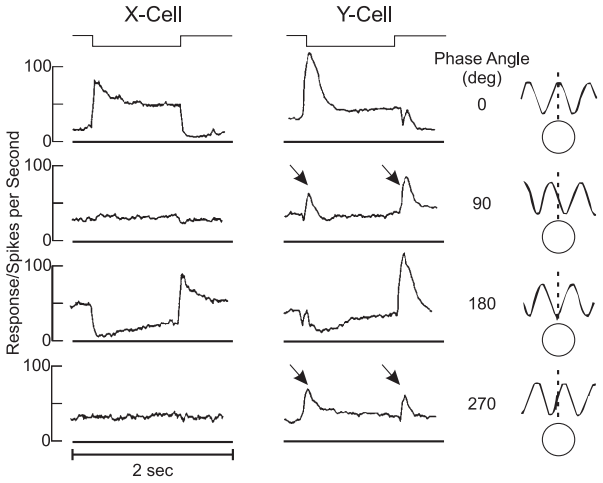

FIGURE 2.6: Frequency-doubling in cat Y-cells. Responses of an Off-center X- (left) and Y-cell (right) to a counterphasing sinusoidal grating (time course indicated on top) are shown for different relative spatial phases of the stimulus (indicated on the right). In the second and fourth row, the stimulus is fully spatially balanced over the receptive field, i.e. the net change of stimulation is zero. This almost exactly cancels the X-cell response (Null-response). In the Y-cell, sharp transient peaks persist at twice the stimulus frequency for this stimulation situation (indicated by arrows), hence the name frequency-doubling (modified from Enroth-Cugell and Robson, 1966).

a transient burst at each contrast reversal (Fig. 2.6, Enroth-Cugell and Robson, 1966; Hochstein and Shapley, 1976a; Kaplan and Shapley, 1982). The responses of Y-like cells under these conditions are *frequency-doubling*, as they respond at twice the frequency of the contrast reversal. Linear X-like cells and PC-cells in primates never show this effect (Fig. 2.6).

Frequency-doubling can also be elicited by stimulation of regions beyond the classical receptive field of Y-cells, as defined by Equation 2.1 (McIlwain, 1964; Krüger and Fischer, 1973). This is known as the *periphery effect* and is mediated by spiking amacrine cells (Demb et al., 1999). The periphery effect is based on a different mechanism from frequency-doubling produced by receptive field center stimulation, because the latter also occurs when spiking is pharmacologically blocked.

The frequency-doubling effect is a result of nonlinear processing in the retina; a linear receptive field will never respond under these conditions. Furthermore, a mathematical description of a receptive field which produces frequency-doubled responses has to be spatio-temporally inseparable. This is required because frequency-doubled responses can only occur if the temporal response to the symmetrical input patterns is altered in a space-dependent way (Victor, 1988).

Hence for Y-like and MC-ganglion cells the spatial and temporal response is not sep-

arable, and a combination of a spatial Difference of Gaussians filter and a temporal bandpass filter is an insufficient description. The exact origin of Y- and MC-cell nonlinearities is still unknown. Pharmacological manipulations indicate that they are not intrinsic to ganglion cells, but a result of interactions within the retinal network (Demb et al., 1999). As a part of this study, different factors which may contribute to nonlinear receptive fields were investigated, and the results are the main topic of Chapter 5.

Figure 2.6 also shows that contrast modulation produces sustained responses in linear X-cells, but transient bursts in nonlinear Y-cells, suggesting that these neurons generally differ with respect to their response duration. The same is observed in the primate retina, where nonlinear MC-cells respond with transients and linear PC-cells in a sustained fashion, and in other mammalian species such as the guinea pig or mouse (see also Fig. 2.4B; Dhingra et al., 2003; Carcieri et al., 2003). The transient type is often called "brisk-transient" ganglion cell, and it has been suggested that these cells also generally show frequency-doubled responses (Demb et al., 2001). In primates, Benardete et al. (1992) suggested the existence of two separate transient types of MC-cells, with different degree of response nonlinearity.

A recent statistical survey of a large population of different ganglion cells in the mouse retina supports the notion of a separation of retinal ganglion cells into separate *transient* or *sustained* classes (Carcieri et al., 2003). However, the presence of separate ganglion cell classes with a different degree of response-nonlinearity could not be confirmed (see also White et al., 2002 for MC-cells). Degree of nonlinearity in these studies is typically measured by dividing the the second (or even) harmonic response component in a cell's fourier spectrum by the the first (or odd) harmonic (Hochstein and Shapley, 1976b). The first and higher odd harmonic response components correspond to the temporal stimulus modulation, and the second and higher even harmonics result from nonlinear processing. Carcieri et al. (2003) showed that, in a larger ganglion cell sample, the degree of response-nonlinearity is unimodally distributed. Hence, it is yet unclear what determines the degree of nonlinearity of a given ganglion cell type, and whether it is correlated with other common features of nonlinear ganglion cells such as transient responses. The analysis of ganglion cell nonlinearities in Chapter 5 attempts to shed light on these seemingly contradictory findings.

Chapter 3

The Retina as a Part of the Visual System

The purpose of this chapter is to provide a brief overview over structural and functional aspects of the early visual system and the role of the different retinal channels within this framework. It is not a comprehensive review, as this would be beyond the scope of this work, and concentrates on aspects relevant for the interpretation of the results in Chapters 7 and 8.

3.1 Functional Segregation in the Visual Cortex

A fundamental property of the visual system is the parallel processing of visual information in different channels, which encode stimulus properties such as luminance, contrast, colour, shape or motion (Merigan and Maunsell, 1993). The existence of two separate processing streams was first suggested by Livingstone and Hubel (1988): the *ventral* stream has been associated with form-analysis and colour vision and the *dorsal* stream with motion- and stereo-analysis (sometimes also called the "what"- and "where"-streams, Fig. 3.1). Experimental evidence in support of such a functional segregation however is still sparse and mostly based on lesioning studies (Schiller and Logothetis, 1990; Merigan and Maunsell, 1993; Gegenfurtner, 2003), which ignore possible interactions between both streams.

As shown in the preceding section, visual information is already segregated into several visual pathways in the retina (i.e. On vs. Off, sustained vs. transient). The axons of retinal ganglion cells project to the lateral geniculate nucleus (LGN), which is a part of

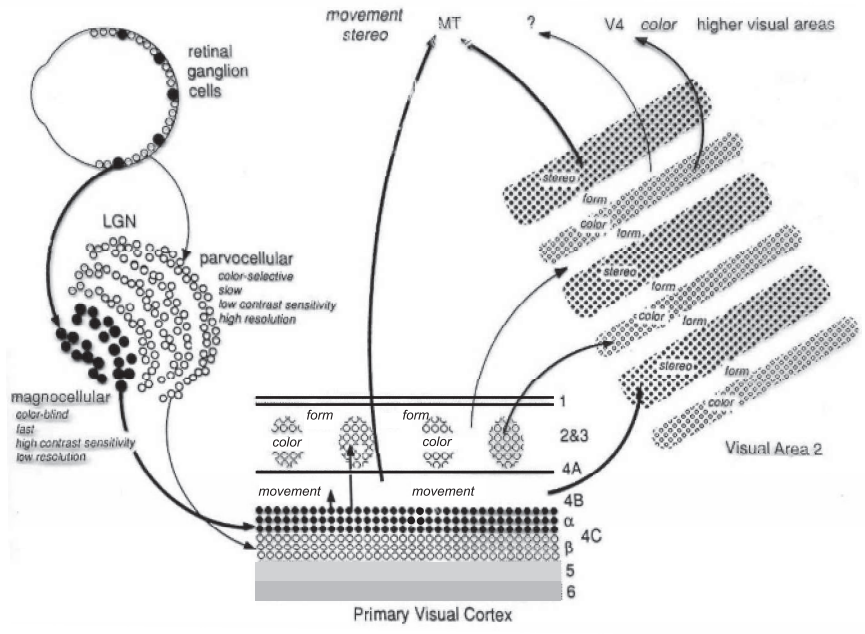

FIGURE 3.1: The primary visual pathway from the retina to the visual cortex. The figure highlights the functional segregation of visual pathways into the ventral and dorsal stream (modified from Livingstone and Hubel, 1988).

the thalamus that relays visual information to the striate cortex (Figure 3.1). The basis for the ventral stream are X-cells in the cat or PC-cells in the primate, which project into the upper four of the six layers of the LGN. Y- and MC-cells, forming the dorsal stream, project into the lower two layers. As a further subpopulation of thalamic neurons are the K-cells (koniocellular) cells in the primate or W-cells in the cat, which account for about 10% of the cells in the LGN (Norton and Casagrande, 1982). These cells seem anatomically more diverse and their retinal correlates and functional roles are not yet fully understood.

From the thalamus, visual information is transmitted to the primary visual cortex (*area 17* or V1). V1 is a complex and large (about 13% of the total surface of the cortex) neural structure devoted to the processing of visual infomation. It consists of several anatomically defined layers, and the projections from the LGN terminate in distinct layers. Figure 3.1 shows that in primates the main projection site is layer 4, which is subdivided into two layers that receive predominantly either input from PC-cells (layer $4C\beta$) or MC-cells (layer $4C\alpha$). Although this picture is incomplete (a more comprehensive view, including the koniocellular pathway, is provided by Callaway, 1998), the fact that the PC- and MC-system (as well as the K-system) are still separated at this level supports the notion of segregated, parallel visual pathways. A similar organisation was found in the cat and many other mammals.

Combining the evidence provided so far, a likely explanation for presence of separate visual pathways in general is that they convey specific information about different parts of the spectrum of spatial and temporal frequencies, which may be used for different purposes (Schiller and Logothetis, 1990). PC-cells and X-cells have a high spatial resolution due to their high density and small receptive fields, but a low temporal fidelity, which makes their signals useful for precise spatial analysis. The opposite is true for MC-cells or Y-cells, so their activity patterns appears more useful for the analysis of temporal changes in the visual world (but see Lee et al., 1995; Rüttiger et al., 2002, who reported a high spatial precision for MC-cell responses). These considerations, and a huge body of data on the physiology of the visual cortex, eventually led to the concept of separate higher visual pathways for form and motion (Fig. 3.1).

However, the evidence how this segregation affects perception is sparse and controversial (Schiller and Logothetis, 1990; Gegenfurtner, 2003). Already at the level of the retina, the notion of separate channels for spatial precision and motion analysis appears wrong, as it has been shown that MC-cells can encode visual stimuli with the same spatial precision as PC-cells at high contrast, and even outerform PC-cells at reduced contrast (Lee et al., 1995; Rüttiger et al., 2002). Furthermore, even during perfect fixation, retinal images are never completely stationary due to small fixational eye movements (Ratliff and Riggs, 1950; Ditchburn and Ginsborg, 1953). Hence during fixation the cortical motion-sensitive pathway, which receives input predominantly from MC-cells, is constantly stimulated and may also contribute to the analysis of structure and form. Finally, it should also be noted that the cellular properties of the PC- and MC-systems, in particular the differences in response-nonlinearity, are not easily discovered at the perceptual level. This suggests that the activity of both streams may be integrated and combined at the cortical level to facilitate a correct interpretation of visual stimuli.

3.2 Simple Cell Receptive Fields

The voluminous body of literature on the visual cortex highlights the complexity of this structure and its physiology. Therefore, only the receptive fields of *simple cells* in the primary visual cortex shall be reviewed here, as they will be of importance for the interpretation of the results in the Chapters 7 and 8. Hubel and Wiesel (1962) discovered that neurons in layer 4 of the cat V1 which respond best to edges and bars and are tuned to a specific orientation of the stimulus. Their experiments led to the conclusion that these neurons, called *simple cells*, have receptive fields with elongated On- and Off-subfields that alternate in space (Fig. 3.2). Hubel and Wiesel proposed a simple

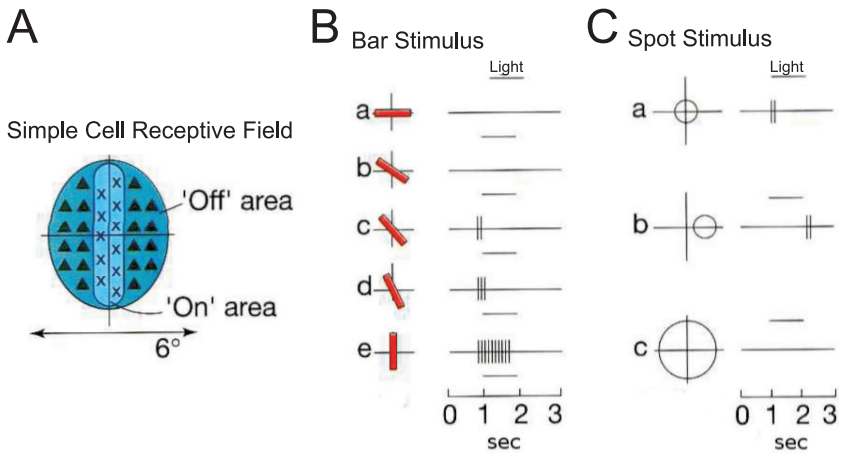

FIGURE 3.2: A typical V1 simple cell receptive field. It consists of alternating excitable (On-area) and inhibitory (Off-area) subfields (left). Stimulation with a bar with different orientations shows that each simple cell has a preferred orientation (middle). The composition of the receptive field into subfields further leads to a selectivity to stimulus size (right).

model, where the receptive field is constructed of afferent input from the LGN that covers a line in visual space. Alternating On- and Off-subregions are supplied by On- or Off-afferents from the LGN. Although frequently reinvestigated and refined, this basic model for simple cells is generally accepted as the basis for spatial filtering in the visual cortex (Reid and Alonso, 1996; Priebe et al., 2004).

As mentioned above, spatial summation in simple cells appears to be largely linear (in fact, a characterisation of simple cells shows various degrees of spatiotemporal linearity; Carandini et al., 1997; Carandini and Ferster, 2000), although they receive input from both the linear and nonlinear cells of the LGN (P/M or X/Y) (Malpeli et al., 1981; Maunsell and Gibson, 1992). A possible mechanism to obtain linear responses from the mixed LGN input is a push-pull circuit, which consists of balanced excitatory and inhibitory connections and leads to a cancellation of the nonlinear components (Glezer et al., 1980; Gaudiano, 1992b; Wörgötter et al., 1998; Anderson et al., 2000; Lauritzen and Miller, 2003). Depending on the relative weights of the excitatory and inhibitory inputs, a push-pull circuit is capable of linearising nonlinear input. It may therefore be possible that nonlinearities in retinal responses are no longer be visible at the cortical level, and are solely an artefact of retinal processing. This is also supported by the finding that nonlinearities of simple cells are largely generated intracortically (Carandini et al., 1997). On the other hand, in Chapter 8 of this work a novel visual illusion will be introduced which is a direct consequence of retinal nonlinearities. This suggests that the influence of nonlinear processing in the retina on cortical responses may have to be re-evaluated and included into models of cortical processing.

Chapter 4

Anatomy and Physiology of the Model Retina

This chapter introduces the model retina used in this study on the basis of the physiology and anatomy of the different retinal neuron classes and their connectivity. The basic neural connectivity in the model, as shown in Figure 4.1, provides the basis for the circuits that lead to primate PC- and MC-cell and cat X- and Y-cell receptive fields (for a more detailed description, see the legend). In the following, first a general introduction of the level of modelling and mathematical description of neurons and receptive fields will be given. Then, each retinal neuron class will be described and reviewed in detail, and the specific model implementation will be discussed. Finally, the technical details of the implementation as a computer model will be summarised.

4.1 General Approach

The model retina used in this work consists of single neurons, and it was attempted to implement realistic connectivity patterns based on anatomical and physiological data. As will be shown below, the passive membrane equation was used as the mathematical level of description for the activity of single neurons. All neurons were implemented as single-compartment structures, and spatial the extend of dendrites or axons was not explicitly implemented. Instead, to account for the different effect of an input at a distal site compared to more proximal sites, the connections between neurons were weighted according to the distance. This method allows for a realistic, but simple implementation of spatial receptive fields which are very similar to those obtained in physiological

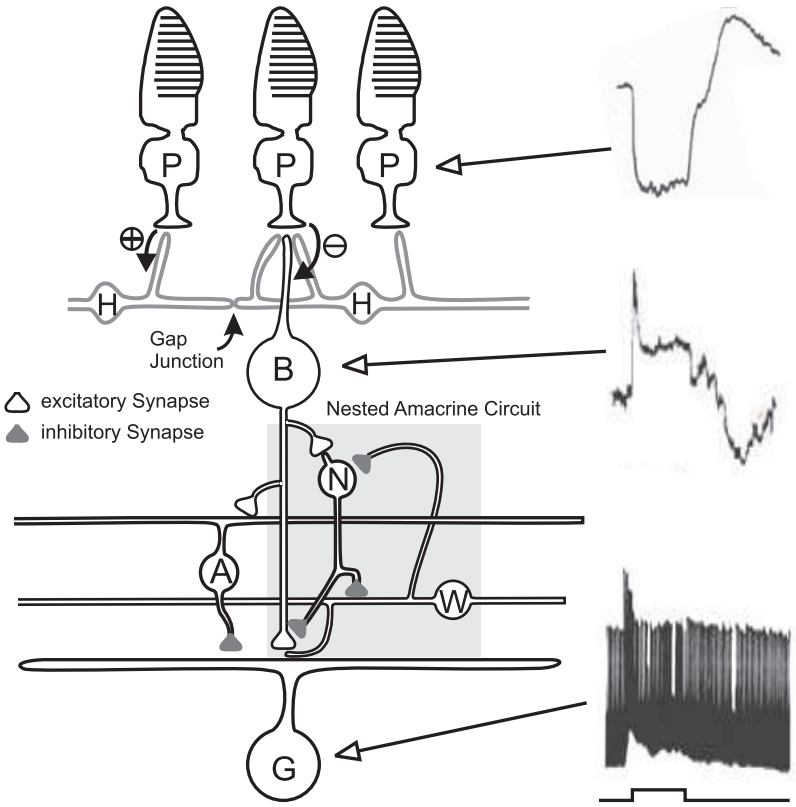

FIGURE 4.1: Schematic circuit diagram of the model retina. Shown are the different cell classes and their synaptic connections for the simulated On-center pathway. Photoreceptors (P) connect to horizontal cells (H) by excitatory synapses (⊕) and to On-center bipolar cells (B) by sign-inverting synapses (⊖). Horizontal cells connect to bipolar cells with sign-conserving synapses, mediating their receptive field surround. The receptive field of On-center X- or PC-ganglion cells (G) consists of excitatory input from On-center bipolar cells to the receptive center and inhibitory input from wide field amacrine cells (A) to the surround. For Y- or MC-cells, the presynaptic bipolar cells further receive inhibition from narrow-field amacrine cells (N) at the axon terminal (forming a subgroup of transient bipolar cells). Narrow field amacrine cells receive excitatory input from bipolar cells and inhibition from wide field amacrine cells (W). Wide field amacrine cells are excited by transient bipolar cells and receive inhibition from narrow-field amacrine cells. Combined, this coupling of amacrine cells forms a nested amacrine circuit (shaded region), which leads to transient responses in Y- and MC-ganglion cells. The insets show typical responses of a photoreceptor, a bipolar and a ganglion cell to a flash of light (modified from Kolb et al., 2005).

experiments (Cohen and Sterling, 1991). Furthermore, synaptic transmission was assumed to be a linear process, and possible influences of short-term synaptic plasticity were neglected.

The situtation is however different in photoreceptors. The cascade of molecular events translating a light stimulus into a electrical response differs substantially from the processes involved in synaptic transmission, and to obtain realistic responses, a more complicated model had to be used. As shown in Section 5.2.1, photoreceptors show a nonlinear relation between light intensity and response, and their response also depends on the level of background illumination. Therefore, in this work an earlier qualitative model for the photocurrent in cones following light stimulation by Schnapf et al. (1990) was extended to reproduce the most important characteristics of their voltage response (Schneeweis and Schnapf, 1999).

The connectivity patterns between many retinal neurons are now well established (Sterling and Demb, 2004; Sterling, 2003), so it was possible to implement most parts of the model's circuitry on the basis of solid experimental work. On the other hand, in particular the specific connectivity and function of many types of amacrine cells is still unknown. There are however indications that many amacrine cells form very specific functional microcircuits (Marc and Liu, 2000), and recent work in the vertebrate retina has identified potential candidate circuits (Roska et al., 1998; O'Brien et al., 2003). In this study, three different types of amacrine cells were implemented, and their connectivity was based on this earlier experimental work.

This whole approach was chosen as a compromise between a computationally more efficient but less realistic linear filter model (as, for instance used by Teeters et al., 1997 or Kenyon et al., 2004) and a detailed realistic, but computationally expensive description of the processes involved in synaptic transmission (see for example Freed et al., 2003). It is clear that this model, while providing a realistic description of the interplay of excitatory and inhibitory currents in generating a single cell's voltage response, can not reproduce the full range of dynamic effects in the retina. There are however two reasons why this model is expected to reproduce the relevant effects in the conditions investigated in this work. Firstly, only photopic conditions at a constant mean luminance were investigated, and it was assumed that no contrast adaptation takes place (Smirnakis et al., 1997; Brown and Masland, 2001; Zaghloul et al., 2005), which reduces the number of mechanisms that had to be implemented. Secondly, while the model of the inner retina is incomplete, it will be shown in Chapter 5 that it can faithfully reproduce a number of important experimental results. These good fits to experimental data strongly suggest that the circuitry and level of modelling chosen here offers a sufficient

description in the context of the effects and conditions studied here.

4.2 Single Neuron Models

Retinal neurons encode stimuli in two different ways. The majority of neurons respond with gradual changes of the membrane potential. The amount of neurotransmitter released then directly depends on the membrane potential - a depolarisation leads to an increase in release. Some neurons produce action potentials, or *spikes*, when their membrane potential exceeds a certain threshold (Fig. 4.1, insets). A spike is a brief and very strong (about $100mV$) all-or-none depolarisation of the membrane. In the retinal network, spikes are generated by some amacrine cells, which transmit activity over larger distances. The output of the retina to higher brain areas by ganglion cells is also encoded as spikes.

The communication between neurons takes place at synapses, where the release of neurotransmitter from the presynaptic neuron causes a modulation of the membrane potential at the postsynaptic neuron. Typically, a connection between two neurons involves multiple synapses of the same type. More uncommon are electrical synapses, where ions and small molecules can pass directly from one to the next neuron through *gap junction*s. Both types of synapses exist in the retina and were included in the model.

A simple, but accurate approximation of the activity of neurons and synaptic input from N presynaptic neurons is given by the passive membrane equation:

$$C\frac{dV(t)}{dt} = \sum_{i=1}^{N} g_i(t) \cdot (V(t) - E_i) + \frac{V_{rest} - V(t)}{R}, \tag{4.1}$$

where C is the membrane capacitance, $g_i(t)$ the conductances evoked by input i, E_i the reversal potential for the input i, R the membrane resistance and V_{rest} the resting potential. When no synaptic input is present ($g_i(t) = 0$), the membrane potential will return to V_{rest}. The effect of synaptic input depends on the reversal potential E_i for the specific synapse. When it is below the resting potential ($E_i < V(t)$), it hyperpolarises the neuron, or acts *inhibitory*. Conversely, when $E_i > V_{rest}$ the neuron will be depolarised and the synapse acts *excitatory.*

4.3 Receptive Fields

All receptive fields in this model were assumed to be Gaussian-shaped. The center and surround inputs to a neuron were separately calculated according to the Difference of Gaussians equation (Eqn 2.1, Section 2.5). The amplitudes for the center and surround input (A_c and A_s in Eqn. 2.1) were both set to one, and the resulting responses were used to calculate the input conductances $g_i(t)$ for the membrane equation (Eqn. 4.1). $g_i(t)$ was either calculated as a linear or nonlinear dependence on the input (see Methods-Sections of the following Chapters).

The parameters for the width of the Gaussians for different neuron types (σ_c and σ_s in Eqn. 2.1, Section 2.5) were, where possible, estimated from anatomical studies and hence correspond to the width of the dendritic tree of the given neuron. Generally, they were then set to yield a 1:10-ratio between the strongest and weakest inputs (Cohen and Sterling, 1991; Dacey and Petersen, 1992; Grünert et al., 1993).

4.4 Photoreceptors

In photoreceptors, a cascade of molecular events converts light into electrical activity. This process, called *phototransduction*, eventually leads to a hyperpolarisation of the membrane potential. In this study, photoreceptor responses were simulated by means of a state-variable description of this process, which allows the inclusion of important details of the signal transduction process. Most of these mechanisms are well established in the literature (for reviews, see Müller and Kaupp, 1998; McNaughton, 1990; Fain et al., 2001; Burns and Lamb, 2003). The model, which provides a *qualitative* description of the processes, is based on a model description of the photocurrent of macaque cones after brief stimulation by Schnapf et al. (1990).

The main components of the phototransduction cascade are summarised in Figure 4.2. In the outer segment of a photoreceptor, light sensitive rhodopsine molecules are embedded in the cell membrane which are transformed into an active state by photons ($R \rightarrow R*$). The activated rhodopsine catalyses the activation of transducin ($T \rightarrow T*$), which in turn activates phosphodiesterase ($PDE \rightarrow PDE*$). This cascade, depicted in Figure 4.2A, amplifies the signal by a factor of about 1 Million. These steps are expressed by:

$$\tau_{Casc}\frac{dS_i(t)}{dt} = S_{i-1}(t) - S_i(t), \tag{4.2}$$

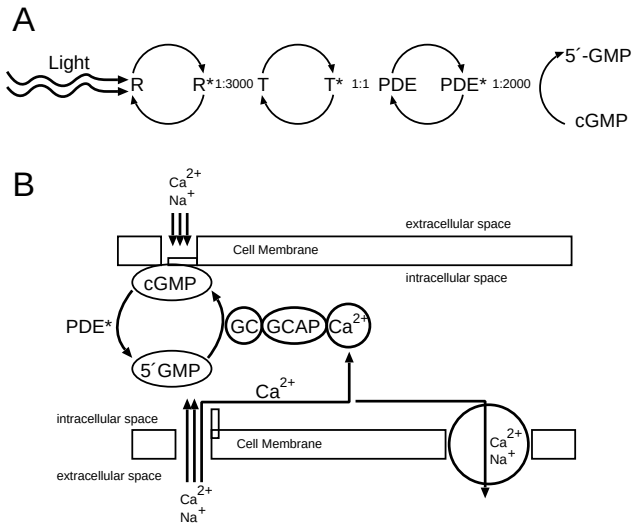

FIGURE 4.2: Schematic illustration of the mechanisms underlying phototransduction (see text).

where $S_i(t)$ denote the activation of the ith cascade and τ_{Casc} the respective time constant. Thus, $S_0(t)$ is the stimulus, and $S_{i=1..n}$ the response of the respective cascade. Eqn. 4.2 implements a cascade of low pass filters.

Activated PDE, which is expressed by the last step of the cascade, triggers a mechanism which generates the electrical response in the photoreceptor (see Figure 4.2B). The second messenger cyclic guanosine monophosphate (cGMP), which keeps the cation channels (Ca^{2+}, Na^{+}, K^{+}) in the cell membrane open, is hydrolysed by PDE. The reduced concentration of cGMP then leads to a closure of cation-channels and thus to a hyperpolarisation of the membrane potential. The concentration of hydrolysed cGMP ($1 - [5'GMP] = [cGMP]$) depends on the concentration of activated PDE ($S_n(t)$) and also on the free calcium ions ($[Ca^{2+}]$). It is calculated by:

$$\frac{d[cGMP](t)}{dt} = \underbrace{-\beta \cdot \left([Ca^{2+}](t) - 1\right)}_{\text{resynthesis}} \underbrace{-S_n(t) \cdot [cGMP](t)}_{\text{stimulus induced}}, \tag{4.3}$$

where β expresses the strength of the re-synthesis reaction of cGMP. The re-synthesis depends on the intracellular concentration of Ca^{2+} via the enzyme guanylylcyclase (GC), which in turn is activated by GCAP (*g*uanylyl-*c*yclase-*a*ctivating-*p*rotein). This reaction can only take place when GCAP does not bind to Ca^{2+} ions, thus only when the intracellular Ca^{2+} concentration is low. The intracellular Ca^{2+} concentration is given by:

$$\frac{d[Ca^{2+}](t)}{dt} = \underbrace{\gamma(1 + c \cdot ([cGMP](t) - 1))}_{\text{influx}} \underbrace{-\alpha \cdot [Ca^{2+}](t)}_{\text{efflux}}. \tag{4.4}$$

The constants α and γ denote the rates of efflux and influx of ions and by $\gamma c([cGMP](t) - 1)$ the light response is transmitted onto the cation concentration and thus to a change of the membrane potential. The constant c expresses the impact of $[cGMP]$ onto the cation concentration.

The constants in Eqns. 4.2, 4.3 and 4.4 were fitted to data from the literature, and their values are provided in the chapters describing the results. Of all ionic species involved in phototransduction, only the intracellular concentration of Ca^{2+} was modelled explicitly, since it mediates the re-synthesis of cGMP. Eqns. 4.3 and 4.4 form a system of first order coupled linear differential equations, which describes the saturation of the response and has a temporal band pass characteristic.

Since the temporal shape of photocurrent and photovoltage V_P differ significantly, voltage dependent currents are likely to shape the photoreceptor responses. As shown experimentally, a hyperpolarisation-activated current has a strong impact on the photovoltage (Bader and Bertrand, 1984; Demontis et al., 1999). It was modelled by:

$$\frac{d[H](t)}{dt} = \left(\frac{1}{e^{(V_P(t) - A_H)S_H} + 1}\right) \cdot (1 - [H](t)) - \delta_H[H](t), \tag{4.5}$$

where A_H defines the activation of the receptor at which the current is half-activated relative to the membrane potential $V_P(t)$, and S_H gives the slope of this activation function. The constants λ_H and δ_{H_τ} define the rates of increase and decay of the ionic concentrations.

Finally, the membrane potential of the photoreceptor is computed by:

$$C_P \frac{dV_P(t)}{dt} = q_P \frac{d[Ca](t)}{dt} + q_I \frac{d[H](t)}{dt}, \tag{4.6}$$

where C_p is the membrane capacity, q_P the unit charge transported by the Ca^{2+} current and q_I the unit charge transported by the I_h current.

Photoreceptors tonically release glutamate, and the depolarised membrane in darkness leads to a high release rate. Light causes a graded hyperpolarisation, which in turn leads to a reduced transmitter release. The synapses transmitting these signals to bipolar and horizontal cells are structurally complex devices that are optimised for maxi-

mal information transfer at low metabolic cost (Haverkamp et al., 2000). Additionally, electrical coupling between cones has been shown to improve the signal to noise ratio in cones (DeVries et al., 2002). This evidence implies fine tuned mechanisms at the synapse, which are carefully adapted to assure a reliable transmission of the light-evoked signals.

Indeed, in the extreme light-sensitive rods nonlinear synapses are essential for the removal of dark noise (van Rossum and Smith, 1998). Given the weak signals they generate under scotopic conditions, their synapses transmit signals in a binary fashion (Baylor et al., 1984). Cones on the other hand receive a sufficient amount of light under photopic conditions to produce signals much larger than the dark noise. As a consequence, the transmitter release of cones is a finely graded signal.

This work considers the retina under photopic conditions, thus a detailed description of the synapse was not required. In the model, the amount of transmitter released was assumed as proportional to the membrane potential. Electrical coupling between cones was omitted as the resulting spatial blur is substantially weaker than blur due to the ocular optics (DeVries et al., 2002).

4.5 Horizontal Cells

Horizontal cells are the interneurons of the outer retina. In the vertebrate retina, two main types were found: the axonless A-type and the B-type with an axon. Physiologically, they can broadly be classified as either as chromaticity or luminosity type. While in lower vertebrates a great variety of horizontal cells has been identified, in mammals only the luminosity type seems to exist (Nelson, 1985; Dacey, 1996).

In the cat, both the A- and B-type are dominated by red-cone input, and probably a weaker contribution from blue cones. In the primate, the H1-type, which has an axon, avoids blue cones whereas the axonless H2-type has a stronger input from blue cones. Neither of these cells in the cat and primate show strong spectral opponency, as found for the chromaticity-types in many cold-blooded vertebrates. In this work, the A-type horizontal cell of the cat (Wässle et al., 1978), that solely contacts cones, and the H1-type of the primate, which is held responsible for shaping the bipolar cell receptive field surround (Dacey et al., 2000; McMahon et al., 2004), were considered. This could be done without loss of generality as no distinction was made between different cone types.

Horizontal cells are interconnected by gap junctions, not by chemical synapses. They form a syncytium of electrically coupled neurons. In such a syncytium, activity evoked

at one spot spreads rapidly to neighboring cells, with a gradual spatial decay (Kaneko, 1971; Nelson, 1977). Thus, the receptive field of a horizontal exceeds the size of the dendritic tree by far. In the model, spatial decay was assumed to be Gaussian, which is a simplification but reduces the description by Bessel functions provided by Nelson (1977) to one parameter. Transmission from cones to horizontal cells was implemented as normal excitatory synapses and connections between horizontal cells were assumed to be undelayed and without a reversal potential.

Horizontal cells in the model antagonise bipolar cells at a reversal potential of chloride ($E_{rev} = -70mV$, see below), but the feedback pathway to cones was omitted because of the uncertainty of its specific physiological and functional properties (Kamermans and Spekreijse, 1999).

4.6 Bipolar Cells

Bipolar cells are responsible for the transmission of light-evoked activity from the outer to the inner retina. About ten morphologically different types exist in mammals (Boycott and Wässle, 1991). Based on their response characteristics, the population can be separated into two broad classes: On-center cells are depolarised by light stimulation, while Off-center cells are hyperpolarised.

Because the light response of photoreceptors is hyperpolarising, which is accompanied by a reduced glutamate release, the synapse to On-bipolar cells is sign-inverting and for Off-bipolar cells sign-conserving. Two different types of glutamate receptors in bipolar cells are responsible for this. Responses of Off-center cells are mediated by ionotopic receptors (iGluRs), which open cation channels (DeVries and Schwartz, 1999). On-center cells express a metabotrophic glutamate receptor (mGluR6), which reverses the response of photoreceptors (Masu et al., 1995). Details about the cascade used by the mGluR6 receptor are still largely unknown. Interestingly, the responses of On- and Off-center bipolar cells are not symmetrical and appear to differ with respect to their contrast sensitivity (Zaghloul et al., 2003).

4.6.1 Receptive Field

The receptive field surround of of bipolar cells is a result of antagonistic action from horizontal cells (Dacey et al., 2000). It is still unclear exactly which mechanism is mediating the inhibition, and at present two possibilities are discussed in the literature.

Both theories are based on the observation that cone photoreceptors have a receptive field surround (Baylor et al., 1971), which suggests that an inhibitory connection from horizontal cells to the cone axon terminal may exist (Satoh et al., 2001). Further support comes from the findings that hyperpolarising current injection into horizontal cells leads to depolarisation of cones (Baylor et al., 1971).

One model assumes that the surround is mediated by GABA. A modulation of the Cl^- -gradient such that the reversal potential E_{rev,Cl^-} is positive to the resting potential in the cone axon would then ensure that GABA has a depolarising response (Vardi et al., 2000). This model is supported by the finding that horizontal cells release GABA (Schwartz, 1982), and that GABA-modulated chloride channels has been found in cones (Kaneko and Tachibana, 1986). Another possibility is that the surround is mediated by non-GABAergic mechanisms which rely on the decreased voltage in the synaptic cleft when horizontal cells hyperpolarise (Kamermans and Spekreijse, 1999). Recent evidence supports the latter model (Verweij et al., 2003; McMahon et al., 2004).

Within the framework of a model based on the membrane equation however, these two possibilities are equivalent, if the nonlinear voltage dependent currents in the cone or bipolar cells are neglected. Thus, in this study, the surround of the bipolar cells was implemented by inverting the horizontal cell response at the resting potential and calculating the postsynaptic current in bipolar cells assuming a reversal potential of a $GABA_C$ synapse (Feigenspan et al., 1993).

In this study, only On-center bipolar cells were considered, which were simulated by the membrane equation (Equation 4.1), without accounting for the specific mechanisms of synaptic transmission. As will be shown, the implementation of Off-center bipolar cells in the same way is problematic, and an alternative will be proposed in Chapter 5.

4.6.2 Temporal Response

About five types of either On- and Off-bipolar cells exist, which differ with regard to their temporal characteristics (Nirenberg and Meister, 1997; Roska et al., 1998; Marc and Liu, 2000; Masland, 2001b). Specifically, two different types emerge, one with more transient and one with more sustained responses. It is yet unclear which mechanisms generate transient responses.

Experimental evidence suggests at least two possibilities: differences between the kinetics of sustained and transient types may be the result of varying channel kinetics (Awatramani and Slaughter, 2000) or inhibition from amacrine cells (Nirenberg and Meister,

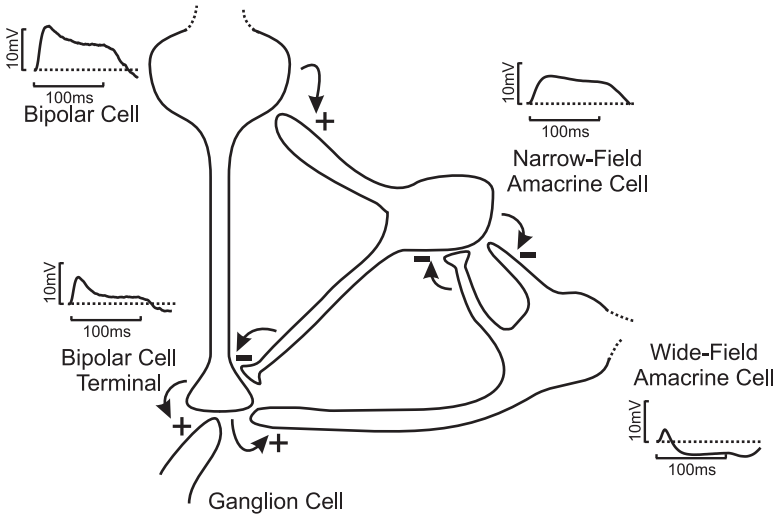

FIGURE 4.3: The nested amacrine circuit. A narrow-field amacrine cell receives input from a bipolar cell and inhibits this bipolar cell at the axon terminal. A wide-field amacrine cell receives excitatory input from the bipolar cell axon terminal. Between both amacrine cell classes reciprocal inhibitory connections exist. The insets show the response of each cell to a full-field flash (100ms).

1997; Roska et al., 1998). The former mechanism relies on different kinetics of desensitisation and has not been included in the model. Further, in Off-center cells it has been shown that the recovery rate of different iGluRs can differ markedly, which has a direct influence on the kinetics of the response (DeVries and Schwartz, 1999; DeVries, 2000). On-center bipolar cells however express only one type of mGluR, so this can not be realised there.

To simulate transient bipolar cell responses, delayed inhibition of the axon terminal by amacrine cells was included in the model. This leads to an attenuation of the late sustained response component. The amacrine cell mediating this inhibition is part of a nested amacrine circuit, which will be covered in detail in the next section. To compensate for the reduced transient component due to inhibition in these cells, their input conductance was increased by a factor of 1.3 compared to the sustained type.

4.7 Amacrine Cells

Ramon y Cajal as one of the first neuroscientists who studied interneurons of the inner retina already noticed their great diversity. He found that these cells usually (but not always) possess no axon, and coined the name amacrine cells, which is derived from the Greek *a makros inos*, which means “without long fibre”. The enormous diversity of

amacrine cells has been confirmed since, MacNeil et al. (1999) more recently identified 28 different types in the rabbit, and even more types may exist (Vaney, 1990). It is generally assumed that the majority of amacrine cells are inhibitory neurons (Dowling and Boycott, 1966), but on the other hand, amacrine cells release a wide range of neurotransmitters as well as other neuroactive substances. Thus, the connectivity between amacrine cells and to bipolar and ganglion cells offers the potential for a great diversity of specialised functional circuits (Marc and Liu, 2000).

For some amacrine cells it was possible to identify a distinct functional role. The AI and AII types for instance are responsible for relaying the signals of the scotopic system from rod bipolar cells to cone bipolar cells (Bloomfield and Dacheux, 2001), and the starburst amacrine cell generates the direction selective response of some ganglion cells (Fried et al., 2002; Euler et al., 2002). The role of most other types however is still elusive, and experimental evidence so far does not even answer the question whether the morphological diversity is accompanied by an equal functional diversity.

Therefore, in the present study it was not attempted to create a comprehensive model of the interactions in the inner retina. Following the ideas of Marc and Liu (2000), experimental evidence was used to establish certain functional microcircuits that may explain specific physiological properties of bipolar and ganglion cells (see Figure 4.3). Three functionally different amacrine cell types were included in the model, which will be described in the following.

4.7.1 GABAergic Interneurons

The first amacrine cell type is an inhibitory GABAergic interneuron with a wide receptive field that receives excitatory input from bipolar cells and inhibits the ganglion cells, as shown experimentally (Flores-Herr et al., 2001). It thereby substantially contributes to the surround of ganglion cells. The morphological correlate of the amacrine cell(s) mediating this inhibition has not yet been identified. A recent study suggests that neuropeptide Y-expressing cells (NPY cells) as a possible candidate as their selective ablation changed the spatial tuning of ganglion cells towards lower spatial frequencies, which was interpreted as a sign of missing surround inhibition (Sinclair et al., 2004). This study further suggests that the extend of the surround may be a consequence of electrical coupling of NPY cells, which have only small dendritic fields - a mechanism very similar to that of lateral inhibition in the outer retina.

4.7.2 Nested Amacrine Circuit

The remaining two amacrine cell types are wide- and narrow-field amacrine cells which form a circuit that truncates the input of transient ganglion cells by inhibiting bipolar cells (Figure 4.3). The rationale is that an amacrine cell provides GABAergic inhibition to bipolar cell axon terminals, which would be very effective because it can *shunt* the activity of the whole bipolar cell. Early studies already indicated that these connections may exist (Dowling, 1968; Burkhardt, 1972), and subsequently Roska et al. (1998) suggested that the early response of this amacrine cell may be suppressed by a second amacrine cell. During stimulation, this allows transient release from the bipolar cell until inhibition increases, hence renders the bipolar cell response more transient.

In this study, this circuit was implemented to study its effect on nonlinearities in transient ganglion cells (Fig. 4.3). Specifically, a narrow-field GABAergic amacrine cell inhibits the axon terminal region of a bipolar cell. A glycinergic wide-field amacrine cell receives excitatory input from transient bipolar cell terminals and also GABAergic inhibitory input from narrow field amacrine cells. The narrow-field cell receives excitatory input from sustained bipolar cells and glycinergic inhibitory input from the nearest wide field amacrine cell. For both cell types, a Gaussian shaped receptive field was assumed.

The insets in Figure 4.3, which show responses to full-field flashes, indicate how the circuit operates. The pathway from the bipolar cell through the narrow-field amacrine cell to the bipolar cell terminal acts as a delayed inhibition which reduces late, tonic response components. The wide-field cell disinhibits the bipolar cell terminal at stimulus onset, thereby further enhancing the early part of the response in the bipolar cell terminal.

4.8 Ganglion Cells

The task of ganglion cells is to encode and transmit visual information, after processing in the retina, to higher visual brain areas. The preceding sections have highlighted that the diversity of processing in the retina gives rise to different parallel channels, and the functional diversity of ganglion cells reflects this and supports the notion of ganglion cells as a set of parallel encoders (Roska and Werblin, 2001). At least a dozen morphological different ganglion cells have been identified in the mammalian retina (Kolb et al., 1981; Masland, 2001a), and probably even more exist in cold-blooded vertebrates (Ammermüller and Kolb, 1995). Attempts to functionally classify the diversity

of the mammalian retina led to the separation into On- and Off-cells and, according to their spatio-temporal response characteristics and anatomy, into the broad X-, Y- and W-classes in cats and PC- MC- and KC-classes in primates (Famiglietti and Kolb, 1976; Boycott and Wässle, 1974; Norton and Casagrande, 1982).

4.8.1 Subtypes in the Cat Retina

X- and Y-cells in the cat retina, the functional equivalents of anatomically identified β- and α-cells (Boycott and Wässle, 1974), received particular attention from experimentalists, probably because these cell types form the main input to the visual part of the thalamus (LGN, see also the following section). The axons of each cell type terminate in different lamiae in the LGN (see below), which support the notion of two separate cell classes. As explained in Section 2.6, the main physiological difference between these two classes is that X-cells show are linear spatial summation and sustained responses, while Y-cells have nonlinear receptive fields and respond with transients (Enroth-Cugell and Robson, 1966). Further, due to their larger dendritic trees, Y-cells have larger receptive fields than X-cells. Finally, Y-cells show a substantially higher contrast gain than X-cells, which has been suggested to be the consequence of receptive field nonlinearities (Shapley and Victor, 1978).

4.8.2 Subtypes in the Primate Retina

In the primate retina early studies suggested that a similar distinction can be made between ganglion cells with narrow and wide receptive fields and sustained and transient responses (Leventhal et al., 1981). These two classes are called parvocellular (PC) and magnocellular (MC) cells, respectively (reviewed in Kaplan and Benardete, 2001). PC-cells have their morphological correlate in midget cells, and MC-cells in parasol cells (Perry et al., 1984). As for X and Y-cells in the cat, their axons project to distinct regions of the LGN (Dreher et al., 1976), and the contrast gain is higher in MC than in PC-cells (Lee et al., 1990).

A closer examination of the properties of PC- and MC-cells however shows that the homology between PC/MC and X/Y-cells is only partially valid. Kaplan and Shapley (1982) reported that of the magnocellular neurons they studied in the LGN, only 25% showed the same degree of nonlinear spatial summation as Y-cells. Benardete et al. (1992) found different forms of contrast gain control in MC, but not in PC-cells, suggesting a homology between different subclasses of MC-cells (MC_X and MC_Y) and cat

X and Y-cells. Also it seems that the degree on nonlinearity is unimodally distributed in primate MC-cells (White et al., 2002), while a bimodal distribution was reported for the cat Y-cells by Hochstein and Shapley (1976a) (but unimodality has been reported for the mouse retina by Carcieri et al., 2003). This evidence suggests that the parvocellular system may have been developed specifically in primates for improved acuity and colour vision. Furthermore, it seems that the classification of X/Y and MC/PC according to the response-linearity could be problematic and in need of a revision (Derrington and Lennie, 1984; Rodieck and Watanabe, 1993; Usrey and Reid, 2000; Carcieri et al., 2003).

4.8.3 Receptive Field Organisation

This study focuses on a linear and a nonlinear subclass of ganglion cells in both the cat and in primates. In the first part (Section 5), X- and Y-cells in the cat retina were investigated as defined by their anatomical and physiological properties. The second part (Sections 7 and 8) focuses on the primate retina, and a linear and nonlinear type was considered that would best fit into the classification as linear PC- and nonlinear MC-cell.

Common for all ganglion cell types in the model is excitatory input from bipolar cells, which originates from sustained bipolar cells for linear ganglion cells and from transient bipolar cells for the nonlinear type. Further, GABAergic inhibitory connections from wide-field amacrine cells contribute to the surround of either type (see above). The relative contribution of the inputs were spatially weightened by Gaussian distributions, with the strongest input into the center of the hypothetical dendritic field of the cell. For all cell types, the inhibitory input extended over 3.3 times the input to the center (Linsenmeier et al., 1982; Lee et al., 1998). The resulting receptive field is then “Difference of Gaussians”-shaped (see Sections 2.5 and 4.3). For each cell type, the size of the center was derived from anatomical data, and it should be noted that the effective physiological receptive field is larger due to optical blurring and the presynaptic circuitry.

4.9 Computer Simulations

The simulation software was developed in the programming language C++. Each cell type was implemented as a C++-class, and cells of the same type were arranged on discrete two-dimensional layers. Each of these (rectangular) layers also contained a

description of the location of each neuron on the hexagonal grid. Stimuli were represented as numerical values on a two-dimensional layer, with a pixel-density of at least five times the density of the photoreceptor layer to prevent spatial sampling errors (this factor was set to ten in those cases where eye movements were included).

The activity of each neuron was calculated according to the Equation 4.1 in double precision. For numerical integration, either the Euler-method (for the results of Chapter 5) or second order Runge Kutta method (for the results of Chapters 6-8) was used with a time-step of $0.1ms$. In all cases, these methods provided the necessary numerical stability.

At each time step, the input for each neuron, as defined by its receptive field, was calculated by convolution with an appropriate filter kernel. Convolution was performed in Fourier-space on the stimulus layer and, as fast 2-dimensional convolution in Fourier-space on discrete hexagonal grids leads to sampling errors, by direct multiplication of the filter kernels with the activity of the respective input layer. To increase the simulation speed, all convolution kernels were computed ahead of the simulation and stored in lookup-tables.

During the simulations, the activity of individual neurons was recorded in files for subsequent analysis[1]. Data analysis was then performed on the saved data sets using either dedicated C++-programs, xmgrace [2] or Matlab [3].

The simulations were performed on a cluster of Intel x86/Linux computers, using code generated by the the GNU C and C++-compilers (GCC)[4]. All Fourier transforms in the simulations where calculated using the the FFTW-Library ("Fastest Fourier Transform in the West")[5], and some of the data analysis relied on the GNU Scientific Library (GSL)[6] for integration and curve fitting.

[1] For data storage, the IGB image format, a generic data format to store 4-dimensional data, was used (`http://www.enel.ucalgary.ca/~vigmond/flounder`).
[2] `http://plasma-gate.weizmann.ac.il/Grace/`
[3] Mathworks, Inc.; `http://www.mathworks.com/`
[4] `http://gcc.gnu.org`
[5] `http://www.fftw.org/`
[6] `http://www.gnu.org/software/gsl/`

Chapter 5

Nonlinearities in X- and Y-Cells of the Cat Retina

As outlined in Section 2.6, spatiotemporal summation in X-cells in the cat and PC-cells in the primate is essentially linear, but cat Y-cells and primate MC-cells both show similar pronounced nonlinearities. These nonlinearities are thought to be a consequence of a contrast gain control mechanism and also lead to the observed frequency-doubling for contrast reversed grating stimuli (see Section 2.6, Fig. 2.6). Especially cat Y-cells are experimentally well characterised, but the origin of these nonlinearities is still unclear.

Early studies suggested that Y-cells receive input from small nonlinear receptive field subunits, because the nonlinear receptive field component is sensitive to higher spatial frequencies than the linear component (Hochstein and Shapley, 1976a; Victor, 1988). Commonly, nonlinear amacrine cells were suspected to form these subunits (Fisher et al., 1975; Hochstein and Shapley, 1976a; Frishman and Linsenmeier, 1982) and several nonlinearly responding amacrine cell types have been identified (Freed et al., 1996). Yet no study has so far clearly identified a particular amacrine cell type that may be responsible for the frequency-doubling nonlinearity in ganglion cells. Evidence exists that nested feedback from narrow- and wide-field amacrine cells onto bipolar cell axon terminals may contribute to transient responses (Roska et al., 1998; Passaglia et al., 2001; Nirenberg and Meister, 1997), which is a common feature of Y- and MC-cells. On the other hand, a study which was based on the pharmacological inactivation of parts of the retinal circuitry provided evidence for a less important role of the amacrine cells in generating nonlinear responses (Demb et al., 2001).

As an alternative hypothesis it has been suggested by Gaudiano (1992b) that nonlinear ganglion cell responses could arise from the response properties of photoreceptors.

PARAMETER	EQN.	DESCRIPTION	VALUE
τ_{Casc}	4.2	Time constant of the 1^{st} low-pass filter (i=1).	10 ms
β	4.3	Strength of cGMP re-synthesis.	$0.6ms^{-1}$
α, γ	4.4	Rates of efflux and influx of ions.	$0.6ms^{-1}$
c	4.4	Impact of $[cGMP]$ on $[Ca^{2+}]$.	$0.42ms^{-1}$
A_H	4.5	Activation of the h-current.	$-0.4V$
S_H	4.5	Slope of the activation function for I_h.	$10V^{-1}$
δ_H	4.5	Increase/decay rates for I_h.	$0.025ms^{-1}$
C_P	4.6	Membrane capacity.	$100pF$
q_P	4.6	Unit charge transported by the Ca^{2+} current.	$1 \cdot 10^{-9}C$
q_I	4.6	Unit charge transported by the I_h current.	$6 \cdot 10^{-9}C$

TABLE 5.1: Constants, variables and parameters of the photoreceptor model. It consists of the following stages: (1) three cascaded low-pass filters (Eqn. 4.2), (2) hydrolisation of the second messenger cGMP (Eqn. 4.3) and Ca^{2+}-dependent resynthesis, (3) in- and outflux of $Ca2+$ (Eqn. 4.4), (4) the hyperpolarisation-activated I_h current (Bader and Bertrand, 1984; Demontis et al., 1999) (Eqn. 4.5) and the calculation of the photovoltage (Eqn. 4.6). Concentrations of second messengers and cations are calculated in dimensionless units relative to the boundaries [0, 1] and the photovoltage is calculated in Volts.

This assumption was derived from a modelling study where a specific push-pull circuitry along with the wide receptive field of Y-cells was found to be the main source of nonlinear behaviour (Gaudiano, 1992a,b,c, 1994; Gaudiano et al., 1998). In the simple model used in these studies it was assumed that all ganglion cell types receive mixed input from the ON- and OFF-bipolar channels, but recent experimental evidence only supports an unidirectional interaction from ON to OFF-cells (Zaghloul et al., 2003). However, because the influence of amacrine cells on nonlinear responses has been shown to be only minor (Demb et al., 2001), it may be possible that the photoreceptor response in combination with convergence properties can influence a ganglion cell's linearity.

In this chapter, the results of a detailed model study of cat X- and Y-cells reinvestigating these ideas will be presented. By quantifying the contributions from the realistically modeled photoreceptor and a nested amacrine circuit to ganglion cell nonlinearities, it will be shown that both have a distinctive influence on the linearity of ganglion cell responses.

5.1 Materials and Methods

5.1.1 Model Retina

The model aims to simulate a patch of the central cat retina under photopic conditions. A general description of the model is provided in Section 4, here the specific parameters of the model will be summarised. Model neurons are arranged on a two-dimensional, regular hexagonal grid representing 4.8 by 4.8 deg visual angle of the area centralis. Distance between two photoreceptors was chosen as $6\mu m$, assuming an estimated photoreceptor density of $25000\ cones/mm^2$ in the area centralis (Steinberg et al., 1973; Wässle and Boycott, 1991). This distance corresponds to a visual angle of approximately 1.7 arcmin (Vakkur and Bishop, 1963). Optical blurring has been included by attributing a Gaussian shaped spatial sensitivity profile to each photoreceptor with a standard deviation of 6 arcmin (Smith and Sterling, 1990). The analysis focuses on On-center cells, because the corresponding literature data allows for quantitative modelling of this cell class, while more unknowns remain for the Off-center cells (see Sections 5.2.10 and 5.3). The relevant model parameters used in this chapter are provided in tabular form in Tables 5.1 and 5.2.

5.1.2 Stimuli

As stimuli, non-coloured luminance modulated full-field flashes and sine-wave gratings were used. Except where noted, 100% Michelson contrast was used. The sine gratings were contrast reversed with a temporal frequency of 4Hz and the spatial frequency was varied between 0.25 and 5.56 cycles per degree (cpd).

5.2 Results

5.2.1 Photoreceptor Responses

The responses and properties of simulated photoreceptors are shown in Figure 5.1. The top row demonstrates the nonlinear characteristics of the responses, which will be one central aspect used to explain the nonlinear behaviour of ganglion cell responses. Parts E and F compares simulated to real photoreceptor characteristics. Additionally, a *linear* photoreceptor was implemented as a low-pass filter, without any saturation or other

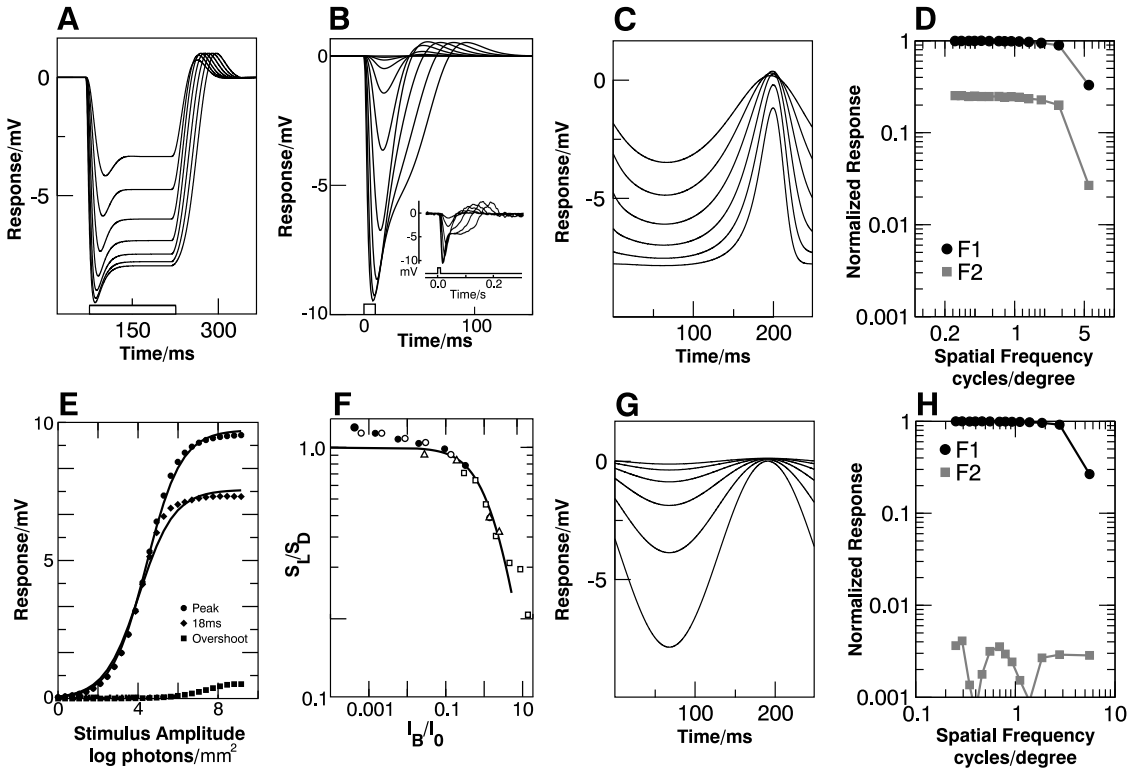

FIGURE 5.1: Characteristics of the simulated photoreceptor (for details, see main text). A-C, Responses to a flash (A, 150ms, B, 10ms, stimulus shown on bottom) and to sinusoidally modulated luminance (C, 4 Hz) at different light intensities ($3.5-7$ log photons$/mm^2$). The inset in B shows data from a macaque cone (modified from Schneeweis and Schnapf, 1999). D, The first (F1) and second harmonic (F2) response component at different spatial frequencies. Stimulus was a sinusoidally modulated sine grating with a mean luminance of 4log photons$/mm^2$ and the 90 deg phase centred above the cell. The drop-off at high spatial frequencies is due to the optical blurring of the stimulus. E, The response amplitude of the photoreceptor as function of the light intensity, measured at the peak (circles), 18ms after stimulus onset (squares) and at the peak of the depolarisation after stimulus offset (diamonds). Stimulus was a 10ms flash. The lines show fits with the Michaelis Menten function $R = R_{max}\frac{I}{I+I_0}$, where R_{max} is the maximal and R the actual response amplitude, I the stimulus intensity and I_0 the stimulus intensity that leads to a half maximal response. F, Flash sensitivity of the simulated photoreceptor (line) and data from four different cones from the macaque (data taken from Schneeweis and Schnapf, 1999). Sensitivity S_L is expressed as the response divided by the flash intensity and is normalised by the dark-adapted sensitivity S_D. The abscissa is in units of the background intensity I_B divided by the background intensity that halves S_D. G, Response of the "linear" photoreceptor model (see text) to sinusoidally modulated luminance (stimulus as in C). H, Spatial frequency tuning curve of the "linear" photoreceptor model (stimulus as in C).

	σ_c/deg	σ_s/deg	$E_{rev,inh}$	τ
Horizontal Cell	0.72 [1]	-	-	20ms
Bipolar Cell	0.12 [2]	0.72 [3]	$-70mV$ [4]	10ms
Transient Bipolar Cell Terminal	0.12 [5]	0.72 [5]	$-70mV$ [6]	10ms
Wide-Field Amacrine Cell	0.50	-	$-70mV$ [7]	10ms
Narrow-Field Amacrine Cell	0.12	0.50	$-70mV$ [8]	10ms
Type-1 Amacrine Cell	0.12	-	-	10ms
X Ganglion Cell	0.18 [9]	0.59 [10]	$-70mV$ [11]	10ms
Y Ganglion Cell	0.50 [9]	1.65 [10]	$-70mV$ [11]	10ms

[1]Nelson (1977),
[2]Nelson (1977),
[3]via Horizontal cells,
[4]GABA C; Feigenspan et al. (1993),
[5]identical to Bipolar Cell,
[6]identical to Bipolar Cell,
[7]GABA A; Flores-Herr et al. (2001),
[8]Glycine; Flores-Herr et al. (2001),
[9]Cohen and Sterling (1991); Freed and Sterling (1988),
[10]Linsenmeier et al. (1982),
[11]GABA A; Flores-Herr et al. (2001)

TABLE 5.2: Parameters used in the simulations. The receptive field center (σ_c) and surround (σ_s) radius is the anatomic extend of the subfield that receives synaptic input. $E_{rev,inh}$ is the reversal potential for inhibitory synaptic transmission and τ the membrane time constant. The nested amacrine circuit (see Section 4.7) includes a glycinergic wide-field and a GABAergic narrow-field amacrine cell. The type-1 amacrine cell provides surround inhibition to ganglion cells.

nonlinearity. Its behaviour is shown in parts G and H. It was used as a tool for circuit dissection by allowing for the differentiation of photoreceptor-induced nonlinearities from other nonlinearities.

Typical responses of the model photoreceptor are shown in Figure 5.1A, B and C. The response to a 10ms or 100ms flash at various intensities (A and B) shows a sharp initial transient hyperpolarisation of the membrane potential which is followed by a sustained response and terminated by a short depolarisation at light offset. This behaviour is very similar to recordings of the photovoltage from the macaque cone photoreceptor (Schneeweis and Schnapf, 1999, see inset in B) apart from a slightly slower repolarisation in the macaque data at high luminance of unknown origin. Similar to the responses to flashes, a sinusoidal modulation of the luminance (C) leads to a pronounced asymmetry between the light and dark phase of the response. As shown experimentally for rods, this harmonic distortion is mainly caused by the I_h current (Demontis et al.,

1999), which acts as a delayed rectifier. This is also reflected in the Fourier analysis of the responses. The strong second harmonic component in D indicates a substantial distortion of the stimulus.

A common property of photoreceptors is a saturation characteristic which follows the Michaelis Menten function, and that of background desensitisation according to Weber's law (McNaughton, 1990; Fain et al., 2001). Both are well reproduced by the model, as shown in Figures 5.1E and F. In close correspondence with experimental data measured by Schnapf et al. (1990) and Schneeweis and Schnapf (1999), the saturation of the response fulfils the Michaelis Menten relation (Fig. 5.1E). The decrease of the flash sensitivity with increasing background illumination is also in accordance with experimental data (Fig. 5.1F; Schneeweis and Schnapf, 1999).

Figures 5.1G and H show, in comparison, the behaviour of the photoreceptor responses after linearisation. A "linear" photoreceptor consists only of a cascade of low-pass filters specified by equation 4.2, hence acts as a simple linear filter. Note that therefore the second harmonic (F2) is virtually non-existent for the linear photoreceptor in H.

5.2.2 Nonlinearities in the Outer Retina

As shown above (Fig. 5.1D-F), the response of a photoreceptor to an equal increment or decrement in luminance is not of the same magnitude, it rather depends on that actual state the photoreceptor is at a given time. This effect is also well visible in the simulated responses of horizontal cells using a stimulus paradigm introduced by Lee et al. (1999).

If the stimulus consists of a temporally sinusoidal modulated luminance change at a low mean luminance, the resulting waveform does well reflect the waveform of the sine wave (Fig. 5.2A, B). The stimulus is now modified by adding a second sinusoidal modulation with a higher temporal frequency and lower amplitude to the slow "carrier wave" (Fig. 5.2C). At low mean luminance, the shape of the input signal is preserved (Fig. 5.2D). At higher luminances however, the sensitivity for the high frequency modulation drops as the light intensity of the slow carrier wave increases (Fig. 5.2E, F). For comparison, the recordings of Dacey and colleagues are shown in Figure 5.2G.

The effect is easy to understand if one considers how the simulated photoreceptor works. Equation 4.2 in Section 4.4 describes the hydrolisation of cGMP during light stimulation. This is mediated by the concentration of activated PDE ($[PDE*]$), which linearly depends on the stimulus intensity. The change of the concentration of $cGMP$ by hydrolisation ($cGMP \rightarrow GMP$) however is described by the multiplicative relation

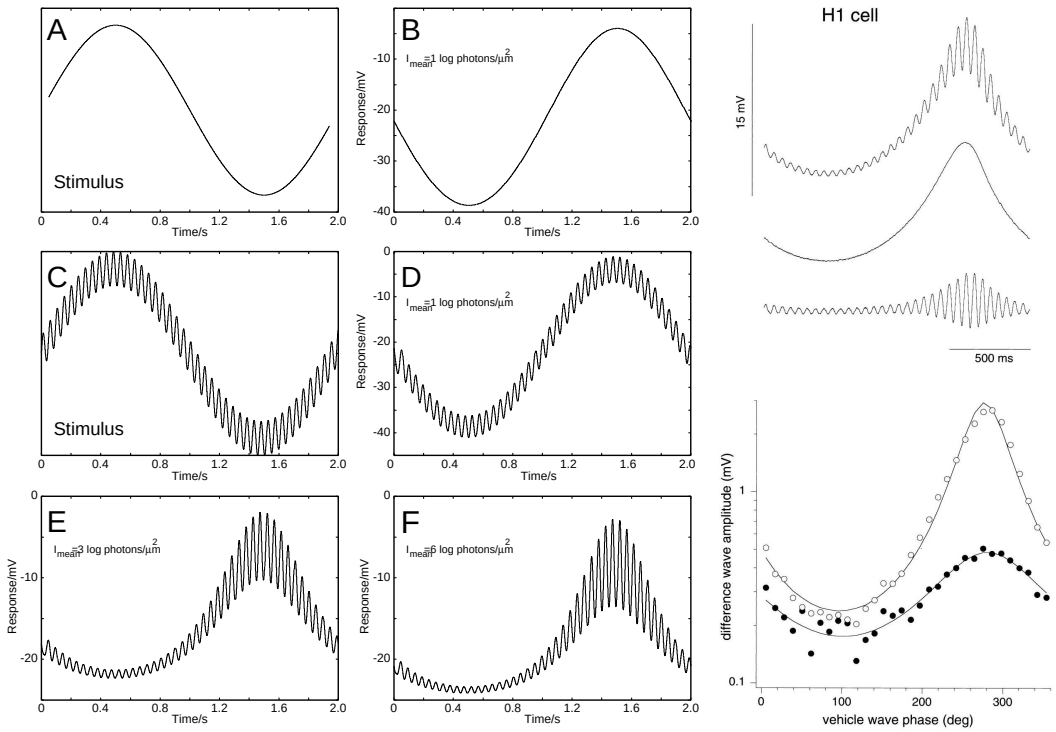

FIGURE 5.2: Sensitivity of horizontal cells depends on the background luminance. A-B, A slow, high contrast sinusoidal luminance modulation (A) leads to a similar modulation in horizontal cells (B). C, The stimulus used in D-F consits of the slow modulation shown in A, onto which a high frequency low contrast sinusoidal modulation was superimposed. D-F, Responses to the stimulus in C at different background luminances (indicated as I_{mean} in the graph). The response to the fast modulation is increasingly compressed for a high background luminance (compare D and F). G, Recordings from a horizontal cell show the same effect. The traces show from top to bottom a response to the stimulus shown in C, a response to the low frequency modulation and the difference between the two traces. The lower graph shows the principal Fourier amplitude of the responses at a background luminance of 1,000 troland (open circles) and 100 troland (filled circles). The figure was taken from Lee et al. (1999).

$[PDE*](t) \cdot [cGMP](t)$, which means that the gain of the photoreceptor depends on the background luminance (the work of Nikonov et al. (2000) supports the existence of a similar mechanism in rods). Thus, when the carrier wave is closer to its minimum, the sensitivity of the receptor to the small modulations is higher than for the peaks. This leads to the observed compression of the response at the peaks.

5.2.3 Responses of all Retinal Cell Types

Traces of simulated activity of the different retinal cell classes for contrast-reversed gratings are shown in Figure 5.3. The diagram shows two sets of responses to either a counterphasing (A) or a sinusoidally modulated (B) grating stimulus at five different

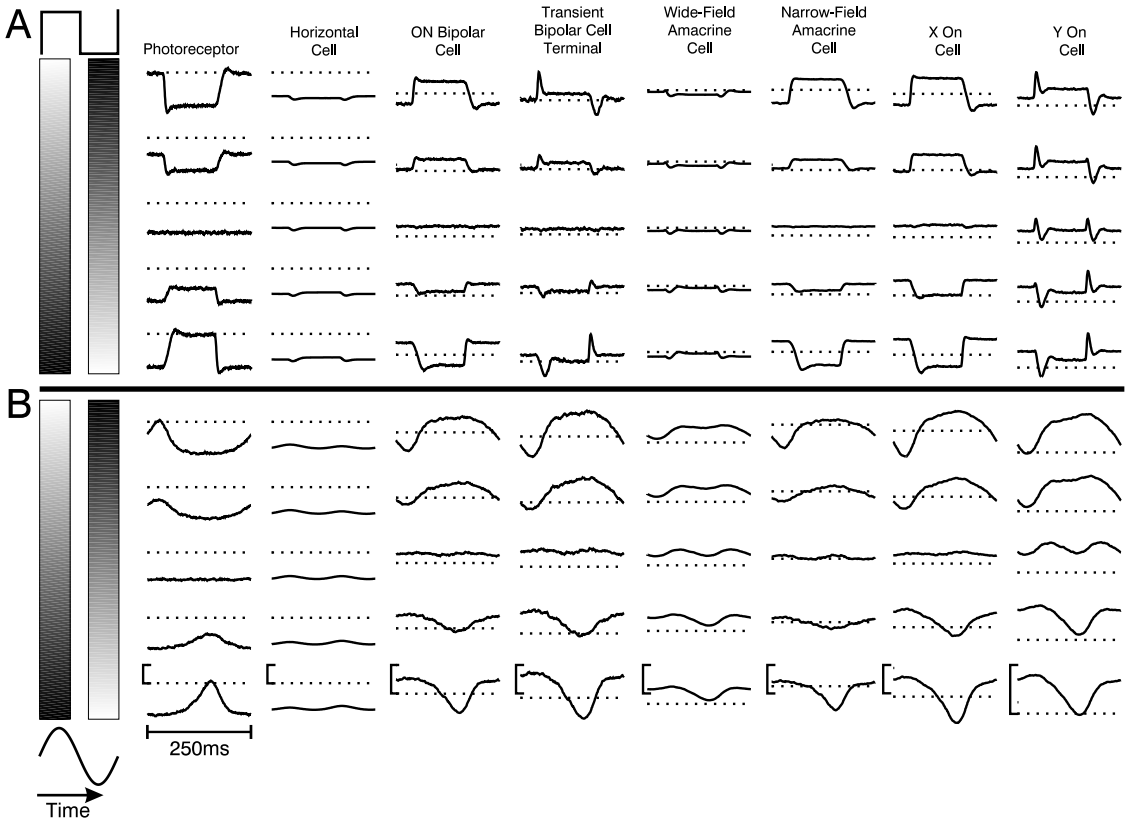

FIGURE 5.3: Responses of the different simulated cell types for stimulation with a contrast-reversed sine grating. The contrast reversal was either counterphasing (A) or had a sinusoidal temporal wave-form (B). The spatial frequency was 0.8 cpd. The vertical position of the responses indicates the location of the cells relative to the spatial stimulus phase, as shown on the left margin. Dotted horizontal lines indicate the dark potential of each cell type. The vertical calibration at the bottom bars indicate $5mV$. In this case, the second harmonic component of the wide-field amacrine cell and Y-cell reaches 70% and 50% of the first harmonic amplitude, respectively.

spatial phases. For cells located at zero-phase of the stimulus (center traces) there is no mean luminance modulation across their receptive fields for every point in time. A photoreceptor placed at exactly this location will indeed not respond (leftmost-center traces in A and B). Significant second harmonic deviations from Null-responses are only visible in the Y-cells and wide field amacrine cells (see especially B).

The top and bottom traces represent the $\pm 90°$-phases of stimulation and accordingly responses are dominated by first harmonics in all but the horizontal cells. In wide-field amacrine cells and Y-cells, a substantial second harmonic distortion is observed.

Horizontal cells behave somewhat differently. At first, there are small, but still clearly visible second harmonic deviations from the Null-response. Such tiny but distinct second harmonic responses are also clearly visible at a closer look in the data of Lankheet

et al. (1992, their Fig. 3). In this simulation, the spatial frequency was 0.8 cpd in order to show the frequency-doubled activity of Y-cells. This leads to the situation that the wide receptive field of the horizontal cell is not optimally stimulated such that the first harmonic modulations are not visible here.

The existing small second harmonics in the horizontal cells suggests that there is a nonlinear influence early in the retinal pathway, while the behaviour of the wide field amacrine cells indicates additional, later occurring nonlinear input to the Y-cells. In general it seems that cells with wide receptive fields tend to show stronger deviations from the Null-response than cells with small receptive fields. As will be shown later, the receptive field size is indeed one important parameter for the linearity of retinal cells.

The transient bipolar cell terminal responds very phasic to a counterphasing grating (A). This is due to the delayed inhibition of the amacrine pathway, which reduces the late, tonic response (see Fig. 4.3 in Section 4.7). Y-cells, which receive input from transient bipolar cell terminals, consequently respond more transiently than X-cells. Another observation is that generally the maintained response to uniform stimuli as well as the mean response to gratings of Y-cells is smaller compared to X-cells. This is due to the inhibition by the amacrine-bipolar cell circuit and is in accordance with experimental findings (Sato et al., 1976; Troy and Robson, 1992).

Figure 5.3 also illustrates that frequency-doubling only occurs in the temporal, but not in the spatial response of Y-cells. A comparison of the vertically aligned traces of Y-cell activity shows that the second harmonic responses are always depolarising and are not separated from the first harmonic responses by a gap of reduced depolarisation. Hence the spatial activity pattern in Y-cells shows, as a result of the nonlinearity that leads to frequency-doubling, also a certain degree of harmonic distortion, but not spatial frequency doubling. This result is consistent with recent electrophysiological data (White et al., 2002) and contradicts the assumption that the frequency-doubling illusion (Kelly, 1966, 1981), where the spatial frequency of a rapidly contrast-reversed grating appears to double, is a direct consequence of the Y-cell nonlinearities that lead to temporal frequency doubling (Maddess and Severt, 1999).

5.2.4 Tuning of Horizontal-, Bipolar- and Amacrine-Cells

Figure 5.4 shows the spatial frequency tuning curves for all modeled cell classes except photoreceptors and ganglion cells. The curves for the first and second harmonics intersect only for horizontal and wide-field amacrine cells, for the other cell classes the first harmonic always dominates. This indicates nonlinear behaviour in these two cell

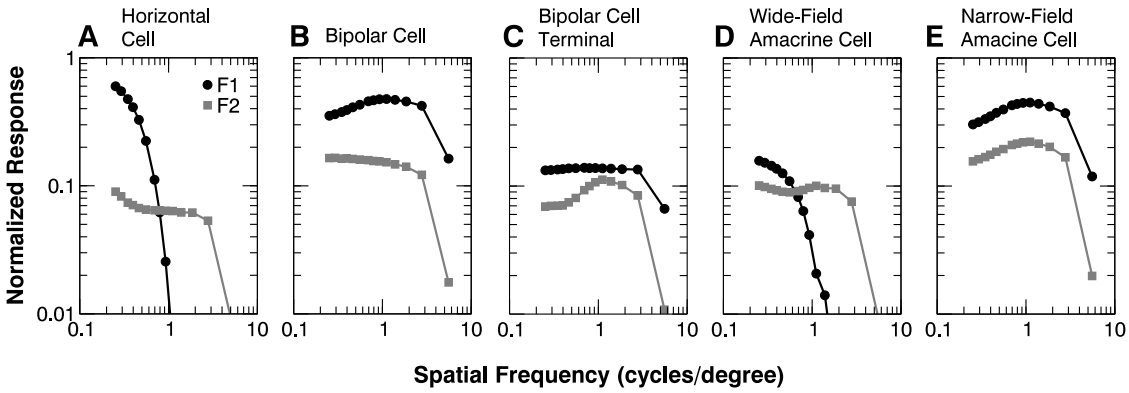

FIGURE 5.4: Amplitude of the first (F1, circles) and second harmonic (F2, squares) response components of horizontal-, bipolar-, and amacrine- cells as function of the spatial frequency. Stimuli were sinusoidally modulated sine wave gratings, and responses were obtained at the $90°$-phase. The curves are scaled to the maximum first harmonic response of the nonlinear photoreceptor in Fig. 5.1D.

types at spatial frequencies where the second harmonic response component exceeds the first harmonic component. It is especially pronounced in the wide-field amacrine cells, where the second harmonic is almost equally strong as the first even for the low spatial frequencies. The bipolar and narrow field amacrine cell, on the other hand, behave largely linear.

For the simulated horizontal cell, the second harmonic response component is weaker than for the photoreceptor. At at low spatial frequencies, it is about a factor of 10 smaller than the first harmonic component, which is in accordance with experimental data by Lankheet et al. (1992). More recent recordings from H1 horizontal cells in the macaque (Lee et al., 1999; Smith et al., 2001) show a similar harmonic distortion that could be reproduced with the photoreceptor model (see Section 5.2.2). On the other hand it was not possible to reproduce these responses using the linearised photoreceptor. This supports the notion that horizontal cell nonlinearities derive from the photoreceptors.

As noted above, both wide-field amacrine and horizontal cells integrate over a large spatial area. As a consequence, they essentially collect and accumulate the asymmetrical parts of the photoreceptor responses leading to second order peaks in their responses. The aspect of spatial integration of nonlinearities will also be central to the discussion of the spectra of Y-cells in the following sections.

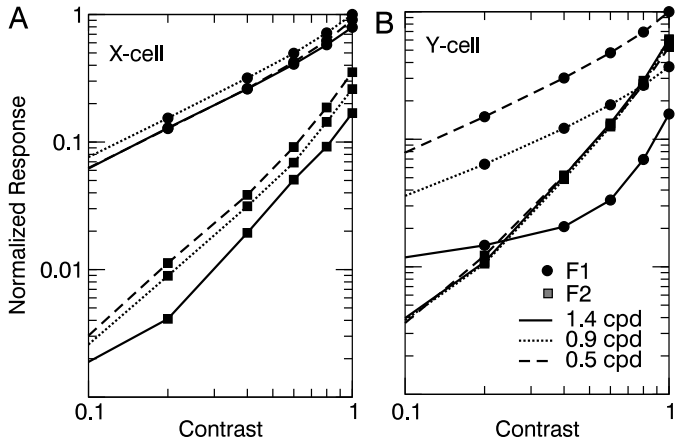

FIGURE 5.5: First (F1, circles) and second harmonic (F2, squares) response amplitudes of an X- (A) and a Y-cell (B) at different contrast levels. Stimuli were sinusoidally contrast reversed sine gratings at different spatial frequencies at maximum modulation (i.e., $90°$-phase). The responses are normalised to the maximum of the strongest first harmonic response of each cell.

5.2.5 Contrast Sensitivity of Ganglion Cells

Figure 5.5 shows the amplitudes of the first and second harmonic response component as function of the contrast for simulated X- and Y-cells. For both cell types, the first harmonic increases monotonically and approximately proportional with contrast. In experimental studies under photopic conditions, the slope of this curve is typically lower (Troy et al., 1993), indicating that additional contrast gain control (Shapley and Victor, 1978) and adaptation mechanisms (Smirnakis et al., 1997) act in the retina which have not been included in the model. The second harmonic responses increase stronger with increasing contrast than the first harmonic and are stronger for Y-cells. For both cell classes, second harmonics are detectable from above about 20% contrast. This is close to the observed experimental threshold for second harmonics in Y-cells which are detectable just above 15% contrast (Hochstein and Shapley, 1976a).

5.2.6 Spatial Frequency Tuning of Ganglion Cells

Figure 5.6 shows spatial frequency response curves (solid lines) obtained from the membrane potential of X- and Y-ganglion cells and from modified siblings of them, which were derived by changing some properties of the circuitry. All these modifications, which are described below, only affect the second harmonic of the responses; the first harmonic curves remain almost entirely unchanged.

First harmonic spatial frequency response curves for completely modeled X- and Y-

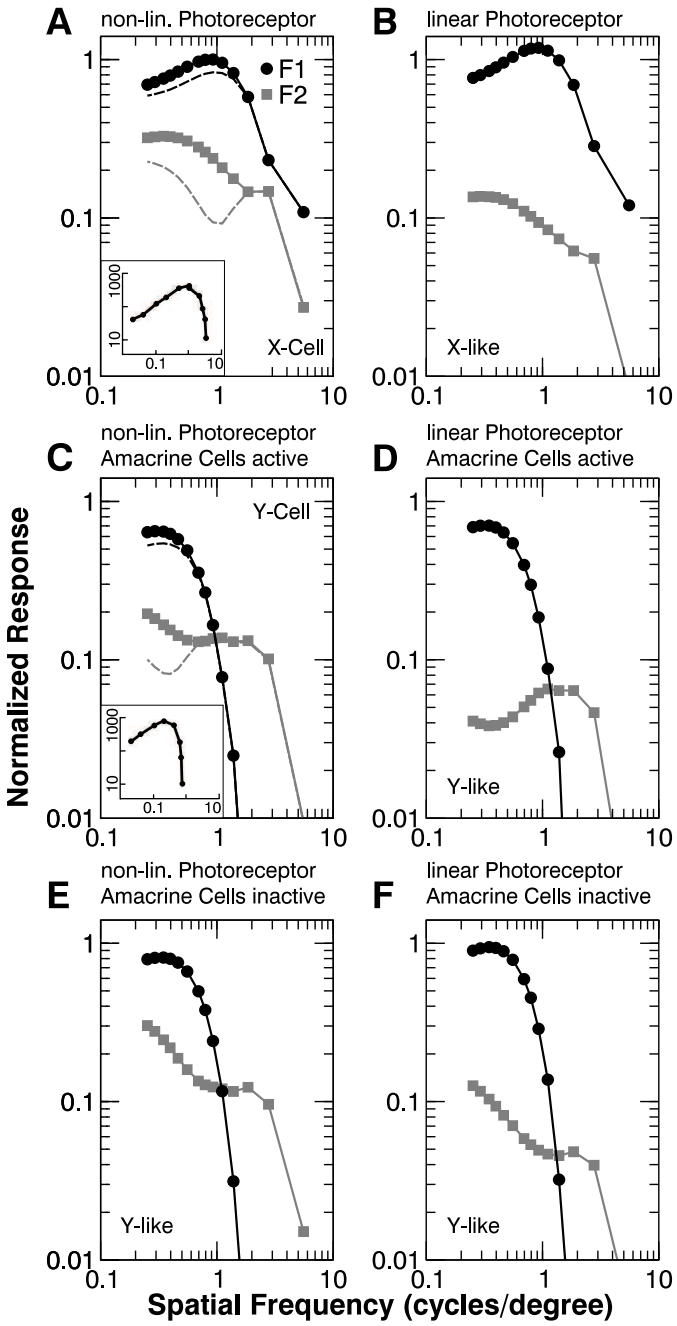

FIGURE 5.6: Amplitude of the first (circles, F1) and second harmonic (squares, F2) response components of an X- (A) and a Y-ganglion cell (C) and modified siblings of them. The insets in A and C show first harmonic responses obtained experimentally (modified from Freeman, 1991, his Fig. 1). The X-like cell (B) is identical to the X-cell apart from having used the "linear" photoreceptor model. Y-like cells (D-F) differ from the Y-cell with respect to the photoreceptor model and their presynaptic circuitry. The curves were obtained at maximum modulation (i.e., 90°-phase) with sinusoidally modulated gratings. All curves are scaled to the maximum first harmonic response of the X-cell (A). The dashed lines in A and C show the spatial frequency tuning curves after rectification of the membrane potential at the resting level. Here a linear relationship between membrane potential and spike rate was assumed.

cells (A, C) closely resemble those reported in the literature (see insets in A,C, Freeman, 1991; Troy et al., 1993, 1999). Second harmonic responses for Y-cells match those reported for membrane potential recordings by Demb et al. (1999), but differ in shape from those studies that recorded action potentials (Enroth-Cugell and Robson, 1966; Hochstein and Shapley, 1976a). This is a consequence of the half-wave rectified characteristic of the impulse rate functions, which cuts away the subthreshold part of the response. It leads to a strong attenuation of the second harmonic component at low spatial frequencies. To illustrate this, dashed lines in A and C show tuning curves after half-wave rectification.

The peak in the first harmonic response component results from the receptive field center size of the cell, which determines its spatial filtering characteristics. The second harmonic response shows that X-cells respond fairly linearly over a wide range of spatial frequencies, while Y-cells behave nonlinear at high spatial frequencies.

To investigate the different factors contributing to the nonlinearity of the simulated cells, in the following some properties of the model have been changed. Figure 5.6B (as well as D, F) was obtained by linearising the photoreceptor responses, while keeping all other parameters identical to those used in A or C, respectively. This removes all nonlinear contributions of the photoreceptor to the network (see Fig. 5.1 for a comparison of the photoreceptor responses). For the X-cell, this essentially leads to a uniform reduction of the second harmonic response components (compare B with A), indicating that nonlinear responses are reduced in a similar way for all spatial frequencies. Y-cells also show a reduced second harmonic response (compare D with C), but the nested amacrine circuit clearly affects the second harmonic response, so no simple downward shift is observed.

Panel E represents a Y-cell modeled without the nested amacrine circuit, which in the following will be called an 'amacrine-lesioned Y-cell'. Within the constraints of our model, such a cell could be imagined as an X-cell with an overly large receptive field. Nevertheless, for high spatial frequencies the second harmonic response dominates over the fundamental response. This supports the notion that the nonlinear behaviour of ganglion cells is related to the receptive field size.

Linearisation of the photoreceptor responses has, for an amacrine-lesioned Y-cell, exactly the same effect as for a normal X-cell: The second harmonic curve is again shifted downwards (compare E with F). Note, that, despite of these linearisations, still a weak second harmonic response exists in both the X- and Y-cell responses. This reflects the harmonic distortion caused by synaptic transmission, if modeled by the passive neural membrane equation (Eqn. 4.1, Section 4.2). It shows that the often neglected boundary

effects of the reversal potentials for ionic currents during synaptic transmission are also a potent source of nonlinearities. Therefore, a full linear response would only possible if none of the ionic reversal potentials introduce saturation points to the voltage response, which otherwise always lead to response distortions.

Comparing the 'amacrine-lesioned Y-cell' with a normal Y cell shows how the nested amacrine circuit affects the second harmonic responses. For the linearised cases (D, F) the effect is most clear. For low spatial frequencies, the nested amacrine circuit attenuates and for high spatial frequencies it enhances the second harmonic component in the responses. A qualitatively similar but weaker effect occurs with a nonlinear photoreceptor (C, E).

Linearisation of the photoreceptors as well as the removal of the nested amacrine circuit both act 'linearising' on the responses. The overall magnitude of this effect, however, is different for both procedures and it seems that linearisation of the photoreceptors has a stronger influence as compared to the removal of the amacrine circuit. This can be assessed by comparing panels (C) with (E), which shows the rather mild influence of amacrine-lesioning as opposed to a comparison of panels (C) with (D) where a much stronger, though non-uniform, drop of the curve of the second harmonic responses is visible.

5.2.7 Dissecting the Nested Amacrine Circuit

In order to better understand the non-uniform influence of the nested amacrine circuit, its subcomponents were selectively shut down. Here, only responses obtained from ganglion cells with linearised photoreceptors were considered in order to concentrate on the nested amacrine circuit as a source for nonlinearities.

The influence of the circuit subcomponents can be understood when comparing the partly active nested amacrine circuit (Fig. 5.7B, C) to the situation when it is fully shut down (A). First, the curves in Figure 5.7 A and B are almost identical showing that wide-field cells alone do not influence linearity.

The situation is different in Figure 5.7C. Here only the narrow-field cell is active. The consequence is a strong general inhibition and a substantial attenuation of the second harmonics at low frequencies. Finally, the combined action of narrow- and wide-field cell leads to the shape of the curves in D. For a detailed explanation of the underlying effects, see the legend of Figure 5.7.

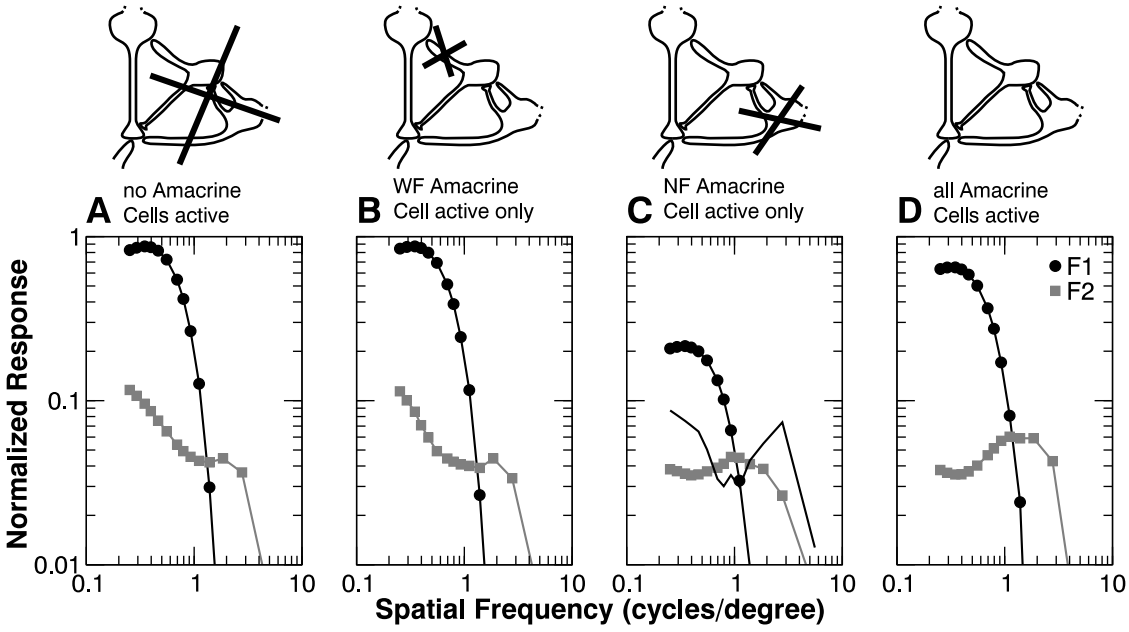

FIGURE 5.7: Amplitude of the first (circles, F1) and second harmonic (squares, F2) response components of a Y-like ganglion cell while in-activating certain subcomponents of the nested amacrine circuit while using the linear photoreceptor model. The same stimulus as in Figure 5.4 has been used and curves are scaled to the maximum first harmonic response of the X-cell in Figure 5.6A. Parts A and D are reproduced from Figure 5.6F and D and show the cases with inactivated and fully active nested amacrine circuit, respectively. In B the excitatory input from the bipolar to the narrow-field cell is shut down while the bipolar cell terminal still provides input to the wide-field amacrine cell. The negative output of the wide-field cell enters the narrow field cell from which a recurrent negative connection exists. As a result the narrow field cell remains mainly hyperpolarised to the reversal potential of the inhibitory currents and does not inhibit the bipolar cell terminal. Therefore, the curves are almost identical to those in A. In C, the wide-field cell is shut down. This leads to a removal of disinhibition at the bipolar cell terminal and thus to a strong reduction of the first harmonic component. In comparison to A and B, it also leads to a specific depression of the second harmonic at low frequencies. This behaviour can be explained by second harmonic content of the membrane potential above the threshold introduced by the reversal potential of the inhibitory currents in the target cell (which is close to the resting potential) at different spatial frequencies. To visualise this influence, the thin curve in C shows the second harmonic of the narrow-field cell obtained after half-wave rectifying the responses at the reversal potential. The second harmonic of the rectified response of the narrow-field cell is weak for medium-high spatial frequencies, because the narrow-field cell is partly hyperpolarised in this range. Thus, the thin curve is essentially a mirror image of the second harmonic curve of the ganglion cell, which reflects the fact that the narrow-field cell indirectly inhibits the ganglion cell.

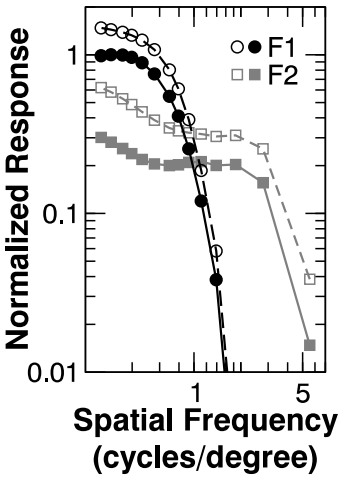

FIGURE 5.8: Spatial frequency tuning curves of a simulated Y-cell (filled symbols) and the same cell, after blocking all inhibitory synapses in the inner retina (open symbols). Circles indicate the first (F1) and squares (F2) the second harmonic response component. Responses are scaled to the maximum of the first harmonic response of the Y-cell. The same stimulus as in Figure 5.4 has been used.

These results partly reproduce experimental results (Frishman and Linsenmeier, 1982). In this study, the GABA antagonist picrotoxin had a similar attenuating effect on the frequency-doubled responses that is observed when removing the GABAergic connections from the narrow-field amacrine cells to the bipolar cell terminals in the model (about 40% decrease at high spatial frequencies, Fig. 5.7A). Further, an enhancement of the first harmonic component of about 50% is observed. The removal of the wide-field cell, which is in the model equivalent to the application of strychnine however had also an attenuating effect on the second harmonic response (20%-40% reduction at high spatial frequencies, Fig. 5.7C). This is in contradiction to Frishman et al., who report a increase of nearly 200%. This might be caused by other direct glycinergic input on Y-cells which have not been included in the model (Freed and Sterling, 1988), or by other effects that are caused by the injection of the antagonists into the cat's bloodstream. The first harmonic component, however, was attenuated to about 50%, which is again in accordance with Frishman's results.

5.2.8 Removing all Inner Retinal Inhibition

In a recent paper, Demb et al. (2001) have applied a mixture of specific GABA- (all types) and glycine-receptor antagonists in order to block all inhibition in the inner retina. They report an increase of the second harmonic response, especially at high contrasts. Accordingly, the authors conclude that this experimental procedure, which

mainly affects the amacrine circuitry, leads to an increased nonlinear behaviour at the ganglion cells. As a consequence, they further conclude that the influence of amacrine cells on the nonlinearity of ganglion cell responses might be less strong than originally suggested.

This experiment was reproduced using the model by shutting down the nested amacrine circuit and also the other remaining amacrine influence from the type-1 amacrine cell, which mediates surround inhibition to ganglion cells (Fig. 5.8). This effectively creates a ganglion cell with a strongly reduced surround with the center size of a Y-cell. Both, the first and second harmonic responses increase by approximately a factor of 1.5. This is in accordance with the findings of Demb et al. It seems, however, that elimination of inner-retinal inhibition has basically a broad enhancing effect which affects all response components in the same way (see the first harmonic curve in Fig. 5.8).

5.2.9 Influence of Photoreceptor Convergence on Ganglion Cell Nonlinearities

In Figure 5.6A, E it was observed that a part of the nonlinear behaviour may result from the receptive field size, because these panels differed only in this respect. Accordingly, in Figure 5.9 the complete cell models and their dissected versions by changing the receptive field size were investigated. This is equivalent to a change of the number of photoreceptors converging on the receptive field center. This particular parameterisation of the receptive field size has been chosen because the receptive field size changes with retinal eccentricity parallel to the photoreceptor density, while the cone to ganglion cell ratio is less variable (Wässle and Boycott, 1991). It allows for a better comparison of X- and Y-cells at different eccentricities. In this way anatomically realistic X- and Y-cells (shaded regions in Fig. 5.9, A, B) were created but also many others which have unrealistic photoreceptor convergence numbers.

As before, the curves for the first harmonic response are almost identical for the different conditions. The strong first harmonic response at a convergence number of around 30 photoreceptors reflects the match between the chosen stimulus frequency (0.93 cpd) and receptive field size. In addition, in all cases the first harmonic dominates for small and the second for large convergence numbers.

The main effect of the different circuit dissection procedures is a shift of the second harmonic curve along the ordinate, while the shape of the curve remains the same. Only for small convergence numbers a slightly different curvature is observed in panels (A,

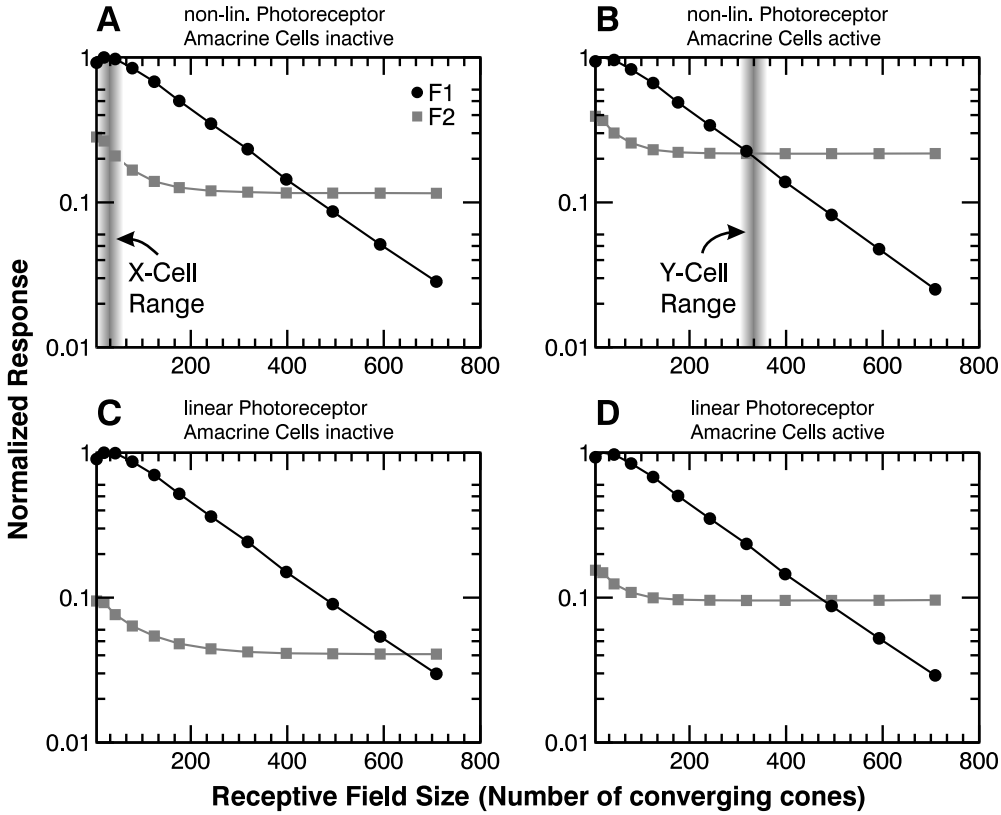

FIGURE 5.9: Normalised amplitudes of the first (circles, F1) and second harmonic (squares, F2) response component of ganglion cells as function of the receptive field size. The receptive field size has been parameterised by the number of cones converging onto the receptive field center via bipolar cells. Stimulus was a sinusoidally modulated sine grating of 0.93 cpd. A, Data for a ganglion cell without modelling the nested amacrine circuit (X-like). The shaded region indicates the convergence number for an X-cell at 1 deg eccentricity. B, Data for a ganglion cell including the nested amacrine circuit (Y-like). The shaded region indicates the convergence number for a Y-cell at 1 deg eccentricity. C, D, Data for ganglion cells as in A and B, respectively, but with a "linear" photoreceptor model.

B) versus (C, D). The highest values for the second harmonic response were obtained with nonlinear photoreceptors and an active amacrine circuit (Fig. 5.9, B), which is a set of simulations containing the realistic Y-cells (shaded). The simulations with nonlinear photoreceptors but an inactive amacrine circuit (A), which contain the realistic X-cells (shaded), produce slightly stronger second harmonics than those with linear photoreceptors and an active amacrine circuit (D). The smallest values for the second harmonic are obtained, quite expectedly, for linear photoreceptors and an inactive nested amacrine circuit (C).

The location of the intersection between both curves is suited as an indicator of the "degree of nonlinearity" of the specific situation. Cells behave nonlinear when the intersection occurs at small convergence numbers and vice versa. In Figure 5.10, the

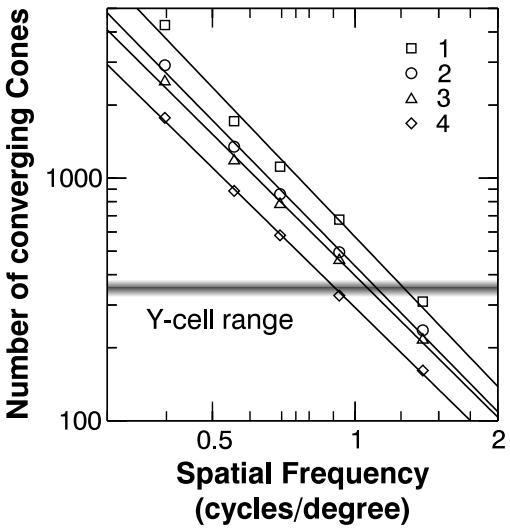

FIGURE 5.10: The degree of nonlinearity as a function of the cone convergence. Shown are those cone convergence numbers where the first and second harmonic response curves in Figure 5.9 intersect as function of the spatial frequency of the stimulus. Stimuli were sinusoidally modulated sine wave gratings and only receptive field sizes in the range of Y-cells (shaded region) and larger were considered, because realistic X-cells are largely linear anyway. For the spatial frequency range from 0.4 to 1.4 cpd, the shapes of the first and second harmonic curves are similar to the curves in Figure 5.9 and it was possible to determine the point of intersection. At lower spatial frequencies, the location of the intersection was at convergence numbers that exceeded the size of the simulated cell grid. The curve labelled (1) belongs to the case where the amacrine cells are inactive and the "linear" photoreceptor has been used. In curve (2) the nested amacrine circuit has been activated. Curve (3) represents the nonlinear photoreceptor without amacrine cells (X-like) and curve (4) the nonlinear receptor and active amacrine cells (Y-like). The shaded region indicates the convergence number for a Y-cell at 1 deg eccentricity. The curves 1-4 in this diagram can be fitted by linear functions $c_i = mx + b_i, i = 1, ..., 4$ (shown as lines) with a slope of $m = -1.97 \pm 0.06$ for all four curves and with $b_1 = 6.349$, $b_2 = 6.073$, $b_3 = 5.981$, $b_4 = 5.679$). A shift parallel to the y-axis in the double-logarithmic domain is equivalent to a multiplication in the linear domain, and the resulting relation $b_4 = -b_1 + b_2 + b_3$ allows for the estimation $b_{4,est} = 5.705 \approx b_4$. This shows that a multiplicative relation provides a reasonable fit for the interaction of different sources of nonlinearities in the model retina.

convergence number at which the intersection occurs is shown as function of the spatial frequency of the stimulus for the different cases.

The top curve (1) represents the most linear case, modeled with the linear photoreceptor and an inactive amacrine circuit. The degree of parallel shift of the other curves relative to the top curve indicates the "degree of nonlinearity" introduced through the different circuit modifications. Curve 2 (linear photoreceptor + active amacrine circuit) is closer to the top curve than curve 3 (nonlinear photoreceptor + inactive amacrine circuit). Thus, across all spatial frequencies the photoreceptor nonlinearity adds more to the nonlinear behaviour of ganglion cells as compared to the nested amacrine circuit. The bottom curve, which belongs to the simulations with nonlinear photoreceptor and active amacrine circuit represent the most nonlinear case.

A mathematical analysis and comparison of the different cases revealed that the photoreceptor- and amacrine-induced nonlinearities interact approximately in a multiplicative fashion (for an explanation, see the legend of Figure 5.10). Thereby, the influence of the amacrine cells is about 25% weaker as compared to the photoreceptor.

5.2.10 Off-Cell Responses

So far, only responses of On-center ganglion cells were considered, because the situation with Off-responses is slightly more complicated and not entirely understood. Figure 5.11 shows on the right hand side real and simulated responses of two different types of Y-Off-cells reported in the literature (brisk and sluggish Off-cell; Cleland and Levick, 1974; Demb et al., 1999). Only the responses are shown where the stimulation is balanced over the receptive field. The convergence pattern which leads to these responses is schematically shown as a sum (Σ) indicating that a spatially relatively broad distribution of bipolar cell inputs leads to the wide receptive fields of Y-cells. The sluggish Off-response is derived from an unmodified retinal network simulation using the mirror-symmetric setup as for the On-responses. For the brisk cell, photoreceptor responses undergo a nonlinear transformation (see gray box, top) at the cone to bipolar cell synapse, as also suggested by Demb et al. (2001):

$$V_{BC,nl} = \frac{3mV}{1 + exp(-(V_{BC,l} - 4mV)/3mV)} - \frac{3mV}{1 + exp(4mV/3mV)}, \qquad (5.1)$$

where $V_{BC,l}$ is the membrane potential after linear synaptic transmission and $V_{BC,nl}$ the resulting membrane potential.

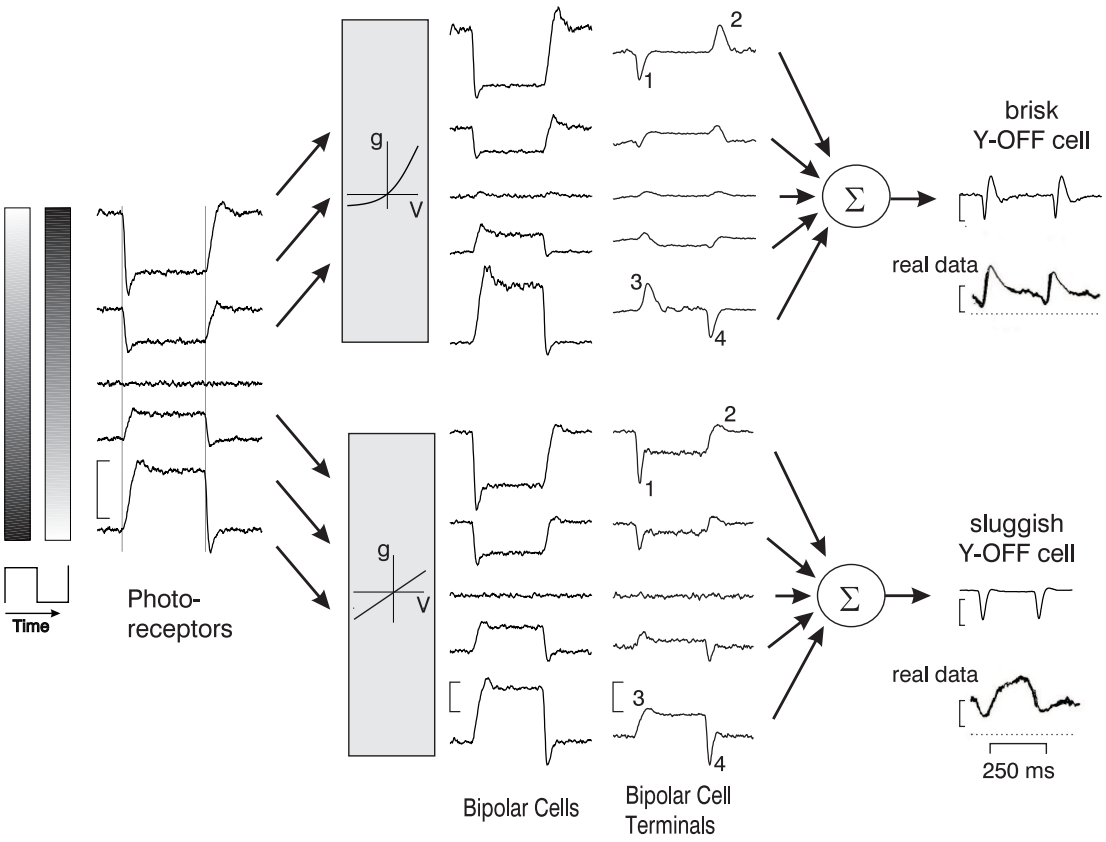

FIGURE 5.11: Responses of two types of Y Off-ganglion cells to a contrast reversed sine wave grating. The figure shows schematically the sequential processing stages for two different Off-channels beginning at the photoreceptors (left) which connect via bipolar cells and their transient axon terminal (middle) to a Y-cell (right). The vertical alignment of the responses shows the cell locations relative to the stimulus phase (middle trace represents the 0 degree phase). The two channels split up at the photoreceptor to bipolar cell synapse with a nonlinear (upper traces) as compared to a linear (lower traces) voltage (V) to conductance (g) transformation (indicated by the curves in the gray boxes). This leads to a different asymmetry at the bipolar cell response. Spatial summation by the ganglion cells (right traces) leads to the brisk (top) or sluggish (bottom) behaviour. Below each ganglion cell response, traces from Demb et al. (1999) are shown. Vertical calibration bars represent 5mV.

In both cases, a frequency-doubled response is visible, which is hyperpolarising for the mirror-symmetric pathway (sluggish), but depolarising for the pathway containing the nonlinear transformation (brisk). The differences between sluggish and brisk cell responses originate from the different slopes of the rising and falling flanks of the photoreceptor responses (see vertical reference lines). For the pathway of the sluggish cell, the photoreceptor responses are directly transferred to the bipolar cells without much change. The transient characteristic of the bipolar cell terminal amplifies the steep hyperpolarising flanks more than the shallow depolarising flanks leading to pronounced hyperpolarising peaks and rather small depolarising peaks at the terminal (compare

bottom: 1,2 and 3,4). Linear summation of these responses leads to a monophasic hyperpolarisation of the sluggish cell at each contrast reversal.

For the brisk cell, the rectifying nonlinearity (Eqn 5.1, see upper gray box in Fig. 5.11) leads to a balancing effect for the peak heights of hyper- and depolarising peaks in the bipolar cells, which have now similar amplitudes. The transfer characteristic of the bipolar cell terminal amplifies these transients in the same way. However, due to the steeper slope of the hyperpolarising flanks, the hyperpolarising peaks occur earlier than the depolarising peaks. This produces a pronounced temporal asymmetry of, especially, the top and bottom traces of the bipolar cell terminal responses in the brisk pathway (compare top: 1,2 and 3,4). Summation of these responses leads to a depolarisation of the brisk cell after a very brief transient hyperpolarisation at each contrast reversal.

A comparison to real data shows that the model captures the main response characteristics of sluggish and brisk cells. However the model does not fully reproduce the slow sustained character of the frequency-doubled hyperpolarisations. A physiological correlate of the heuristically introduced nonlinear transmission might be based on the kinetics of the kainate receptor that mediates synaptic transmission to Off-bipolar cells (DeVries and Schwartz, 1999). Similar to the photoreceptor kinetics, kainate receptors produce a strong initial (transient) current which is followed by a weaker tonic current. In the tonic phase of the current, the receptors are desensitised and a further transmitter release again leads to a strong transient current (Wilding and Huettner, 1997). The net effect is that a depolarisation of the photoreceptor at light offset causes a stronger transient in Off bipolar cells than for a hyperpolarisation. This reverses the asymmetry in the photoreceptor, which leads to the frequency-doubled depolarisations in Off ganglion cells.

5.3 Summary and Discussion

In this chapter, the influence of different properties of the retinal circuitry on the nonlinearity of ganglion cell responses was compared by using the model retina. Two possible sources of nonlinear ganglion cell behaviour were investigated: (i) photoreceptor nonlinearities and (ii) influences from amacrine cells. Modifications of the original model demonstrated that both had a distinct influence on the linearity of ganglion cell responses, and that it is the spatial integration of these nonlinear signals that leads to the observed Y-cell nonlinearities. The large receptive fields of Y-cells integrate more of the nonlinear photoreceptor responses as compared to the smaller X-cells, hence their

nonlinear responses. The nested amacrine circuit on the other hand contributes less strongly and in a less uniform way.

5.3.1 Restrictions of the Model

The model introduced in this study was set up to capture the most important aspects of retinal anatomy and physiology, focusing on cat data. Other data was used where this was not available. In the following the potentially relevant omissions of the model will be discussed.

The model of the photoreceptor is an extension of a description of the photocurrent as given by Schnapf et al. (1990). Its characteristics substantially contribute to the nonlinear responses of ganglion cells, thus the mathematical description and choice of parameters is crucial for the model behaviour. The simplifications made here can be summarised as:

1. The temporal properties of the amplification cascade regarding the activation and recovery of the involved messengers have been ignored as well as pigment bleaching (for an analysis, see Laitko and Hofmann, 1998).

2. All interactions between messengers have been temporally and spatially linearised in order to allow for an easier mathematical treatment.

3. Only one nonlinear current-voltage relation (the I_h-current, Demontis et al., 1999) has been implemented that is crucial for the shape of the initial transient of the response (extended analysis of ionic conductances in photoreceptors provide Yagi et al., 1997; Demontis et al., 1999).

However, as the model reproduces the most important characteristics of vertebrate photoreceptors (Fig. 5.1), it appears justified to consider it as sufficient in the context of the addressed questions.

The other cell classes are modeled in a conventional way by using the membrane equation and adding important cell specific characteristics to it.

The horizontal cell network has been simplified in several ways: the spatial spread of the activity is Gaussian-shaped, which is a sufficiently adequate estimate for horizontal cell receptive fields (Lankheet et al., 1990). Furthermore, the feedback pathway to cones has been ignored. This approximation was used because the mechanisms that generate the

horizontal cell receptive field are not yet understood. The main effect of this network is a subtractive adaptation mechanism relying on the mean light intensity by acting as antagonists in the bipolar cell receptive field.

With respect to their intrinsic properties, bipolar cells were modeled as a uniform class. Specific intrinsic mechanisms could potentially add to the nonlinear behaviour of the circuitry (as discussed in Section 4.6). The results however are generally in good agreement with the experimental data, which indicates a less important role of these intrinsic mechanisms. On the other hand, the model is not able to capture the increased contrast gain of Y-cells for reduced contrast found experimentally (Figure 5.5). This indicates that additional mechanisms must be at work, and it was recently suggested by Snellman and Nawy (2004) that in On-bipolar cells of the mouse retina cGMP may selectively enhance weak responses of photoreceptors. This would be a possible mechanism to increase the weak contrast gain of cone photoreceptors and thus may lead to an increased gain of ganglion cells. On the other hand, Figure 5.5 shows that decline of the amplitude of the second harmonic response is in accordance with experimental data, which again suggests that the influence of this mechanism on nonlinearities may be weak.

The role of the different amacrine cells is currently probably the most confusing aspect of retinal function given their great diversity. Thus it can not be excluded that additional subtypes may contribute to ganglion cell nonlinearities. Little is known about their connectivity and function. Therefore, the model omits many of the existing subtypes (Strettoi and Masland, 1996; Kolb, 1997; Masland, 2001a) and instead, two known amacrine circuits were included: Type-1 amacrine cells (Flores-Herr et al., 2001) and the nested amacrine circuit (Nirenberg and Meister, 1997; Roska et al., 1998; Passaglia et al., 2001). Again, the good agreement with experimental data suggests that these are the main components which contribute to nonlinear behaviour of ganglion cells. The detailed analysis of the amacrine circuit (Figure 5.7) also provides predictions for future experiments.

X- and Y-ganglion cells have been treated as a uniform class regarding their physiological properties. This rules out any internal property that promotes nonlinear responses in Y-cells (Robinson and Chalupa, 1997; Cohen, 1998). The synaptic transmission from bipolar to ganglion cells normally involves AMPA and NMDA type receptors (Matsui et al., 1998; Cohen, 1998, 2000), of which only the AMPA type has been modeled. The NMDA receptor introduces a rectification for membrane potentials below $-40mV$, which could reduce the asymmetry and linearise the final responses of ganglion cells. This effect was not investigated, and results by Cohen and Miller (1994) indicate a less important role of NMDA receptor mediated transmission in the light response of

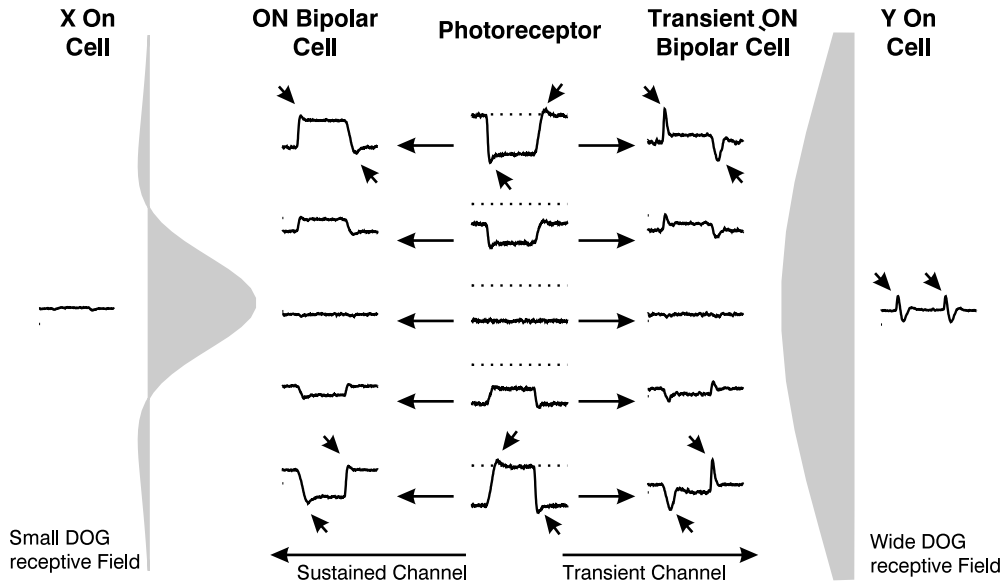

FIGURE 5.12: Schematic diagram illustrating the origin of Null-responses in X-cells (left) and frequency-doubled responses in Y-cells (right). Traces are vertically aligned relative to a contrast reversed sinusoidal grating (middle trace represents the 0-deg phase). The X-cell receives most of its input from the central photoreceptor and faithfully reproduces the Null-response. For every given retinal eccentricity, Y-cells receive a higher number of photoreceptor inputs than X-cells, which is equivalent to a larger receptive field. Photoreceptor responses, however, are asymmetrical with respect to light on- and offset (marked by arrows), and this asymmetry is enhanced further by the nested amacrine circuit that shapes the responses of the transient bipolar cell terminal. Summing these responses across a Y-cell's receptive field results in depolarisations at each contrast reversal.

primate ganglion cells.

5.3.2 Nonlinearities in Ganglion Cell Responses

Unavoidably, all neuronal responses, graded or spiking, are nonlinear. Even without additional nonlinear influences, the reversal potentials of ionic currents lead to boundary effects, which lead to harmonic distortion of signals arriving via synaptic transmission. As a consequence, the model cell spectra beyond the photoreceptors still contain higher harmonics even in the case of an inactive nested amacrine circuit and a linearised photoreceptor. Nonlinearities caused by synaptic transmission can thus be regarded as the first and pervasive source of nonlinear behaviour in the retinal network.

In the realistically modeled photoreceptors the mechanisms of phototransduction, combined with a nonlinear voltage-gated current create the input nonlinearity of the system. The resulting nonlinear effects manifest themselves in the responses of the other cell

classes due to the specific spatial convergence characteristic. For ganglion cells, this is illustrated in Figure 5.12.

Gaudiano already suggested that receptive field size could play a role in the generation of retinal nonlinearities (Gaudiano, 1992b,c, 1994; Gaudiano et al., 1998). Like the present model, the input nonlinearity of his model is caused by the compressive behaviour of the photoreceptor. These signals are then assumed converge onto ganglion cells such, that each input is determined by one On-center and one Off-center bipolar cell (*push-pull* connectivity). The saturation points of these inputs differ, which leads to a nonlinear input-output relation. Both the center and surround of a ganglion cell are mediated by pairs of bipolar cells. This connectivity leads to responses in ganglion cells. which are primarily signalling local contrast, as suggested byTroy and Enroth-Cugell (1993). Gaudiano's model is able to reproduce important features of X- and Y-cells, although the only difference between the two types are the saturation points and the receptive field size.

The model is attractive because few parameters account for the differences of two apparently fundamentally different ganglion cell classes. On the other hand, as presented Gaudiano's model contradicts basic anatomical and physiological findings. So far, only an unidirectional interaction from On to Off-bipolar cells has been identified (Zaghloul et al., 2003). More problematic is the assumption that saturation points for bipolar cell inputs differ for X- and Y-cells, which implies a differing physiology. On the other hand, the model presented here makes use of similar mechanisms by assuming amacrine cells as inhibitory interneurons, which effectively reverse the signal from On- cells into an Off-signal. Although the analogy of both model was not further considered, a reinvestigation of Gaudiano's model with more realistic assumptions about retinal neurons may thus be interesting. It has for instance been demonstrated that a balanced push-pull connectivity could linearise the responses of neurons in the visual cortex (Pollen and Ronner, 1982; Ferster, 1988; Wörgötter et al., 1998).

The third source for nonlinearities arises from the intra-retinal connectivity, most prominently through amacrine circuitry. First experimental indications that amacrine cells in general have a *weaker* effect on retinal nonlinearities as compared to other sources came from the results of Demb et al. (see Figure 4 in Demb et al. (2001) and Figure 5.8 here). The present model confirms their observations and allows augmenting their conclusions by the observation that the nested amacrine circuit enhances the nonlinearity of Y-cells for high- but reduces it for low spatial frequencies. However, other sources of nonlinearities might exist that have not been considered.

One possible source could be depression at excitatory synapses (Thomson and Deuchars,

1994; Zucker and Regehr, 2002), which could also lead to a harmonic distortion of the signal. The data of Demb et al. (1999, Figure 2 there) shows a distinctive difference of the behaviour of the first and second harmonics of ganglion cell responses in response to drifting versus counterphasing gratings: only during contrast reversal a strong second harmonic exists. This behaviour could be reproduced with the model, because for moving gratings the temporal properties of the amacrine circuit perfectly compensate the asymmetries in the photoreceptor responses. If a strong depressing synapse from the bipolar to the ganglion cell would exist, a strong distortion of the signal would be expected in both cases. This suggests that synaptic depression has only a weak effect on the nonlinearity of ganglion cells responses.

Another possible source of nonlinearities is that different types of bipolar cells exist, which selectively provide linear or nonlinear input to X- and Y-cells (Wu et al., 2000). In the cat retina, On-X-cells receive half of their excitatory input from transient b1 bipolar cells and the rest from the sustained types b2/b3 (Cohen and Sterling, 1992; Freed, 2000a). On-Y cells receive excitatory input almost entirely from the b1-type (Freed and Sterling, 1988). The source of transient behaviour of b1-bipolars is still unknown. The model suggests that it could arise *retrogradely* through the properties of the nested amacrine circuit, which generates transient responses in bipolar cells. Thus, one could interpret those model bipolar cells which connect to Y-cells as the b1-type while those which connect to X-cell represent the group of b2,b3-bipolars.

Chapter 6

The Influence of Fixational Eye Movements on Retinal Neural Responses

During fixation, involuntary ocular micromovements constantly lead to retinal image motion (Ratliff and Riggs, 1950; Ditchburn and Ginsborg, 1953). Fixational eye movements comprise three main components: a small and fast tremor (ocular microtremor), larger and slow drift movements and small saccades (microsaccades). Their role in visual perception has been studied extensively in psychophysical experiments involving stabilisation of the retinal image. Yet, the experimental data is often contradictory, which mainly is a consequence of the technical difficulties that arise with retinally stabilised images (reviewed by Steinman and Levinson, 1990 and Steinman, 2003). An exchange of letters between R.W. Ditchburn and E. Kowler and R.M. Steinman on the relevance of microsaccades in the journal *Vision Research* nicely illustrates this debate (Ditchburn, 1980; Kowler and Steinman, 1980).

Experimental results clearly show that retinally stabilised images fade away after some time, which can be attributed to neuronal adaptation processes (Ditchburn and Ginsborg, 1953; Riggs et al., 1953). In addition, 80 years ago theoretical considerations led Averill and Weymouth (1925) to suggest that eye movements may the basis for visual acuity beyond the theoretical Nyquist limit of the visual system (hyperacuity). These ideas were later further elaborated by Marshall and Talbot (1942), but so far no conclusive evidence exists to support or reject this hypothesis. Further, Clowes (1962) demonstrated that detection of hue differences at equal luminance was improved for the free viewing eye, but impaired for a retinally stabilised stimulus, where the larger mi-

crosaccades were removed. More recent data by Rucci and Desbordes (2003) provides convincing evidence that fixational eye movements can have a beneficial effect on visual perception. Their paper reports that discrimination of briefly presented stimuli is impaired under retinally stabilised conditions.

On the other end of the experimental spectrum, several studies demonstrate convincingly that fixational eye movements influence the responses of visual neurons in the retina (Greschner et al., 2002; Olveczky et al., 2003) and in the visual cortex (Gur et al., 1997; Bair and O'Keefe, 1998; Martinez-Conde et al., 2000; Hennig et al., 2002). These studies generally suggest that fixational eye movements have a beneficial role for visual perception. However, there still is a considerable gap between these electrophysiological findings and related psychophysical studies.

On a neural level, several factors could contribute to the response characteristics in the presence of fixational eye movements. Response amplitudes may for instance be enhanced if the resulting stimulus velocity matches the temporal tuning of individual neurons. Further, spatiotemporal nonlinearities may yield different response patterns under stabilised and natural viewing conditions. These ideas will be investigated in the following sections and were inspired by the finding that responses neurons in the primary visual cortex to weak stimuli can be enhanced by small eye movements (Hennig et al., 2002; K. Funke, N.J. Kerscher and F. Wörgötter, unpublished data). As will be shown, this effect can only be explained by assuming nonlinear processing.

This and the following two chapters will provide a detailed investigation of the influence of fixational eye movements on ganglion cell responses. These sections will focus on the primate retina, in particular on MC-cell nonlinearities, and it will be asked how they could affect visual perception. While the following chapters will consider two psychophysical, perceptually relevant paradigms (hyperacuity and apparent motion), here first the general influence of fixational eye movements on the responses of retinal neurons will be investigated.

6.1 Materials and Methods

6.1.1 Model Retina

In this and the following chapters, the model was used to simulate the parvocellular and magnocellular On-center channel in the primate retina under photopic conditions. As

PARAMETER	EQN.	DESCRIPTION	VALUE
$\tau_{Casc,i}$	4.2	Low-pass filter Time constants of (i=1-3).	$2ms$
β	4.3	Strength of cGMP re-synthesis.	$1ms^{-1}$
α, γ	4.4	Rates of efflux and influx of ions.	$0.4ms^{-1}$
c	4.4	Impact of $[cGMP]$ on $[Ca^{2+}]$.	$0.1ms^{-1}$
A_H	4.5	Activation of the h-current.	$-0.4V$
S_H	4.5	Slope of the activation function for I_h.	$10V^{-1}$
δ_H	4.5	Increase/decay rates for I_h.	$0.025ms^{-1}$
C_P	4.6	Membrane capacity.	$100pF$
q_P	4.6	Unit charge transported by the Ca^{2+} current.	$1 \cdot 10^{-9}C$
q_I	4.6	Unit charge transported by the I_h current.	$6 \cdot 10^{-9}C$

TABLE 6.1: Constants, variables and parameters of the primate photoreceptor model.

in the previous chapter, the model is based on the description given in Section 4, and in the following only the relevant details will be provided.

The activity of PC- and MC-cells was calculated for in the central 1.8 deg of the fovea, with an inter-cone separation of $0.55'$ (Curcio et al., 1987). The bipolar cell density was assumed equal to the photoreceptor density (Wässle and Boycott, 1991). PC-cells receive input from a single bipolar cell, and their density of PC-cells was set equal to the photoreceptor density (Wässle and Boycott, 1991). Further, a ratio of the density of MC-cells:PC-cells of 1:9 was assumed (Silveira and Perry, 1991).

The following set of parameters was used for all neurons: the membrane capacitance was set to $C = 150pF$, the membrane resistance to $R = 100M\Omega$ and the resting potential to $V_{rest} = -60mV$. For the excitatory inputs, mediated by the neurotransmitter glutamate, the reversal potential was set to $E_{rev,exc} = 0mV$. The reversal potential for inhibitory inputs mediated by GABA was set to $E_{rev,inh,GABA} = -70mV$ and by glycine $E_{rev,inh,GLY} = -80mV$. Input conductances are either linear functions of the presynaptic potential, which is expressed as $g_i(t) = V_{pre} \cdot 0.3nS/V$, or, in transient bipolar cells, it was set to $g_{i,T}(t) = V_{pre} \cdot 0.4nS/V$. Additionally, the glutamate release for bipolar and amacrine cells was truncated at $-3mV$ below resting potential, which yields an expression for the input conductance:

$$g_i(t) = \frac{V_{pre} \cdot 0.3nS/V}{1 + exp(-\frac{V_{pre}-3mV}{10mV})} \tag{6.1}$$

The parameters of photoreceptor model were slightly modified from the model for the cat retina in the previous chapter. They are summarised in Table 6.1. Additionally, initial low-pass filtering in Equation 4.2 was done as a three-step cascade, as this could bet-

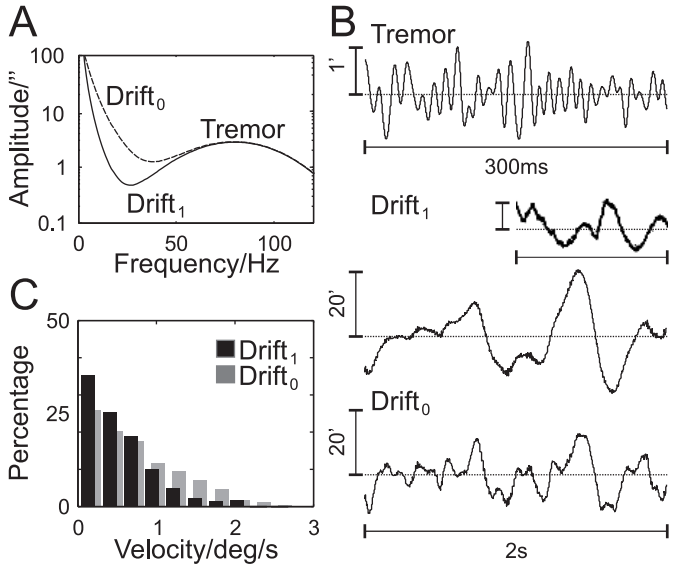

FIGURE 6.1: Simulated fixational eye movements. A, Power spectra of the simulated eye movements. Two different distributions were used. B, Example traces of simulated eye movements for the different conditions. The inset shows 2s of show drift movements as recorded by Murakami (2004) (vertical calibration bar indicates 20'). C, Velocity distributions of the two types of slow drift movement. The velocities were obtained after resampling the eye movement traces at 1kHz, to allow for comparison with data obtained from modern eye tracking systems.

ter reproduce the sustained activity after a very strong, brief stimulation (see Fig. 5.1B, inset).

6.1.2 Optical Blurring

Optical blurring was simulated by convolving the stimulus with the PSF given by Westheimer (1986) for the human fovea:

$$PSF(\rho) = 0.933e^{-2.59\rho^{1.38}} + 0.047e^{-2.34\rho^{1.74}} \tag{6.2}$$

where ρ denotes the visual angle in minutes of arc (arcmin) (see also Fig. 2.1B).

6.1.3 Eye Movements

Fixational eye movements include slow drift movements and the ocular microtremor. Microsaccades were not included since they are rare during normal vision and can be suppressed voluntarily without training (Steinman et al., 1967).

Simulated fixational eye movements were generated by a convolution of Fourier-transformed white noise with a characteristic power spectrum. The power spectrum of the microtremor was modeled as Gaussian normal distribution with a peak at 80 Hz and standard deviation of 25 Hz (Bolger et al., 1999; Spauschus et al., 1999). For the ocular drift, the spectral power has been shown to decline according to a power law (Eizenman et al., 1985). Thus, drift movements were generated from a white noise power spectrum using the following expression:

$$P(f) = \frac{A}{(1 + T_1 f)^2 \cdot (1 + T_2)^2} \tag{6.3}$$

where $f[Hz]$ is the frequency. The value $T_2 = 0.1s$ was kept constant for all following simulations shown in this and the following chapter, A and T_1 were variable. Two different types of ocular drift were generated for the simulations for comparison how individual differences may affect the results. For the first (called $Drift_1$), parameters were $A = 3000''$ and $T_1 = 1.3s$, for the second (called $Drift_0$) $A = 300''$ and $T_1 = 0.1s$ were used. In both cases, the tremor was superimposed on the drift spectrum (Fig. 6.1A).

The main features of the simulated eye movements are summarised in Figure 6.1B and C. The tremor consists of fast, irregular movements with a mean amplitude of $15'' - 20''$ (Riggs and Ratliff, 1951; Ditchburn and Ginsborg, 1953; Steinman et al., 1973). Drift movements are larger (mean amplitude $6.5'$ for $Drift_1$ and $4.3'$ for $Drift_0$; Ratliff and Riggs, 1950; Ditchburn and Ginsborg, 1953; Murakami, 2004) and slower (mean velocity $0.5deg/s$ and $0.7deg/s$, respectively; Murakami, 2004).

6.2 Results

Figures 6.2A-C show simulated responses of different retinal neuron classes for a single contrast step without and in the presence of fixational eye movements. The responses were taken at different locations with respect to the stimulus location.

The responses for a static stimulus reveal the basic properties of the different simulated neurons (Fig. 6.2A). The response amplitudes reflect the receptive field properties of the respective cell class. The photoreceptor response is spatially blurred due to the ocular optics. Horizontal cells respond over wide distances due to their large receptive fields. In their spatial properties, bipolar and PC-cell responses are similar to the photoreceptor responses and MC-cell responses are slightly spatially blurred due to their larger

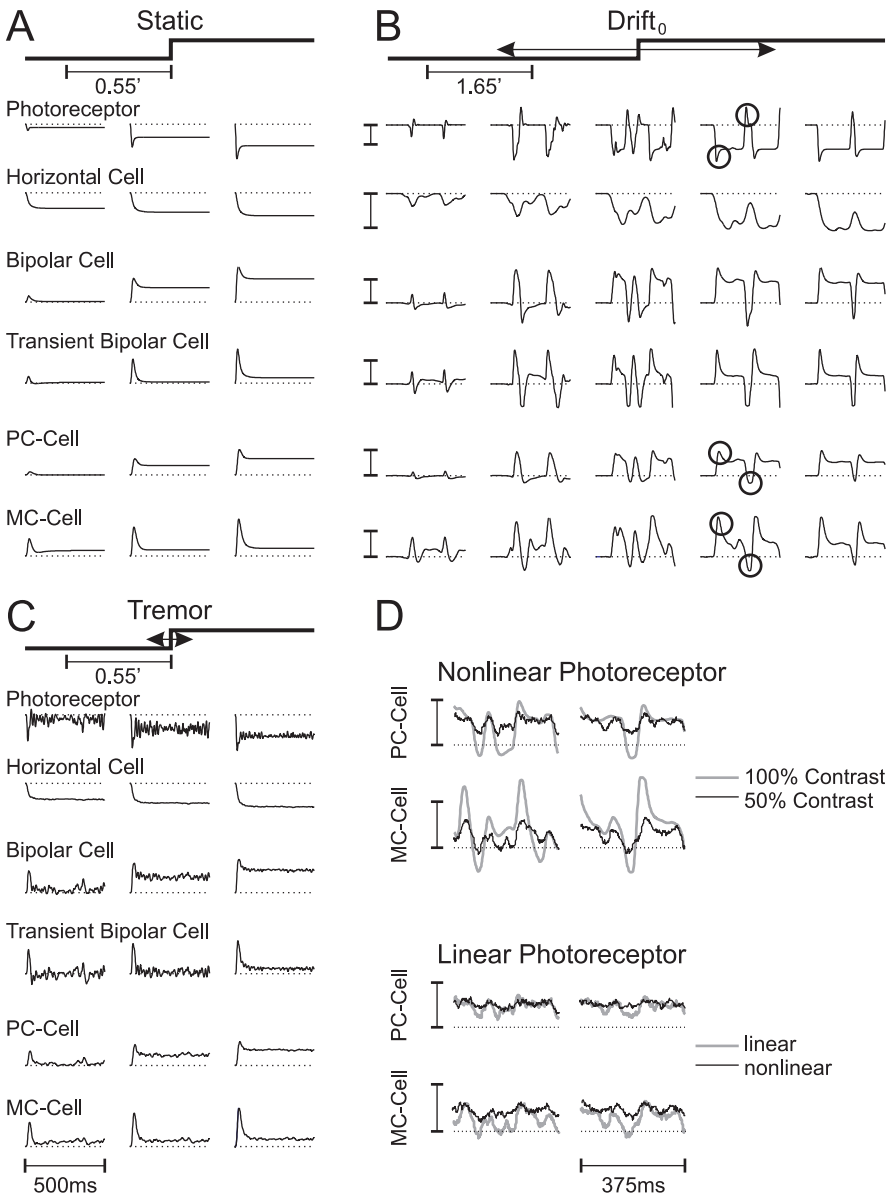

FIGURE 6.2: Responses of simulated foveal neurons to a contrast step. A-C, Responses for the static eye (A), slow drift movements ($Drift_0$, B) and the microtremor (C) at 100% contrast. Horizontal alignment indicates the location of the neurons relative to the stimulus (depicted at the top of each panel). In C, circles indicate onset- (peaks) and offset-transients (troughs). The mean amplitude of the respective eye movements are indicated by the double arrow at the top of each panel. D, Responses of PC- and MC-cells to a contrast step at 50% during slow drift movements ($Drift_0$) at two different locations relative to the stimulus. The upper half compares the responses at 50% contrast (black traces) with those at 100% contrast (gray traces), and the lower half compares responses of the full model (gray traces) with those obtained after linearising the photoreceptor (black traces, see Section 5.2.1). All vertical calibration bars indicate to 10mV.

receptive fields.

The temporal response for the static stimulus is always bimodal, with a transient overshoot at light onset, followed by a sustained response. At light offset, neurons respond with a second transient of opposite polarity (not visible in Fig. 6.2A but see circles in Fig. 6.2B). Off-transients are typically weaker and more delayed than On-transients, which is a consequence of nonlinearities, predominantly in the photoreceptor (see Chapter 5).

Eye micromovements cause the stimulus to jitter across the retina, which leads to a spatial distribution of the excitation (Fig. 6.2B-C). For drift movements, their large amplitudes cause a broad dispersion of the responses covering up to 35 photoreceptors (Fig. 6.2B), clearly visible in all simulated cell classes. The small microtremor however fails to drive strong responses if simulated in isolation (Fig. 6.2C). With a mean amplitude of less than a photoreceptor diameter, the modulation is still strong in the photoreceptor and bipolar cell responses, but attenuated in ganglion cells due to spatiotemporal integration. The only effect clearly visible here is an amplification of the onset transient especially for weakly responding neurons (compare Fig. 6.2C and A).

Drift movements clearly change the temporal response of ganglion cells (Fig. 6.2B). As compared to a static stimulus, PC-cells, which have a substantial sustained response component, react to drift in a more transient way in the vicinity of the edge of the stimulus. This behaviour is even more pronounced in MC-cells, which is strikingly different from the single onset-transient for a static static stimulus. The observed response transients are initiated, as mentioned above, by photoreceptor nonlinearities and the nested amacrine circuit, which leads to a particular difference between On- and Offset transients: Onset responses are fast and pronounced, while offset transients are slower and weaker (compare responses marked by circles in Fig. 6.2B).

The transient behaviour of MC-cells is also evident at reduced stimulus contrast levels, as illustrated in Figure 6.2D. The comparison of the traces obtained at 100% and 50% (upper half in panel D), which were all simulated using the same eye movements, shows that the response is attenuated, in particular for PC-cells while the temporal pattern of the responses remain similar.

To assess the influence of the different model components on these responses, the lower part in panel D compares responses of the full model with those obtained after linearisation of the photoreceptor, as it was done in Chapter 5. The effect of this modification is small in PC-cells, but results in weaker transients in MC-cells. This is in agreement with the finding in Chapter 5 that photoreceptor nonlinearities play an important role in

the response properties of nonlinear Y-like ganglion. The additional effect the nested amacrine circuit has on MC-cell responses is also visible, as their modulation is still stronger than that of linear PC-cells.

6.3 Summary and Discussion

The central finding reported here is that drift movements lead to strong transient responses. In particular, the responses to stimulus on- and offsets are imbalanced, with strong, brief onset-transients and slower and weaker offset-transients. The results show that this effect is particularly pronounced in MC-cells, and it directly results from the nonlinearities discussed in the previous chapter.

How can this more transient behaviour affect upstream processing and visual perception? A direct consequence of this imbalance is that eye movements lead to increased activity levels of the ganglion cell population in the vicinity of stimulus regions which contain spatial contrast differences. As strong transients are typically elicited by more abrupt changes in contrast, stimuli that contain high spatial frequencies should be particularly effective in driving these responses. This effect could possibly enhance responses for weak stimuli, which would be indistinguishable from noise when they are retinally stabilised.

Further, the transient responses in the presence of eye movements encode spatial correlations in the stimulus: the neural responses along an elongated edge are enhanced simultaneously. Hence multiple ganglion cells will send stimulus-evoked spikes to the visual cortex within a very brief interval. As one retinal spike contributes just about 3% to the activity of its cortical target neuron (Kara and Reid, 2003), this effect could strongly increase the probability of a cortical response to a weak stimulus. In summary, the effect observed here could therefore facilitate the detection of weak stimuli, as suggested by Hennig et al. (2002) and Rucci and Desbordes (2003).

Chapter 7

The Influence of Fixational Eye Movements on Hyperacuity

A demanding task for the visual system is *hyperacuity*, or *vernier acuity*, which is the detection of spatial offsets smaller than the spacing between two photoreceptors (reviewed by Westheimer, 1979; Geisler, 1984). Hyperacuity differs from visual resolution tasks (limited by the Nyquist frequency of the system, see Section 2.3), as it requires spatial interpolation (Fig. 7.1). Therefore, hyperacuity is, in contrast to resolution tasks, only limited by the strength of the signal relative to that of the noise in the visual system. The difference between the psychophysical thresholds for resolution acuity ($30' - 60''$ in the fovea) and hyperacuity (foveal $3'' - 6''$) is striking and one may suspect that hyperacuity should be very sensitive to disturbances. On the other hand, it has been shown that hyperacuity thresholds are little affected by moving the stimulus with up to 4 deg/s velocity (Westheimer and McKee, 1975), and that they do not increase for a reduction of the stimulus contrast down to about 25% (Watt and Morgan, 1983; McKee, 1991). Further, hyperacuity thresholds are similar for a range of different stimuli (Westheimer, 1979), suggesting that it is a robust phenomenon that is constrained by the very fundamental limits of the visual system.

Studies of hyperacuity on the neural level have demonstrated that it depends on receptive field properties and variables such as the extend of spatial integration and nonlinear processing, such as contrast gain control in MC-cells (Lee et al., 1993, 1995; Wachtler et al., 1996; Shapley and Victor, 1986; Rüttiger and Lee, 2000). These studies generally considered a brief transient responses of neurons following the onset of the stimulus. It therefor remains unclear how longer stimulus durations, in particular in the presence of fixational eye movements, affect hyperacuity.

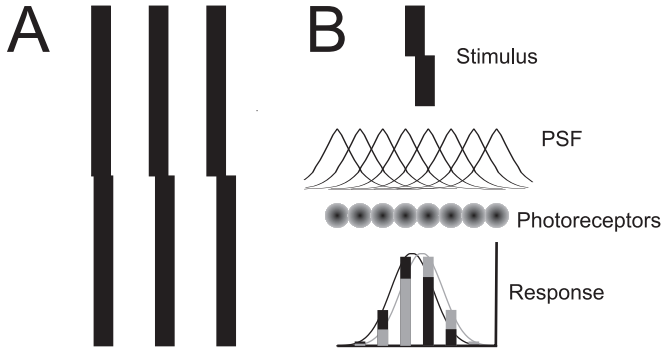

FIGURE 7.1: Illustration of the phenomenon of visual hyperacuity. A, Typical hyperacuity stimuli: two vertical lines with a vernier horizontal offset in the middle. B, Hyperacuity on a neural level. The two bottom curves represent the spatial activity pattern of photoreceptors (circles) of two slightly offset bars (top), after blurring by the ocular optics (middle curves). The offset is less than the separation of two receptors, but due to the optical blurring, a difference between the response patterns to the two bars is visible in the spatial activity pattern (compare black and gray bars in the bottom graph). If this difference is sufficiently strong, the small offset is visible to an observer.

Previously, fixational eye movements have been suggested to contribute to hyperacuity (Averill and Weymouth, 1925; Marshall and Talbot, 1942). These studies propose an improved spatial sampling, as eye movements lead to frequent stimulation of neighbouring photoreceptors. Further, a possible role of transient neural responses was already suggested by Marshall and Talbot (1942). This theory was inspired by the *dynamic theory of visual acuity* by Hering (as reviewed by Steinman and Levinson, 1990), but no conclusive experimental evidence exists so far to support or reject it. In this chapter, the dynamic theory of visual acuity will be re-investigated by using a model of primate PC- and MC-cells. Signal detection theory was employed to estimate neural hyperacuity thresholds, which will allow for a comparison to psychophysical data. The results will confirm and augment the basic assumptions of Marshall and Talbot and highlight the importance of fixational eye movements and retinal nonlinearities for visual perception near threshold.

7.1 Materials and Methods

7.1.1 Model Retina

As in the previous section, the model is based on the description given in Section 4. All parameters were the same as specified in the preceding chapter.

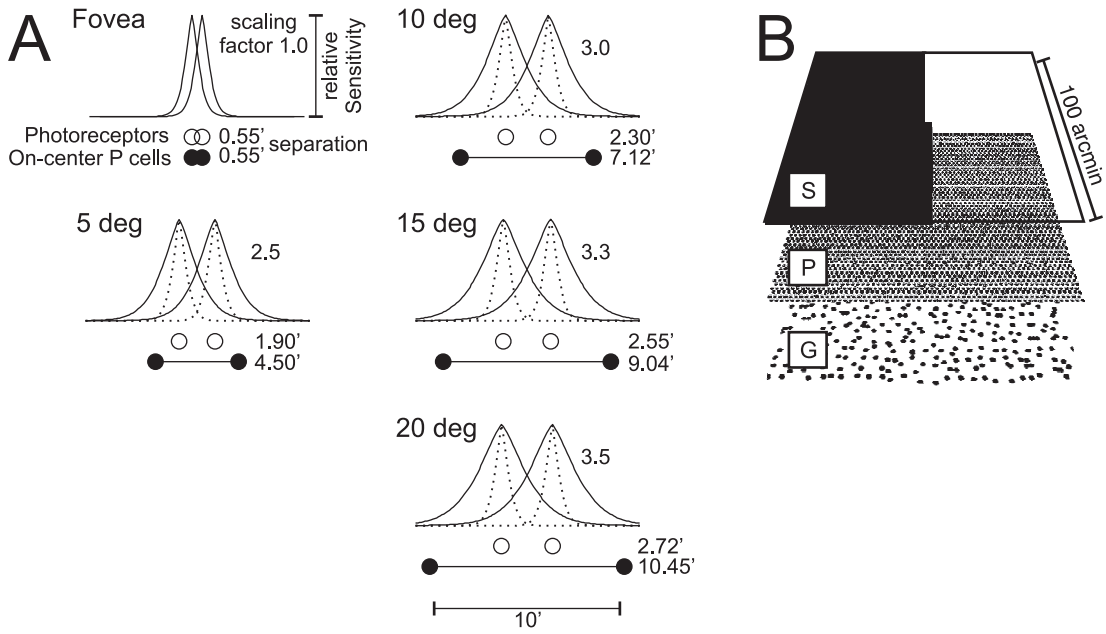

FIGURE 7.2: Spatial configuration of the retina model. A, Summary of the main determining factors for spatial resolution at different retinal eccentricities. All relative sizes are to scale with the foveal dimensions (top left). Shown are the point spread functions simulating ocular blurring (curves, scaling factor relative to the fovea is indicated to the right of each curve), the separation of photoreceptors (open circles, values shown at the right) and of On-center midget ganglion cells (filled circles, values shown at the right). B, Spatial layout of the stimulus (S), photoreceptors (P) and ganglion cells (G) on two-dimensional grids. The example illustrates the arrangement at 5 deg eccentricity.

Simulations were carried out at five different retinal eccentricities: in the fovea for PC- and MC-cells and at 5, 10, 15 and 20 degrees eccentricity for PC-cells only. The photoreceptor layer consisted of either 3600 (0-10 deg) or 14400 neurons (15 and 20 deg).

Ganglion cells were either placed on a perfect hexagonal grid or their positions were randomly shifted. Random displacements were obtained from Gaussian distributed random numbers with a SD of 12% of the cell separation (Dacey, 1993).

The ganglion cell density for each eccentricity was estimated from anatomical data of the central and temporal human retina (Dacey and Petersen, 1992; Goodchild et al., 1996; Sjöstrand et al., 1999), assuming that PC-cells amount to 80% of all ganglion cells across the visual field, and half of them are On-center (Perry et al., 1984; Grünert et al., 1993). The anatomical receptive field diameter for PC-cells at each eccentricity was estimated by assuming a coverage factor of one (Wässle and Boycott, 1991; Dacey, 1993). The Gaussian center radius was set to 17% of the cell separation, producing a grid of neurons with non-overlapping anatomical receptive fields. This is equivalent to

a ratio of approximately 10:1 between the strongest and weakest inputs to the neuron, as estimated for the cat On-beta cell (Cohen and Sterling, 1991). Parameters for the different eccentricities are given in Figure 7.2A. MC-cells were only studied in the fovea, where the receptive field center size was set to $1.1'$. The two-dimensional spatial configuration of the stimulus, photoreceptors and PC-cells is illustrated in Figure 7.2B.

In an additional set of simulations, the size of center and surround of PC-cells was increased by 2.0 to consider coverage factors above unity.

7.1.2 Synaptic Noise

It has been shown that the noise in the spiking response of ganglion cells is dominated by synaptic noise, and that the spiking mechanism itself is rather precise (van Rossum et al., 2003; Demb et al., 2004). The variability of the membrane potential has been shown to increase with increasing depolarisation, but is constant in the spiking of ganglion cells (Croner et al., 1993; Freed, 2000b; Demb et al., 2004).

In this study, the output of ganglion cells was analysed at the level of the membrane potential response, however with the aim to investigate the signals that reach the cortex. Therefore in this model, the response variability of ganglion cells was implemented as additive, contrast-independent noise. This noise was drawn from a Gaussian distribution with a width of 1.0 mV (Demb et al., 2004), and added to the ganglion cell membrane potential. In the following, the simulated noise will be called “synaptic noise”, which indicates its origin. This noise however corresponds to the variability found in the spiking response of ganglion cells.

7.1.3 Optical Blurring

Optical blurring was simulated by convolving the stimulus with a point spread function (PSF) as given by Equation 6.2 in Chapter 6. To account for the additional blurring in the retinal periphery due to off-axis errors and the increasing receptor aperture size in the periphery, the PSF was scaled to fit experimental data (Thibos et al. (1996), scaling factors are given in Fig. 7.2A). The resulting spatial Nyquist frequencies for the photoreceptor and ganglion cell grid and the sampling limit imposed by the optical blurring are summarised in Figure 2.3B in Section 2.1.

7.1.4 Stimuli

Stimuli consisted of two vertical bipartite fields with variable relative horizontal displacement (Fig. 7.2B). This resembles a typical vernier stimulus with wide bars as compared to the extend of receptive fields and lateral interactions. The stimulus was chosen to eliminate the effect of stimulus size Beard et al. (1997), a variable not considered in this work. Stimuli were presented at 100% contrast unless stated differently.

7.2 Results

This section consists of three parts. First, a method to calculate hyperacuity thresholds from the population response of retinal ganglion cells will be introduced. In the second part, spatial aliasing induced effects of reduced vernier detectability in the peripheral retina will be investigated an it will be shown that eye movements can improve on this. Finally in the third part, it will be demonstrated that unbalanced spatio-temporal nonlinearities in the ganglion cell responses following eye micro-movements can lead to an improved vernier detectability also in the central retina.

7.2.1 Analysing Responses to a Vernier Stimulus

In the following section the spatial and temporal analysis method will be described that was used to determine vernier detectability. This method is model free, based on ideal observer analysis, and allows for the definition of vernier detection thresholds, which can be compared to results from psychophysical experiments.

7.2.1.1 Spatial Analysis at a given Point in Time

If a vernier offset in a hyperacuity task is detectable by an observer, it must also be traceable in the spatial population response of the ganglion cell layer (Fig. 7.3A), which constitutes the output of the retina. To measure the degree of detectability of a vernier offset, receiver operating characteristics (*ROC curves*) were calculated to quantify the separability of two contrast steps with a vernier offset. This procedure, described in the following, is equally applicable to experimentally recorded single cell activity.

First, sections of the upper and lower half of the spatial response profile in the ganglion cell layer, representing the two sections of the vernier stimulus, were averaged vertically

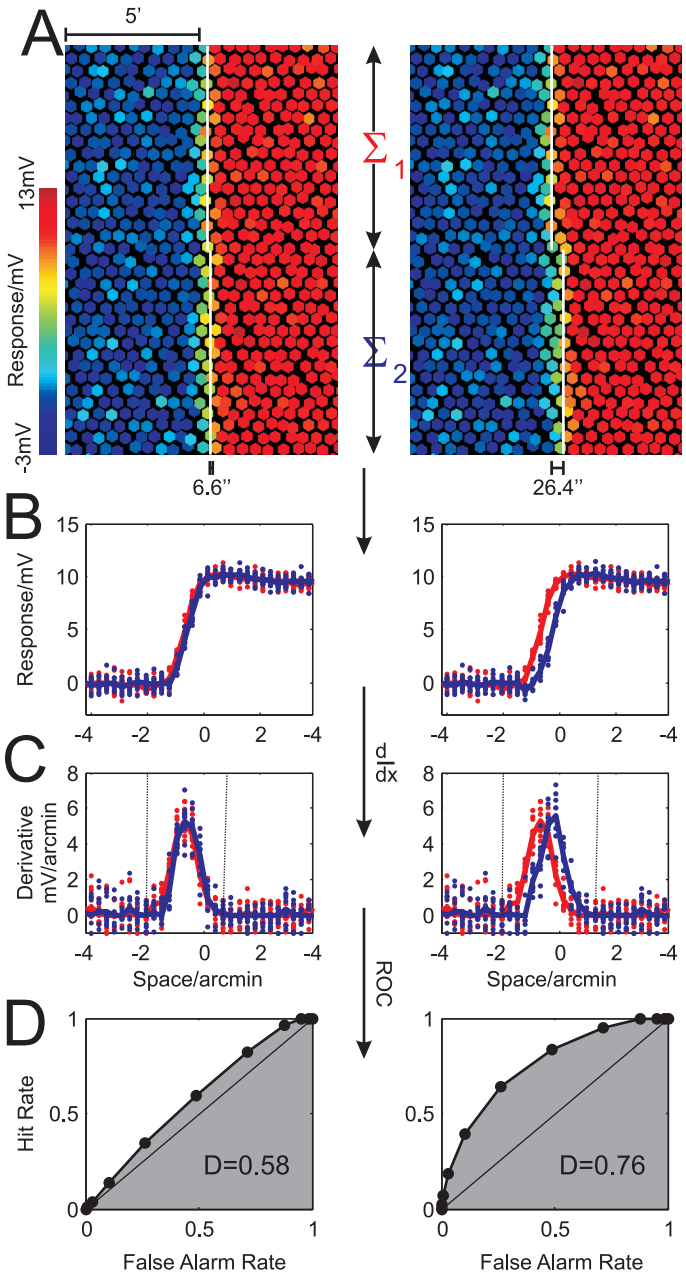

FIGURE 7.3: Spatial analysis of the vernier stimuli. A, Spatial membrane potential response of the ganglion cells to a vernier stimulus 30ms after stimulus onset (fovea, left: vernier offset $0.11'$, right: vernier offset $0.44'$). The contrast step of the stimulus is indicated by white lines. B, Spatial response profile for the upper (red) and lower half (blue) of the responses in A (solid lines, dots show responses of individual ganglion cells), calculated as the average over 20 rows of ganglion cells (Σ_1 and Σ_2). C, Spatial derivative of the responses in B. Circles show values for individual neurons and solid lines their mean, half-wave rectified at zero. Vertical lines show the region where the ROC analysis was carried out. D, ROC curve calculated from the curves in C. The value of the integral of the ROC curve (shaded gray) is shown for each curve (D: detectability index).

and plotted as a function of the horizontal location (Fig. 7.3B). The spatial averaging reflects the convergence of ganglion cells, via the LGN, onto a single neuron in V1 (Shulz et al., 1993). To account for the spatial scatter of the receptive field positions in the visual cortex (Dow et al., 1981), in the analysis the location of each ganglion cell on the noisy grid was re-mapped to its location on a perfect hexagonal lattice. The resulting activity profiles closely fit cumulative Difference of Gaussians functions, as expected from the ganglion cell receptive field shape.

In the next step, spatial derivatives of the profiles were calculated and half-wave rectified at resting potential (Fig. 7.3C). This operation resembles a cortical edge detection mechanism (Hubel and Wiesel, 1962) and yields the positive part of Difference of Gaussian shaped distributions. Finally, ROC curves were calculated from these profiles to obtain an estimate of the degree of overlap for the distributions (Fig. 7.3D).

Usually, ROC curves are used to calculate how well a signal is separated from noise. This method assumes that signal and noise are represented by overlapping probability distributions, which can be measured experimentally. In this case, ROC-analysis is used to calculate how well the derivational profiles (Fig. 7.3C) can be separated, which is a direct indicator for the presence or absence of a vernier offset in the stimulus. The method used here therefore does not differ from the normal procedure to calculate the separability of a signal from noise: A sliding threshold was shifted stepwise across the two response derivational profiles (Fig. 7.3C), called R_1 and R_2 in the following. For each threshold δ, the following integrals were computed:

$$H(\delta) = \frac{\int_{\delta}^{\infty} R_2(x)dx}{\int_{-\infty}^{\infty} R_2(x)dx} \tag{7.1}$$

$$F(\delta) = \frac{\int_{\delta}^{\infty} R_1(x)dx}{\int_{-\infty}^{\infty} R_1(x)dx} \tag{7.2}$$

$H(\delta)$ corresponds to the "hit-rate" for the response at a given threshold δ, as this value indicates which proportion of the response profile contains the information that the lower bar offset to the right with respect to the upper bar. $F(\delta)$ indicates the likelyhood for wrong decision or "false hit", that is a response is taken as a "hit" although it belongs to the left distribution (which indicates a straight line). A ROC curve then can be obtained by plotting $H(\delta)$ as a function of $F(\delta)$ (Fig. 7.3D).

This method was more suitable than to directly calculate d' ("d-prime"), a common measure of the separation of two distributions (Swets, 1996), because the profiles ob-

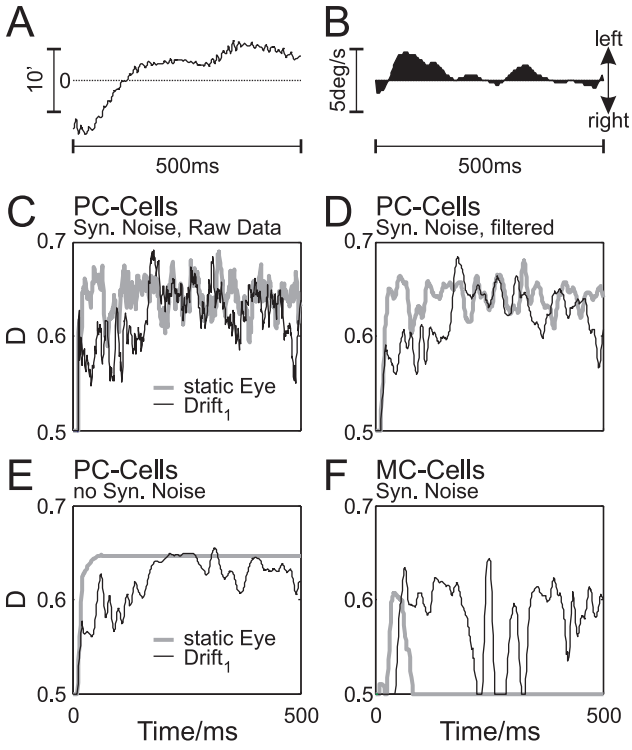

FIGURE 7.4: The effect of eye movements on the detectability of a vernier offset. A, Simulated eye movements (positive values represent motion to the left relative to resting position). B, Velocity of the slow drift component. C-F, Time-course of the detectability D for different situations. Each panel shows D for a static eye (gray traces) and in presence of eye movements (as shown in A,B). D was calculated every 1ms of the response (shown in C for PC-cells) and filtered by calculating a 10ms running average (D-F). Traces are shown for PC-cells (D), PC-cells simulated without synaptic noise (E) and MC-cells, simulated with noise (F). In all examples, the vernier offset was $0.22'$ for PC-cells and $0.44'$ for MC-cells.

tained from the simulations typically differ in amplitude and width, or may be skewed due to eye movements (see below). The integrals of the ROC curves, ranging $[0.5, 1]$, were then taken as a measure for the detectability of the vernier offset (D in Fig. 7.3D). It has been shown that this value, sometimes called the *area index*, corresponds to the proportion of correct choices in a two alternative, forced choice experiment (Geen and Swets, 1966). Thus, when $D = 0.75$ defines the detection threshold, in Figure 7.3 the vernier offset in the example on the left is undetectable and on the right detectable. D was set to 0.5 when it could not be estimated in cases were the derivational spatial response approached the noise amplitude.

7.2.1.2 Influence of Stimulus Presentation Time

To analyse the effect of eye micromovements for a single presentation of a vernier stimulus, a *sliding* ROC analysis was carried out in time steps of 1ms over a 500ms stimulation interval. Raw traces of D for a static eye show a high degree of variability (shown for PC-cells in Fig. 7.4C, gray trace), which is a consequence of the synaptic noise included in the model. Cortical neurons however perform temporal band pass filtering on the incoming signals. Therefore, the detectability D was filtered by calculating the running average of the traces over 10ms (Fig. 7.4D, gray trace). This filtering reduces the variability of the detectability, but leaves a substantial amount of modulation compared to the almost unmodulated traces obtained without noise (compare gray traces Fig. 7.4D and E).

The tonic responses of PC-cells allow for an uninterrupted estimation of the detectability, which changes only little over time. For MC-cells in a static eye, typically only the first 60ms of the response could be analysed, because their tonic response was too weak to be distinguished from noise (Fig. 7.4F, gray trace).

The inclusion of ocular drift led to an additional modulation of the detectability, both for PC- and MC-cells (Figs. 7.4C-F, black traces). For PC-cells, a loose dependency between direction and velocity of the eye movements and D is found: it is reduced both for high velocities and, as a consequence of the stimulus asymmetry, for rightward motion (Fig. 7.2C). Additionally, a faster modulation is visible, which is mostly a consequence of synaptic noise and the microtremor. In the MC-cell population, drift movements prevent cells from adapting to the low tonic level, and the vernier offset remains detectable almost for the whole presentation time. The dependency on velocity is weaker than in PC-cells, but rightward motion had a similar negative effect.

7.2.1.3 Determining Detection Thresholds

It should be noted first that in a psychophysical experiment detectability depends heavily on the task. When having to discriminate between a left or right vernier (discrimination task) the visual system probably requires less integration time than when being asked if a vernier offset exists or not (detection task), because it is possible to introduce a bias in the former case. Thus, in the first analysis (discrimination) only the peaks of the filtered traces of D (D_{max}) were considered as the cue for vernier offset detection. Alternatively, we also used the temporal mean of D for a given presentation time (500ms, D_{mean}), which represents a temporal integration mechanism (detection). Interestingly

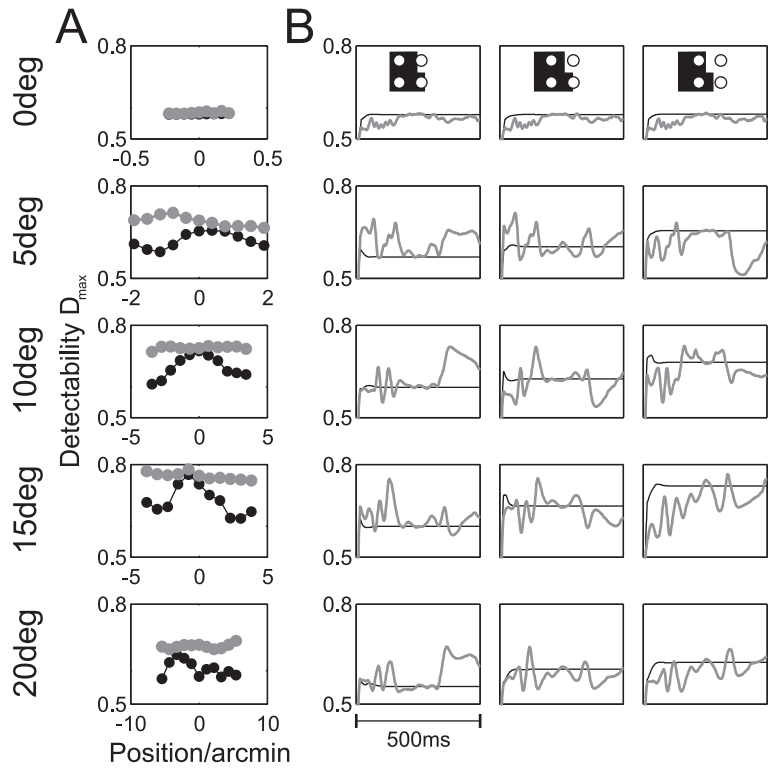

FIGURE 7.5: The relation between the detectability and stimulus position. A, The detectability D is shown for resting eyes (black) and eye movements ($Drift_1$, gray) as a function of the stimulus location relative to the ganglion cell receptive fields at five different retinal eccentricities (indicated on the right of the figure). Vernier offsets are: 0 deg: $0.11'$, 5 deg: $0.76'$, 10 deg: $0.38'$, 15 deg: $1.53'$, 20 deg: $1.632'$. B, Time course of D at different stimulus locations relative to the ganglion cell receptive fields. The insets in the top row schematically illustrate the respective stimulus placement relative to four ganglion cells (circles).

these two measures yield different results, as shall be described next, which can be compared to psychophysical observations.

Generally, the discrimination- or detection-threshold was defined as that particular vernier offset where D_{max} or $D_{mean} = 75\%$.

7.2.2 Spatial Aliasing Effects

In the peripheral retina, neural undersampling, rather than the ocular optics, limits the spatial resolution power (see Section 2.3). To examine a possible effect of the stimulus location on the detectability of a vernier offset and the influence of eye movements, vernier stimuli were presented at different positions relative to the ganglion cell receptive fields. This investigation was limited to PC-cells to isolate the effects described here from those caused by nonlinearities (see below). Only the peaks of the detectability

(D_{max}, discrimination task) were considered, which produced hyperacuity discrimination thresholds in the experimentally observed range (see below).

Figure 7.5A shows D_{max} as a function of the stimulus position for different eccentricities. In the fovea, stimulus position has very little influence on D (top plot in Fig. 7.5A), because the ocular optics prevent neural undersampling. Towards the retinal periphery, the influence of the stimulus location increases in the absence of eye movements (Fig. 7.5A, black circles). The spatial variation of D in the periphery shows a periodicity with a length equal to the minimum horizontal distance between two ganglion cells on a hexagonal grid ($\sqrt{3}/4 \cdot d$, when d is the grid constant). Thus, this effect is a direct consequence of neuronal undersampling, which impairs vernier offset detection in the periphery.

Eye movements strongly reduce spatial aliasing effects in the periphery (Fig. 7.5A, gray circles). The spatial variability is almost completely removed at all eccentricities. As visible in the traces of D in Figure 7.5B, for each stimulus position the temporal variation of the detectability is much stronger in the periphery than in the fovea. In particular, the variations are very similar for different stimulus positions in the fovea, but roughly anti-correlated in the periphery. This illustrates that the improvement in the periphery relies on eye movements moving the stimulus in regions on the retina where detectability is higher (spatial averaging effect = SAR-effect). These results suggest that a qualitative difference exists between foveal and peripheral hyperacuity in the presence of eye movements.

Next, hyperacuity thresholds were estimated for all eccentricities (Fig. 7.6A). The variability of D at different stimulus locations was taken into account by using the average across all locations. This corresponds to a psychophysical experiment with many stimulus repetitions and a small trial-to-trial variability of the exact stimulus location.

Without eye movements, hyperacuity thresholds increase from about $20''$ in the fovea to $230''$ at 20 deg eccentricity, as may be expected from the decreasing cell density towards the periphery. As shown, the influence of eye movements is small in the fovea, but increases towards the periphery. While the influence of the isolated tremor is negligible, both types of drift movements lead to a significant improvement at higher eccentricities (e.g. from $230''$ to about $180''$ at 20 deg). Comparing the two drift conditions shows a slightly higher improvement for the slower drift $Drift_1$ at lower eccentricities, which disappears in the periphery.

Overall, the absolute values of the hyperacuity thresholds obtained from the simulations are in good agreement with experimental data for either very small or large stim-

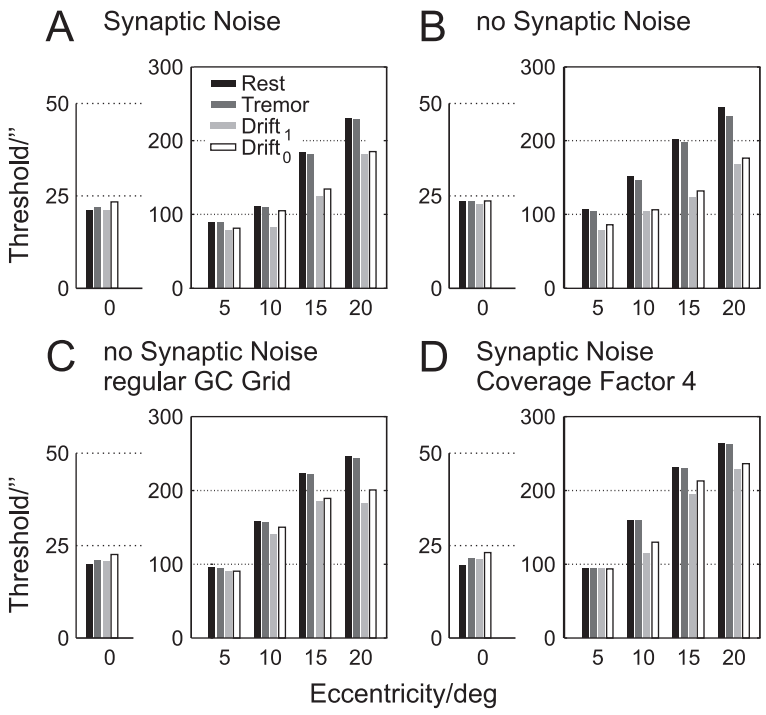

FIGURE 7.6: The influence of eye movements on hyperacuity in the peripheral retina. A, Model hyperacuity thresholds for PC-cells at eccentricities from 0-20 deg and the different eye movement conditions. B, As A, but without synaptic noise. C, as B, for PC-cells on a regular hexagonal grid. D, as A, but comparing the full model (A) to a PC-cell grid with a coverage factor of four. All thresholds are for 500ms stimulus presentations and are averages over different stimulus locations.

uli (Whitaker et al., 1992; Harris and Fahle, 1996). The values at 5 deg eccentricity however are higher than in these experiments, which may be caused by a higher P-cell density (Dacey and Petersen, 1992; Dacey, 1993) and/or increased cortical magnification in this region (Adams and Horton, 2003), which was not considered in this study.

The scaling of the thresholds as a function of the eccentricity is also in good agreement with experimental data (Whitaker et al., 1992), except for the relatively high value at 5 deg. In particular, both for resting and moving eyes a deviation from linear scaling to lower values is visible at 10 deg eccentricity. This effect is especially strong in the presence of drift movements and also evident in the data of Whitaker et al. (1992).

To assess the influence of noise, thresholds were calculated without synaptic noise (Fig. 7.6B). Overall, they are higher for a static eye when synaptic noise is removed, but similar, when drift movements were included. At higher eccentricities (15 and 20 deg), synaptic noise slightly increases thresholds for drift movements. This comparison suggests that generally the presence of uncorrelated noise has a positive effect on hyperacuity. Its influence however disappears in the presence of drift eye movements.

Furthermore, removal of the semi-random placement of ganglion cells on the hexagonal grid shows a strong, eccentricity dependent effect (Fig. 7.6C). In the fovea, thresholds are almost identical, but with increasing eccentricity performance is reduced for the regular arrangement. This performance reduction is particularly strong when drift movements are present. At 20 deg, this effect again disappears. Hence, to certain extend, an irregular placements of ganglion cells could improve hyperacuity due to an effectively more dense sampling (Ruderman and Bialek, 1992). In the central retina, optical blurring prevents this effect. At 20 deg, substantial neural undersampling is the determining factor for hyperacuity, which cannot be countered by random placement.

The previous results rest on the assumption that the anatomical receptive fields of PC-cells are arranged without spatial overlap (i.e. a coverage factor of one). It should be emphasised that in the model, physiological receptive fields nevertheless overlap due to the optical blurring. A coverage factor of one was found for midget cells in the primate, but other ganglion cell types typically have coverage factors > 1 (Wässle and Boycott, 1991; Dacey, 1993).

An increase of the coverage factor to four led to a general increase of thresholds, which depends on the eccentricity and eye movements (Fig. 7.6D). Thresholds are largely unaffected in the fovea, but increased in the periphery. The strongest performance reduction is found at 10 deg for resting eyes and tremor and at 15 deg for drift movements (compare Fig. 7.6A and D).

Without eye movements, the negative effect of increased receptive field diameters is a direct consequence of the increased spatial dispersion of the response. Results for the fovea are unaffected because spatial filtering is determined by optical blurring. At higher eccentricities, neural aliasing effects are reduced by the increased receptive fields. This however also leads to a weaker performance in the presence of eye movements, because the additional blurring leads to a loss of precise spatial information.

In summary, in this section it was reported that effects of neural undersampling can be efficiently removed by eye movements, which would otherwise impair hyperacuity in the retinal periphery. At the same time, the higher spatial precision that accompanies undersampling also benefits performance in a hyperacuity task.

7.2.3 Spatiotemporal Response to a Vernier Stimulus

In the following section, it will be analysed in more detail how the central retina reacts to vernier stimuli in the presence of fixational eye movements. Spatial aliasing does not

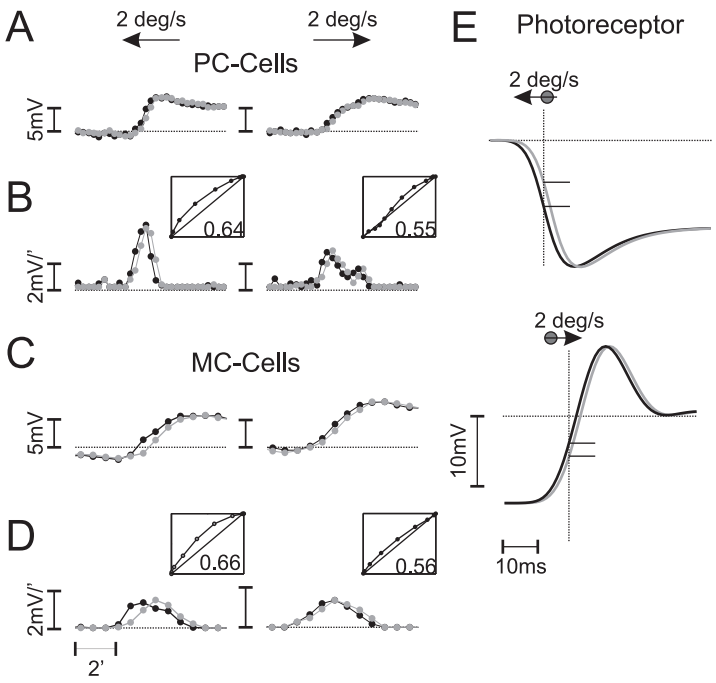

FIGURE 7.7: Effect of eye movements on the spatial activity distributions of simulated neurons. A-D, Snapshots of the average spatial population response of PC-cells (A) and MC-cells (C) and their spatial derivatives (B and D; responses to upper half of the stimulus are coloured black and to the lower half gray). Snapshots were taken during a leftward (left plots) or rightward motion (right plots) of the stimulus (velocity is indicated for each snapshot). Insets show the ROC-curve for each case and the corresponding detectability D. As in Figure 7.3, the graphs represent the vertical average over 20 cell rows. In all examples, the vernier offset was $0.22'$ for PC-cells and $0.44'$ for MC-cells. E, Photoreceptor responses for left- (top) and rightward motion (bottom). Responses to the upper half of the stimulus are back, those to the lower half gray. The response differences at the times where the snapshots in A-D were taken (vertical lines) are indicated by horizontal lines. Vernier offset was $0.22'$.

play any role in the central retina; however, a certain temporal effect, which relies on onset-transients (see Section 6, Fig. 6.2) can nonetheless lead to acuity improvement.

7.2.3.1 Phasic Resolution Enhancement

Fixational eye movements lead to changes of the spatial activity distribution of ganglion cell responses. Examples for simulated PC- and MC-cells are shown in Figure 7.7A-D. With the given stimulus asymmetry, leftward motion leads to improvement in detectability, while for rightward motion responses are strongly smeared out and detectability is reduced. This is the case for both PC- and MC-cells.

This effect is initiated by the nonlinear properties of photoreceptors, as illustrated in Figure 7.7E. Moving the bright part of the contrast step into the receptive field of a

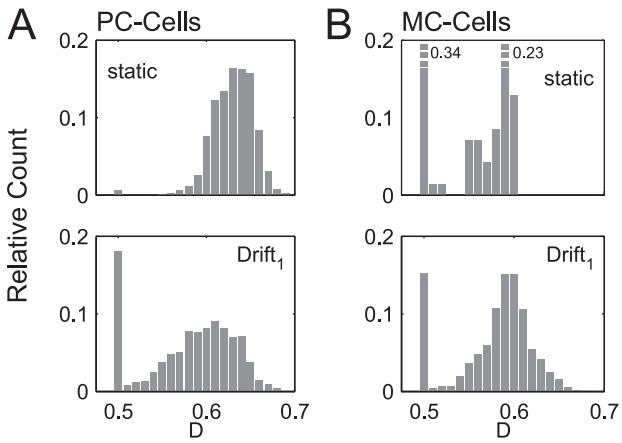

FIGURE 7.8: Distribution of the detectability values D for PC-cells (A) and MC-cells (B) for a static (top) and moving eye (bottom). Histograms for PC-cells and MC-cells with eye movements were computed from a 2 sec response. For MC-cells in the static condition, the histogram represents the onset transient only (70ms). In all examples, the vernier offset was $0.22'$ for PC-cells and $0.44'$ for MC-cells.

photoreceptor (leftward motion) gives rise to a strong, fast hyperpolarisation after about 15ms (fast On-transients, see Section 6, Fig. 6.2). Due to motion, the spatial offset of the vernier stimulus is translated into a brief temporal interval. Two vertically aligned photoreceptors, one located at the upper and one to the lower half of the stimulus, therefore respond temporally slightly out of phase. If this interval is sufficiently long, as in this example, the difference between the responses of photoreceptors and of subsequent neurons is increased, and a better spatial discrimination is possible (phasic resolution enhancement = PRE-effect). For rightward motion, the photoreceptor responses slowly decay, as the stimulus leaves their receptive fields (slow Off-transients, see Section 6, Fig.6.2). Thus, differences between responses in the upper and lower half of the stimulus are less pronounced and the spatial population response is smeared out substantially (Fig. 7.7A-D, response profiles on the right).

This result predicts that vernier acuity should generally be slightly better for moving than for static stimuli. Experimental data by Westheimer and McKee (1977) indicates that this may be the case.

7.2.3.2 Distributions of the Detectability Index over Time

On average, drift movements lead for PC-cells to a reduced detectability in comparison with the static case (Fig. 7.8A, compare top and bottom graphs). The distribution of D is broadened and its mean is lower compared to the static case. D however reaches the same maximum in both cases. Furthermore, in the static case D could almost always

be determined ($D > 0.5$), which was not the case in the presence of eye movements. In this case D was set to 0.5 and this leads to the high peak at $D = 0.5$ in Figure 7.8A, bottom. This is in strong contrast to MC-cells, where D reaches higher values in the presence of drift movements and the mean of the distribution is also shifted towards higher values (Fig. 7.8B, compare top and bottom graphs). Furthermore, for a static eye a substantial part of the MC-response did not yield values of $D > 0.5$, which improves in the presence of eye movements.

This difference between PC- and MC-cells is not intuitive, given that typical velocities of drift movements are less than 3 deg/s, which does not exceed the sensitivity of PC- or MC-cells. An analysis of the model responses however suggests an explanation, which is based on the physiological properties of the simulated neurons. As shown in Figure 7.7E, the spatial precision of the cells relies on the difference of the responses of photoreceptors for the two halves of the vernier stimulus. The photoreceptor response needs about 15ms to develop. At a velocity of 2 deg/s, the vernier stimulus with offset 0.44 traverses two photoreceptors in just 5ms, and for the smaller vernier offset even faster (2ms for a 0.22" offset). Traversing PC-cells is equally fast, as their density is equal to the photoreceptor density. Therefore small spatial offsets are translated only into tiny temporal differences which will lead to almost no difference in the responses of adjacent PC-cells. This explains the reduced spatial sensitivity of PC-cells during eye movements.

MC-cells, on the other hand, respond faster than PC-cells and their density is lower. Thus, differences between photoreceptor responses, which represent the spatial offset in the stimulus, are better represented in the MC-cell population response (PRE-effect). For the same reason their spatial precision depends less strongly on velocity. Instead, the increased difference in photoreceptor responses can be exploited and leads to the relative improved detectability during eye movements observed for MC-cells (Fig. 7.8B).

Hence this explanation essentially rests on the direction-dependent asymmetry in detectability described in the previous section (Fig. 7.7), which is differently pronounced in PC- and MC-cell. This finding is supported by a recent analysis of ganglion cell responses in the primate retina by Rüttiger and Lee (2000). It should, however, be noted that, due to their large receptive fields, the absolute spatial precision of the simulated MC-cells is lower than that of PC-cells (see also below).

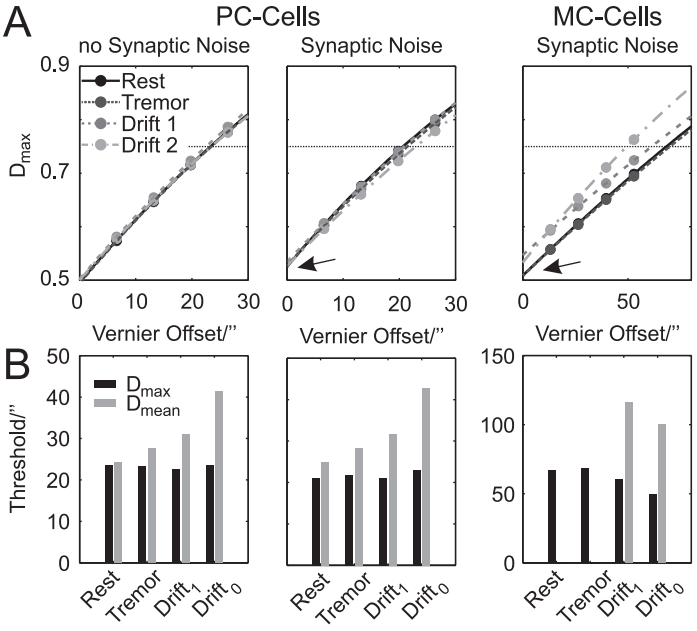

FIGURE 7.9: Foveal hyperacuity thresholds estimated from the model population response. Shown is data from PC-cells without (left) and with synaptic noise (middle) and for MC-cells with synaptic noise (right) for all four eye movement conditions. A, Relation between the vernier offset and detectability D_{max}. Arrows indicate where a bias exists for very small vernier offsets (see text). B, Vernier thresholds estimated from D_{max} (peaks of the detectability, black bars) and D_{mean} (mean of detectability, gray bars) for all conditions. All values were obtained from a single 500ms stimulus presentation.

7.2.3.3 Influence of Eye Movements on Hyperacuity Thresholds

As above, detection thresholds were obtained by systematically changing the vernier offset and calculating the corresponding detectability D. The relationship between D_{max} or D_{mean} and the vernier offset was fitted by a polynomial function (Fig. 7.9A). Plotting the detectability D_{max} as a function of the vernier offset shows that the fit yields values > 0.5 for a zero vernier offset (straight lines) in the presence of synaptic noise (arrows in Fig. 7.9A). This may be an explanation for the small bias found in a vernier *discrimination* task (Garcia-Suarez et al., 2004).

Thresholds were calculated for the peak values (D_{max}) and the mean of the detectability (D_{mean}) for a single 500ms presentation without and with eye movements (Fig. 7.9B). Three conditions were compared: PC-cells without and with synaptic noise and MC-cells with synaptic noise.

For PC-cells, the thresholds estimated from D_{max} are almost equal for all conditions (Fig. 7.9B, left and middle panel). The presence of synaptic noise leads to a slightly re-

duced threshold ($21.5''$ vs. $23''$), which reflects the small increase in D_{max} due to noise (Fig. 7.7B,C). This influence is only present for small vernier offsets (compare first two panels in Fig. 7.9A), and has therefore little impact on the thresholds.

The situation is different for MC-cells, where thresholds for D_{max} substantially decrease in the presence of drift movements ($65''$ vs. $61''$ for $Drift_1$ and $49''$ for $Drift_0$, Fig. 7.9B, right panel). This improvement can be directly attributed to the effects of nonlinear processing, as described above (PRE-effect, Figs. 7.4 and 7.8).

The picture changes dramatically for thresholds estimated from D_{mean}. For PC-cells, thresholds without eye movements are similar to those estimated from D_{max}, but increase by up to a factor of two in the presence of ocular drift (Fig. 7.9B, gray bars). Without eye movements, D_{mean} has no meaning in MC-cells, as D can be only be estimated for the transient onset (therefore not shown). In the presence of drift movements however, thresholds also increase by a factor of about two compared to those calculated from D_{max}.

The difference between the results for D_{max} and D_{mean} may account for the differences found for detection and discrimination tasks (Harris and Fahle, 1995, 1996). The results suggest that *detection* of a vernier offset may require temporal integration over a prolonged time, while for a *discrimination* task, short intervals may suffice. In a discrimination task the observer knows that a vernier offset will exist and he/she only needs to decide about its side. The existing offset will bias D into one direction. Hence in principle any short peak in D would suffice to trigger a decision and it is conceivable that a short presentation time will suffice for this task leading most of the time to the correct decision. For a detection task, where it is a priori unclear if a non-zero vernier offset exists, the difficulty lies in the problem to unequivocally detect the zero-vernier case. In this case D oscillates around 0.5 and only longer integration times can reveal that there is indeed no bias to D, which would indicate an existing small vernier offset.

In summary, it appears that fixational eye movements should lead to performance deterioration in the central retina for a detection-task (effect on D_{mean}), which could possibly be tested by comparing vernier detection under retinally stabilised and normal conditions. On the other hand, thresholds for the MC-cell system improve for the discrimination measure D_{max}, when eye movements are present. Since the analysis method used here is model free, this effect should also be measurable at the level of individual MC-cells. To have any perceptual effect, too, it remains to be seen if there are conditions under which the MC-cell system could have a direct influence on vernier discrimination.

So far the results suggests that this seems unlikely, because generally thresholds for

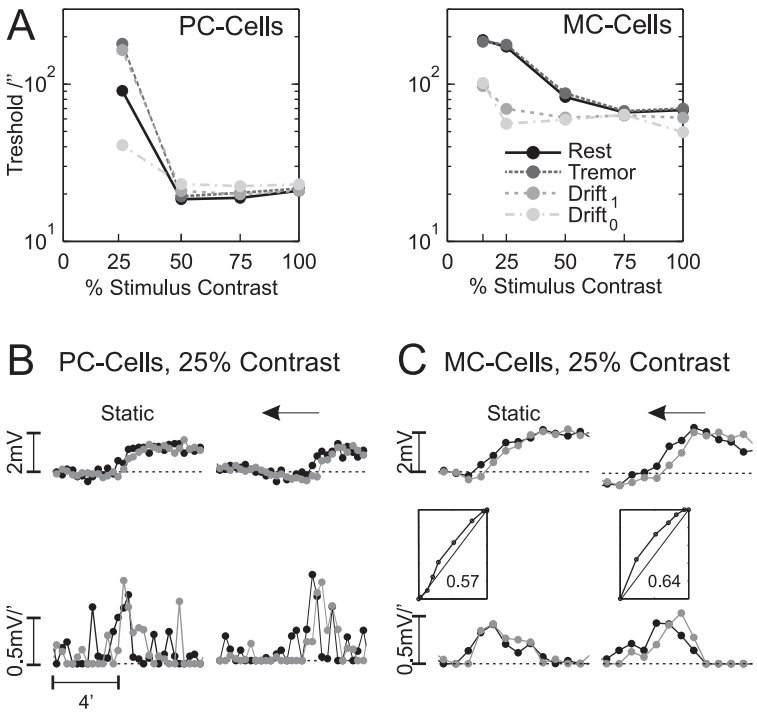

FIGURE 7.10: Contrast dependency of hyperacuity thresholds. A, Thresholds as a function of stimulus contrast for PC-cells (left) and MC-cell (right), estimated from a single 500ms stimulation, for all four eye movement conditions (see legend in right panel). Synaptic noise was included for both cell types. B and C, Snapshots of the average spatial population response of PC-cells and MC-cells (B,C, respectively, plots on top, responses to upper half of the stimulus are coloured black and to the lower half gray) and their spatial derivatives (bottom plots). Snapshots were taken for a static eye (left) and during a leftward motion (right, 2 deg/s) of the stimulus. Insets in C show the ROC-curve for each case and the corresponding detectability D. For PC-cells ROC-curves could not be estimated because of the noise in the activity profiles. As in Figure 7.3, the graphs represent the vertical average over 20 cell rows. In all examples, the vernier offset was $0.44'$ for PC-cells and $0.88'$ for MC-cells.

MC-cells are substantially higher than for PC-cells, which makes MC-cells apparently unsuitable to mediate hyperacuity. This is not surprising as MC-cells have larger receptive fields and are less densely distributed than PC-cells, which should result in a lower spatial precision. In the next two sections it will however be shown that this picture might need to be amended for low contrasts where the model predicts that under certain circumstances MC cells can reach and surpass the acuity of the PC cell system.

7.2.3.4 Eye Movements Improve Hyperacuity at Low Contrast

So far, the effects of eye movements on vernier acuity were investigated for 100% contrast stimuli. Experimental data indicates that vernier thresholds are little affected by

reduction of the stimulus contrast to values as low as 25% (Watt and Morgan, 1983; McKee, 1991). To assess the effect of contrast on hyperacuity in the model, thresholds were calculated from D_{max} at 15%, 25%, 50% and 75% contrast (Fig. 7.10A).

Without eye movements, thresholds remain approximately constant down to about 50% for PC-cells and 75% for MC-cells. Further reduction leads to an increase, and it was not possible to calculate a threshold at 15% contrast for PC-cells, as their response was dominated by noise.

The effect of eye movements was different in PC- and MC-cells. In PC-cells, fast drift movements ($Drift_0$) caused a reduction of the threshold at 25% contrast, but not to the values obtained for higher contrast. At 25% contrast, slow drift ($Drift_1$) and microtremor both led to a reduced performance compared to the resting eye. Hence the situation for PC-cells at low contrast seems equivocal and no real improvement can be expected from eye movements during normal viewing.

In MC-cells, a performance improvement for both types of drift movements is visible with approximately constant thresholds down to 25% contrast, corresponding to experimental results (Watt and Morgan, 1983; McKee, 1991). At 15%, the threshold was increased by a factor of about two. The effect of microtremor was negligible.

Two factors cause the observed behaviour. First, the bad performance of PC-cells is largely a consequence of synaptic noise. For low contrast values, their responses are weak, and noise begins to dominate the spatial derivative of the population response (Fig. 7.10B, left). Fast eye movements lead to an improvement (PRE-effect), which however is strongly masked by noise (Fig. 7.10B, right). Responses of MC-cells are stronger, and their population activity is less dominated by noise (Fig. 7.10C, left). The latter results from the coarser spatial sampling, which attenuates high frequency spatial noise. Most importantly however, the increased spatial sensitivity for moving stimuli (Fig. 7.10C, right) leads to the improved performance at reduced contrast, as described above (PRE-effect, see Fig. 7.7).

The experimental finding of constant hyperacuity thresholds down to 25% contrast (Watt and Morgan, 1983; McKee, 1991) could thus only be reproduced using MC-cell activity. Still, MC-cell thresholds are consistently higher as compared to PC-cells. Psychophysically this would predict a discontinuity in the psychometrical curve when gradually reducing stimulus contrast. At lower contrast, where predominantly the MC-cell system will respond, the psychometrical curve should sharply rise, which is inconsistent with experimental evidence.

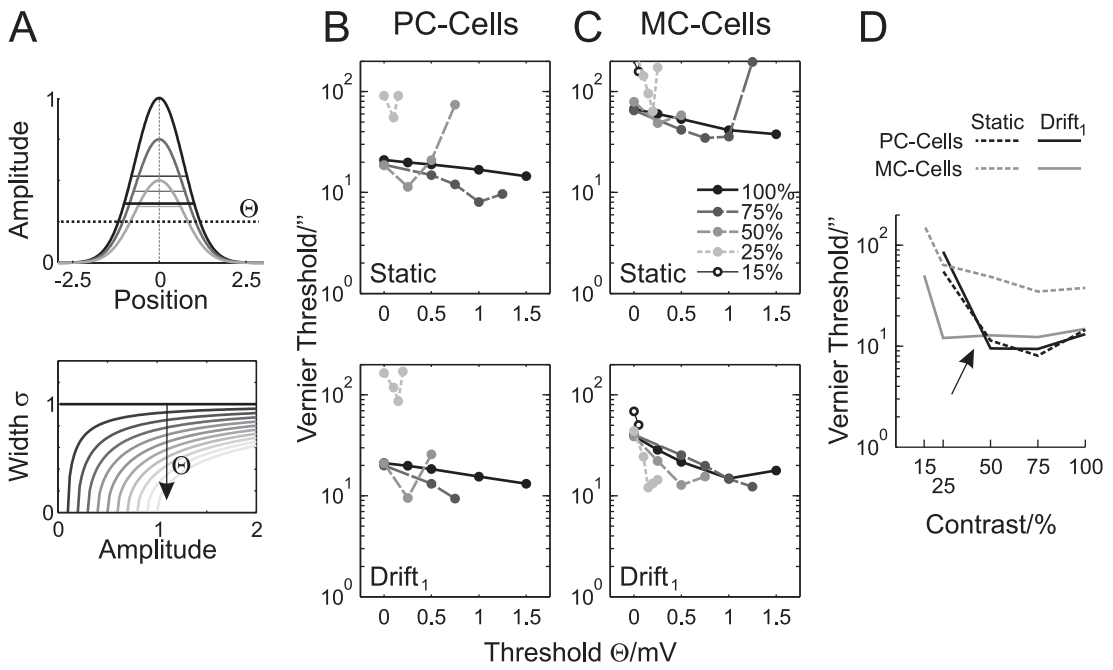

FIGURE 7.11: A, thresholding nonlinearity improves hyperacuity in MC-cells. A, Illustration of the effect of a threshold on the ROC analysis. The derivational activity profiles (as in Fig. 7.3C) were thresholded at various levels Θ above resting activity. This leads to a reduced width σ of the profiles. The width also depends on the amplitude of the distribution (top graph). This relation is plotted in the bottom graph for various values of Θ. The graph shows that increasing Θ (arrow) leads to a reduced σ at a constant amplitude. The ROC-analysis of the ganglion cell activity which yields the detectability D has an inverse dependency on σ, thus increasing the threshold Θ should leads to an increased detectability D. B,C, Vernier thresholds for PC- (B) and MC-cells (C) with and without eye movements ($Drift_1$) plotted as a function of the threshold Θ for different stimulus contrast values. All thresholds are for a single 500ms stimulus presentation. D, The smallest thresholds obtained in B and C, re-plotted as a function of stimulus contrast.

7.2.3.5 Possible Influence of Neuronal Firing Thresholds

This apparent inconsistency may be resolved (possibly at the cortical level) by the fact that the firing threshold in cortical cells is typically higher than the membrane potential at rest. This will lead to the so called "iceberg effect", which is essentially a sharpening of the tuning of neurons in the presence of a firing threshold (Anderson et al., 2000; Volgushev et al., 2000). Hence it is to be expected that at higher stages of the visual system, the linear analysis performed here needs to be augmented by a nonlinear, threshold based mechanism. This mechanism is implicitly already existent in the ROC analysis, where the derivates of the spatial population activity (Fig. 7.3C) were related to cortical edge detector signals. Hence it is straight-forward to apply a *firing threshold* to these peaks and perform the same kind of ROC analysis for different firing thresholds.

As a simple nonlinearity, a static threshold Θ, applied on the derivatives of the spatial response (Fig. 7.3C), was tested. The detectability D of the vernier offset depends inversely on the width of the derivational activity distribution, thus thresholding may indeed lead to an improved performance (Fig. 7.11A).

The results show that this threshold nonlinearity reduces hyperacuity thresholds both for PC- and MC-cells (Fig. 7.11B,C). Without eye movements, an overall improvement of about 40% for PC-cells was observed, independent of contrast (Fig. 7.11B, top). The optimal value of Θ however differs for each contrast level, which reflects differences in the peak amplitudes of the derivational activity profiles. At a high Θ's, vernier thresholds generally increased to very high (meaningless) values because the amplitude of the peaks was reduced to that of the intrinsic noise. MC-cells showed a similar behaviour, but with an improvement of around 50% (Fig. 7.11C, top).

Drift movements further reduced hyperacuity thresholds in particular for MC-cells (shown for slow drift $Drift_1$ in Fig. 7.11C, compare upper and lower graphs). For all contrast levels down to 25%, MC-cells now reached a threshold of about $20''$, similar to PC-cells at high contrast. Generally, at the optimal value for Θ for each contrast, the maximal improvement compared to the static case without threshold was about 76%. For PC-cells, the influence of eye movements is small, here only at 50% contrast a further improvement of about 2" is observed.

These results are in line with the notion of a minor role of PC-cells in hyperacuity tasks. At high contrast and in the presence of drift eye movements, PC- and MC-cells yield a similar performance (contrast range 50-100%, about $15''$, Fig. 7.11D). At lower contrast (15-25%), MC-cells are clearly superior to PC-cells in the presence of eye movements (Fig. 7.11D). In both cases however, the optimal firing threshold Θ depends on the contrast. A candidate mechanism for a variable firing threshold is cortical gain control, combined with a spiking threshold, which could lead to the required iceberg effect (Carandini et al., 1997). Furthermore, it may be speculated that a similar but slower adaptational mechanism could underlie perceptual learning observed in hyperacuity tasks (Fahle et al., 1995).

7.3 Summary and Discussion

The results of the preceding sections can be summarised as follows:

1. For high contrast stimuli, it was found for PC-cells that eye movements lead to a

substantial improvement of hyperacuity in the retinal periphery (Fig. 7.6A). An analysis of responses for slightly displaced stimuli revealed that eye movements strongly reduce aliasing effects, which result from neural undersampling, by continuously scanning the stimulus (SAR-effect, Fig. 7.5).

2. In the presence of drift eye movements, foveal hyperacuity was improved for MC- and PC-cells at reduced stimulus contrast levels (Fig. 7.10A). This effect, which is particularly strong in MC-cells, is initiated by the nonlinear properties of photoreceptor responses and leads to an increased spatial sensitivity of ganglion cells (PRE-effect, Fig. 7.7). It was further shown that the inclusion of a simple thresholding nonlinearity, which could arise from (cortical) firing thresholds, yields similar absolute detection thresholds for PC- and MC-cells, indicating a potential involvement of MC-cells in hyperacuity tasks (Fig. 7.11C). At reduced stimulus contrast values below 50%, the spatial precision of the population response of MC-cells in the presence of drift movements is substantially higher than the of PC-cell response (Fig. 7.11D). Thus, at reduced contrast hyperacuity is possibly solely mediated by MC-cells.

These results were obtained by investigating the ocular microtremor and two types of drift movement. The microtremor in isolation had no effect on hyperacuity tasks, because its movements are too small and fast to elicit strong responses in ganglion cells (Fig. 6.2C). While an influence of microtremor on ganglion cell responses was visible, when superimposed on drift movements, it did not significantly contribute to the effects described here. A comparison of the result further shows that different characteristics of drift movement could yield a different performance, which may, in part, explain differences found between subjects.

7.3.1 Spatial Averaging Induced Aliasing Reduction

This work demonstrated, for peripheral PC-cells and high stimulus contrast, that fixational eye movements could remove spatial aliasing effects. This effect relies strongly on the amplitude of the eye movements, which have to be sufficiently large to shift the stimulus across two adjacent receptive fields into regions with higher sensitivity to vernier offsets. Hence in the far periphery, which was not considered here, the amplitude of slow drift movements should no longer be sufficient to counter aliasing. On the other hand, this effect could, in the same way, also be caused by head-movements and microsaccades, which were also not considered here.

Therefore, the results can, while in good agreement with psychophysical data, only provide evidence for the existence of this effect, and a psychophysical investigation may possibly yield quantitatively slightly different results. In addition, the role of MC-cells was not considered here. As the results for low-contrast stimuli suggest a less important role for PC-cells in hyperacuity tasks, it may be possible that in an experimental situation this effect is mainly determined by the different receptive field properties of MC-cells.

Based on theoretical considerations, this effect was also predicted by Fahle and Poggio (1981), and experimental results by Packer and Williams (1992) suggested a related effect. They reported that contrast detection thresholds for high spatial frequency stimuli (100cpd, interferometrically projected onto the retina), which are only visible as moire patterns, were similar for very short ($1 - 4ms$) and long ($> 500ms$) presentation durations, but significantly elevated for intermediate durations. It was suggested that eye movements interfere with stimulus detection, whose influence is reduced for a very brief stimulus presentation. Equally, for long presentation times, it is more likely that the eyes are stationary for a certain period, which again would allow detection. Hence the present results may represent the reverse case, where detectability improves when eye movements remove aliasing.

7.3.2 Phasic Resolution Enhancement

It has been suggested earlier that MC-cells can provide a higher spatial accuracy than PC-cells (Lee et al., 1993; Rüttiger et al., 2002). The present results confirm this notion, which contradicts the traditional view that high spatial acuity is mediated by the denser PC-cell population. The results further indicate that the performance of MC-cells is little affected by velocities up to 4 deg/s, where PC-cell performance was poor. This is in good agreement with the finding of constant hyperacuity thresholds for stimuli moving at this velocity (Westheimer and McKee, 1975). A possible involvement of eye movements is also hinted in the data by Westheimer and McKee (1977), who reported improved hyperacuity for moving stimuli as compared to very brief presentations.

7.3.3 Assumptions of the Model

The performance of ganglion cells in a hyperacuity task was investigated on the level of the membrane potential after adding noise which simulates the variability of their spiking response. Only On-center ganglion cells were studied. This hybrid approach was

motivated by the fact that the sub-threshold activity of cortical neurons is derived, via the LGN, from the spiking response of both On- and Off-center ganglion cells. Cortical neurons thus have access to the full dynamic range of the retina, which is not present in the spiking response of a single ganglion cell class. Therefore, an investigation of the ganglion cell membrane potential, which also accounts for the variability found in the spiking response, appears to be a suitable way to assess the influence and limiting factors of retinal processing on cortical responses.

Including a realistic spiking mechanism into the model would also have complicated the analysis of the responses, because the results presented here are based on single stimulus presentations, without averaging cross multiple trials. Averaging as a method to analyse spiking responses would therefore have been unsuitable, as it could mask the real intrinsic noise. An alternative would have been to postulate a cortical "readout" mechanism for retinal spikes, which however automatically introduces a new set of problematic parameters. In addition, the spiking mechanism in ganglion cells is known to by very precise (van Rossum et al., 2003; Demb et al., 2004), and could therefore be omitted without a great loss of generality.

The model further ignores the well characterised asymmetry between On- and Off-center ganglion cell responses (Chichilnisky and Kalmar, 2002; Zaghloul et al., 2003). Instead, the influence of this and other possible nonlinearities, such as spiking thresholds in the upstream pathways or nonlinear summation in the cortex (Heeger, 1991; Carandini et al., 1997; Carandini and Ferster, 2000), were approximated using a single, static nonlinearity. Therefore, the hyperacuity thresholds calculated in this chapter can only be an approximation of psychophysically measured values. Of more significance are therefore the relative differences between the different conditions investigated, in particular those assessing the influence of eye movements, as it appears unlikely that they will be strongly affected by these factors.

In conclusion, it should be noted that the results are generally in very good agreement with psychophysical data. Furthermore, parameter variations of single neurons (e.g. reversal potentials or time constants) in a physiologically plausible range typically had an evanescent influence on the results. The only parameters which were sensitive to changes were those describing cell densities and receptive field dimensions, in particular for ganglion cells. Hence it appears that the simplification chosen here were appropriate in the context of the posed questions.

7.3.4 Experimental Predictions

The analysis method used in this work was designed to relate the activity of ganglion cell populations to psychophysical thresholds. Therefore, the results are experimentally testable on both levels.

For an electrophysiological experiment, the ideal observer analysis of ganglion cell population activity could be redesigned for single cell recording to directly reproduce our findings. Responses may be recorded from a single neuron and re-mapped to obtain spatiotemporal activity profiles equivalent to ours. Eye micromovements may be simulated by shifting the stimulus accordingly.

A direct psychophysical confirmation of the results may be achieved by comparing hyperacuity thresholds during normal fixation and for retinally stabilised stimuli. However, retinal image stabilisation is technically demanding (Steinman and Levinson, 1990) and is always accompanied by image fatigue (Ditchburn and Ginsborg, 1953; Riggs et al., 1953). For instance, a comparison of effects of eye movements in the fovea and periphery, as predicted here, may be occluded by the differences in the strength of image fatigue as a result of imprecise stabilisation (Gerrits, 1978). But more recent work by Rucci and Desbordes (2003) appears to have solved the problem of creating comparable conditions with and without eye movements. Another possible method to circumvent these difficulties may be to monitor fixational eye movements during an experiment and subsequently analyse individual trials. Finally, it may be possible to compare hyperacuity for normal vision with that in afterimages. This method however would require a careful matching of both conditions, which may be difficult to achieve experimentally.

An attractive indirect method to confirm the results presented here appears to be to comparison the effect of different stimulus presentation durations. The influence of eye movements is reduced for a brief presentation, so they should contribute less to psychophysical performance. Accordingly, any influence of eye movements should be visible as increased thresholds for shorter presentation times.

The analysis of the simulated responses shows that this effect should be measurable for PC-cells, as the detectability for vernier offsets is highly variable in the presence of eye movements (Fig. 7.4C-E, Fig. 7.8A). For simulated MC-cells however, this effect is much weaker, and eye movements lead to a relatively constant detectability values during a single stimulus presentation (Fig. 7.4F, Fig. 7.8B). Therefore, if hyperacuity is mediated by MC-cells, it is expected that presentation time only matters on very short time scales in the order of tens of milliseconds.

Eye movements were indeed suggested as an explanation for reduced hyperacuity thresholds for longer stimulus durations (Morgan et al., 1983; Yap et al., 1987). But in general, these effects appear to be very small (Westheimer and Pettet, 1990). Therefore, psychophysical experiments can not confirm the present results for PC-cells, but are more consistent with the behaviour of MC-cells as reported here.

This conclusion is further supported by the finding that hyperacuity thresholds are not affected by stimulus velocities up to 4 deg/s (Westheimer and McKee, 1975). Furthermore, a slight improvement was reported for a moving stimulus when compared to a very brief presentation (Westheimer and McKee, 1977). Again, these findings are consistent with the results for MC-cells, but difficult to explain on the basis of PC-cell activity.

This discussion illustrates that it may be difficult to address the present findings using variable stimulus presentation times. The high contrast gain of primate MC-cells however may allow a systematic comparison of hyperacuity thresholds under conditions of strongly reduced mean illumination, where PC-cell responses are weak (Purpura et al., 1988). Under these conditions, integration times are prolonged (Barlow and Levick, 1969) and hence fast eye movements may be less effective in driving MC-cells. This should further reduce the influence of eye movements for short stimulus presentation times. Consistent with this idea, it was reported that at low luminance hyperacuity performance could be improved by moving the stimulus (Westheimer and McKee, 1977).

7.3.5 Influence of Eye Micromovements in Detection Tasks

The results of this chapter augment the ideas of Averill and Weymouth (1925) and Marshall and Talbot (1942). At the time their publications appeared, little quantitative data was available regarding fixational eye micromovements and retinal anatomy. As already pointed out by Barlow (1952), the results confirm that the magnitude of the ocular microtremor is not compatible with Marshall and Talbot's suggestions for foveal hyperacuity. The results however suggest that ocular drift movements can have a significant influence on hyperacuity, both in the fovea and in the retinal periphery, where neural undersampling is strong. A possible role of transient neural responses was already emphasised by Marshall and Talbot (1942), an assumption which is consistent with the present results, in particular for stimuli at low contrast.

While the experimental data to date can not directly prove an influence of eye movements on hyperacuity, a number of studies provide indirect evidence that is compatible with the present data. For instance, eye movements were suggested as explanation for

reduced hyperacuity thresholds for prolonged stimulus durations (Morgan et al., 1983; Yap et al., 1987) and moving stimuli (Westheimer and McKee, 1975, 1977). Furthermore, some studies mentioned in Chapter 6 demonstrated an influence of eye movements in other psychophysical experimental paradigms (i.e., Clowes (1962) for hue discrimination and Rucci and Desbordes (2003) for orientation discrimination). In addition, the following chapter shows a situation where fixational eye movements could lead to modification of retinal ganglion cell activity which appears to have a perceptual correlate.

In conclusion, substantial evidence is now accumulating that fixational eye movements can have an important influence on visual perception. This seems to be the case in particular in the proximity of psychophysical thresholds.

Chapter 8

The Aperture Problem in the Retina

In the previous two chapters, it was shown how the combination of fixational eye movements and retinal nonlinearities can improve detection of stimuli near threshold. A simple analysis of the population response of simulated ganglion cells revealed what an observer would report when presented a typical hyperacuity stimulus. However, while the presence of a vernier offset would be the conscious percept of the observer, the individual features of the ganglion cell responses, i.e. those which lead to an improved detectability in the presence of eye movements, are invisible. Instead they disappear in higher visual areas due to integration and other mechanisms that facilitate the interpretation of a stimulus.

Another example of this kind is the famous *aperture problem* (Wallach, 1935; Hildreth and Koch, 1987), as illustrated in Figure 8.1. The area where a neuron in the visual system is excitable by a stimulus is constrained by the finite dimensions of its receptive field, which is in a sense a window or aperture to the outer world. For example, when an elongated stimulus (e.g. a long bar) is passing over a visual receptive field, the neuron will only respond to the motion component which is orthogonal to the orientation of the stimulus (Fig. 8.1, thin arrows), while axial components do not contribute. This effect occurs essentially for all cells at the lower visual processing stages where receptive fields are small. It considerably limits the ability of individual neurons to reliably encode stimulus properties. On the other hand, the activity of a subset of these neurons usually provides sufficient information to resolve these ambiguities at higher levels. It has, for instance, been demonstrated that the aperture problem is resolved by spatiotemporal integration in the motion sensitive area MT (Pack and Born, 2001).

While this is only one example, large scale integration effects are thought to be generally involved in the generation of stable visual percepts and the individual cell properties

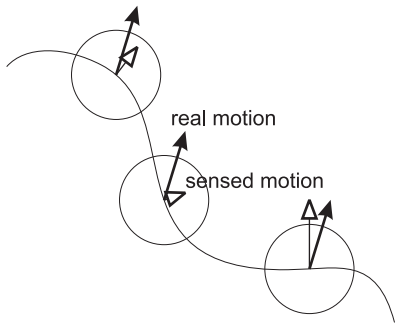

FIGURE 8.1: Illustration of the aperture problem. The circles represent receptive fields of visual neurons at different locations relative to a moving stimulus (line). The global motion of the stimulus is indicated by the thick arrows, but the spatially restricted receptive fields can only sense the orthogonal motion component at each location (thin arrows).

over which integration takes place remain, therefore, normally hidden. As a consequence even the cellular properties of dominant visual processing streams, the parvo- (MC) or magnocellular (PC) systems, are not easily discovered at the perceptual level anymore.

In this chapter, two visual percepts will be described which seem to be directly related to the properties of the first processing stages in the magnocellular pathway. It was found that a stimulus with large homogeneous structures leads to the expression of the aperture problem at the level of retinal ganglion cells, which can not be resolved by later integrative mechanisms. Secondly, it will be shown show that MC-cell nonlinearities can lead to spatial retinal activity patterns that do not correspond to the physical properties of the stimulus, but nevertheless may have a direct perceptual correlate.

8.1 Materials and Methods

8.1.1 Model Study

Model Retina As in the previous chapter, the model aims to simulate the parvocellular and magnocellular On-center channels of the primate retina under cone-dominated illumination conditions. Connectivity patterns and densities were adjusted to reproduce the anatomy of the human fovea. All model parameters were identical to those given for the fovea in Chapter 7, Section 7.1.

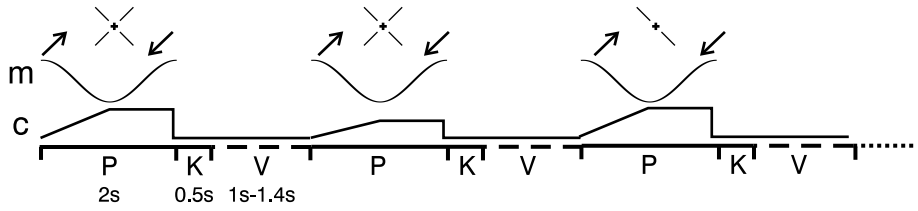

FIGURE 8.2: The protocol for the psychophysical experiment. During presentation (P, 2 s), the stimulus (shown on top) was moving in $+45°$ direction with the waveform of a cosine (traces labelled m). During the first half cycle of the cosine, contrast was gradually increased to the test level (trace labelled c). During the presentation and for an additional interval (K), the subject's response was recorded. This was followed by a variable blank interval (V).

Stimulus A static star shaped stimulus with symmetrically radiating lines at 100% contrast was presented to the model. It had a diameter of $110'$ and consisted of 24 bars, each $2.86''$ wide.

8.1.2 Psychophysics

Two different experimental conditions were used. First, in a qualitative survey 35 naive subjects were presented with the star shaped stimulus and asked to carefully fixate the center (fixation of a red circle). The stimulus was presented either on a CRT (n=22) or TFT screen (n=13). The stimulus was shown at high contrast, and the background luminance varied from 10-100 cd/m^2 (indoor lighting). Subjects were allowed to freely move in front of the screen, i.e. to view from different distances. They were allowed to view the stimulus as long as they wanted. Then they were asked to provide a verbal description of their percepts, which was transcribed. When a subject had not reported the effects relevant for this work, they were explicitly asked for them. In some cases, subjects then confirmed the percept (n=1 for fading, n=5 for splitting).

In the second, quantitative experiment, twelve adult subjects of both sexes with normal (5) or corrected (7) vision participated. Ten were naive to the purpose of the experiment. Stimuli were generated on a ATI Rage graphics card and presented on a Panasonic PanaSync S110 monitor with a frame rate of 91 Hz. Subjects were seated at a distance of 92 cm from the screen and had to use a chin rest that prevented head movements. During the whole experiment, subjects had to view the stimuli monocularly. One eye was covered with an eye patch.

Two different stimuli were presented, a tilted cross or a tilted line. The diameter of the stimuli was $16.6°$, and the inner $26'$ were left blank. Thickness of all lines was $1.3'$ (see

Fig. 8.2 top). The background luminance on the screen was adjusted to 5 cd/m^2. Under these conditions, visual latencies are higher (Maunsell and Gibson, 1992) and longer integration times are necessary for stimulus detection than under photopic illumination conditions (Barlow and Levick, 1969). As a consequence, small and fast eye movements should have a smaller influence on detection, and the response should be dominated by the stimulus motion. During the experiment, subjects were instructed to carefully fixate a small ($3.9'$), red fixation cross that was centred on the screen.

The experiment consisted of two parts. In the first part, repeated ten times, the detection threshold for stimulus contrast was estimated for each subject. The contrast of a static, tilted cross was slowly increased (0.23% contrast increase per 100ms). The subject had to press a key as soon as either the whole or a part of the cross became visible. The mean contrast threshold for all subjects estimated by this method was $3.6\% \pm 1.6\%$.

In the second part (protocol depicted in Fig. 8.2), either the tilted cross or the line was presented at six different contrast levels (-0.6%, -0.2%, 0%, 0.2%, 0.6% and 1.6% relative to the previously estimated threshold). The stimulus was initially shifted $13'$ to the top right along the $+45°$ axis, relative to the fixation cross and then moved once back and forth sinusoidally along this axis with a total displacement of $26'$ over a time of 2 s. During the first half wave (1 s), the contrast was increased from zero to test contrast, while during the second half (1 s) the contrast was kept constant. During (2 s) and up to 0.5 s after the stimulus presentation subjects had to report by pressing a key when they saw a moving line or cross. Recorded reaction times showed that this was sufficient time for all subjects.

The experiment consisted of 120 randomly shuffled trials which comprise two different stimulus conditions (cross or line) and six different contrast levels. The interval between trials was randomly varied between 1 s and 1.4 s. In preliminary experiments, we found that prolonged fixation leads to drastically increased thresholds and reduced reaction times. To ensure a constant performance, the subjects were given a break after 40 and 80 trials to relax the eyes. Under these conditions, performance and reaction times were constant across trials.

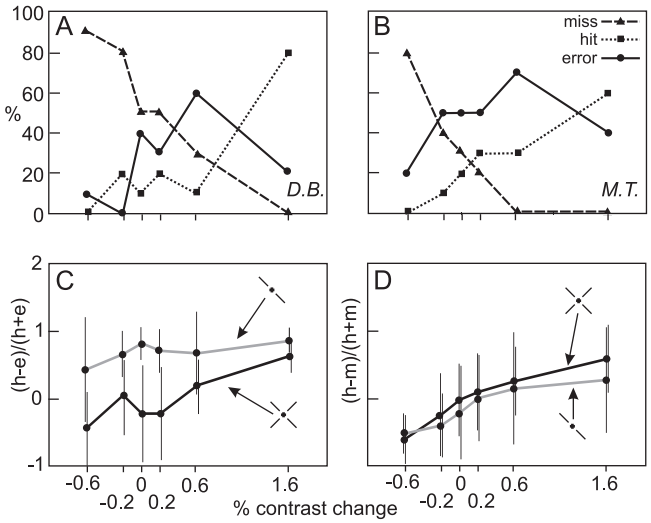

FIGURE 8.3: Line-fading can be induced by motion. (A,B) Percentage of misses (blue lines, triangles), correct (black lines, squares) and erroneous responses (red lines, circles) of two subjects who were presented with a moving oblique cross at low contrast, plotted as a function of stimulus contrast. Correct responses refers to the reporting of a moving cross, false responses to the reporting of a moving line. Contrast values are given relative to the static detection threshold for each subject (2.6% for both subjects). (C) Pooled data for 12 subjects as a function of contrast. Performance is given as relative difference of hits (h) and erroneous responses (e). The black curve shows these values for the control experiment, where only a line was shown, and the red curve for the case where a cross was shown. Contrast values are expressed as in (A,B). (D) as (C), but pooled relative difference of hits (h) and missed stimuli (m) for both cases.

8.2 Results

8.2.1 Psychophysical Correlates of the MC-cell Aperture Problem

In a qualitative assessment, this star stimulus was presented to 35 naive subjects asking them to provide a verbal description of their percept during fixation. All subjects reported that wedge-shaped sectors of this stimulus begin to fade; most often in two wedges opposite to each other. The location of the fading wedges rotates randomly, but not always all orientations are equally affected. Most observers reported that the fading is stronger in an oblique axis. This may be a consequence of the oblique effect (Appelle, 1972), according to which horizontally and vertically oriented structures are better seen than oblique structures. A similar effect has been reported earlier for a similar stimulus known as the MacKay Illusion (see Fig. 8.8C; Pirenne et al., 1958).

In a second, quantitative experiment the hypothesis that the fading percept is a consequence of the aperture problem was tested by asking if it can be induced by moving stimuli. To this end an oblique cross or line stimulus was moved with an amplitude

and velocity similar to slow drift movements, while subjects (N=12) had to carefully fixate a static dot. This procedure was chosen to actively induce a percept related to the aperture problem by biasing the motion of the stimulus on the retinal surface into one particular direction. Several contrast levels close to static detection threshold were used, which were low enough to prevent strong stimulation of the PC-cell system. To avoid onset-transients, the stimulus was gradually faded in. Observers were asked to decide if they saw a moving cross or a line by pressing two different keys. The experiment was purposefully not set up as a two-alternative forced choice test, because observers had not to be cued before the onset of a stimulus, which may trigger anticipatory eye movements.

In Figure 8.3A,B the results obtained with two naive subjects (D.B. and M.T.) are shown, when the cross stimulus was presented. "Hit" refers to the correct key-press, "Error" to the key-press that indicated that the subject has seen a line instead of the actually presented cross and "Miss" shows how many times no response was recorded. As expected, with increasing contrast both subjects have less misses and more hits. Interestingly, close to the static detection threshold both of them produced many errors, indicating that from the cross only the orthogonally moving line remained visible, while the axially moving line could not be detected.

Panels C and D in Figure 8.3 show the pooled performance of twelve subjects, comparing the cross-presentation with the line-presentation, which serves as a control. The measure $(h-e)/(h+e)$ yields one if only hits h are obtained and minus one for errors e only. Cross-presentation leads to a prevalence of negative values at lower contrasts, indicating that observers more often only saw a line (Fig. 8.3C). For all contrasts except the highest, values obtained for cross presentations are significantly lower than for line-presentation ($p < 0.027$, one-tailed t-test). The strongest effect occurs at the estimated threshold contrast for each subject ($p < 0.0001$, one-tailed t-test). In Figure 8.3D hits are compared with misses for both conditions. The obtained curves are not significantly different, indicating that the stimuli did not introduce any detection bias as such.

Taken together, these results suggest that the fading effect found for the star-stimulus could be a direct consequence of on-axis motion of lines of the stimulus, as suggested by the simulations. Biasing retinal motion in one direction successfully rendered the on-axis stimulus elements invisible. The effect occurs even for the long stimulus presentation times used here, however only at very low contrast. A simple explanation for this strong contrast dependency is that at higher contrast fixational eye movements lead to multiple transient responses in ganglion cells during those 2 seconds, which facilitate detection. At low contrasts, fixational eye movements alone do no longer lead to the

required level neural activation to allow detection. During fixation of the star-stimulus, fixational eye movements are the only source of retinal image motion, hence when transient responses have decayed during motion along one axis (for $> 40 - 60ms$), no further activity is triggered which could signal the presence of a stimulus.

8.2.2 The Retinal Expression of the Aperture Problem

The above results suggest that the line-fading may be a property of the magnocellular pathway and that it may be related to the aperture-problem. It was however not possible to directly confirm this hypothesis by monitoring eye movements during these experiments. Instead, the model retina was used to test whether this effect is visible in the population activity of retinal neurons.

Spatial activity patterns of populations of simulated PC- and MC-cells during fixation of a star shaped stimulus (Figure 8.4A) are shown in Figure 8.4. Colour panels on top (Figure 8.4C,D) show parvocellular, those on the bottom (E,F) magnocellular ganglion cell responses[1] . The panels show the membrane potential of each ganglion cell, red indicates a depolarisation and blue a hyperpolarisation relative to the resting potential. Depolarisations thus reflect the activity that the spikes of On-center cells transmit to the higher visual areas of the brain[2].

Two snapshots were taken at the different times t_1 (Fig. 8.4C,E) and t_2 (Fig. 8.4D,F), as indicated in Figure 8.4B, where the horizontal and vertical eye movements are shown. The comparison shows that fixational eye movements lead to a gradual change of the activity of individual ganglion cells consistent the motion of the stimulus across the population. For both cell types, the bars of the stimulus cause a strong depolarisation. The motion of the stimulus leads to a tailing hyperpolarisation as the receptive field surround of the neurons is stimulated.

The main effect of fixational eye movements is visible in Figure 8.4C-F and is very similar to that seen in the psychophysical experiments. The activity of both cell types is reduced in two sectors, which are located along one axis of the stimulus. The orientation of this axis gradually changes as the direction of the eye movements changes. This effect is much more pronounced for the MC- than for the PC-cells (compare panels E, F and C,D). In PC-cells, the membrane potential in the sectors with a reduced response

[1]Films of the spatiotemporal activity patterns for PC- and MC-cells are available at `http://www.cn.stir.ac.uk/~mhh1/Illusion`, Figure S1.

[2]Films of the resulting population firing rate are available at `http://www.cn.stir.ac.uk/~mhh1/Illusion`, Figure S2.

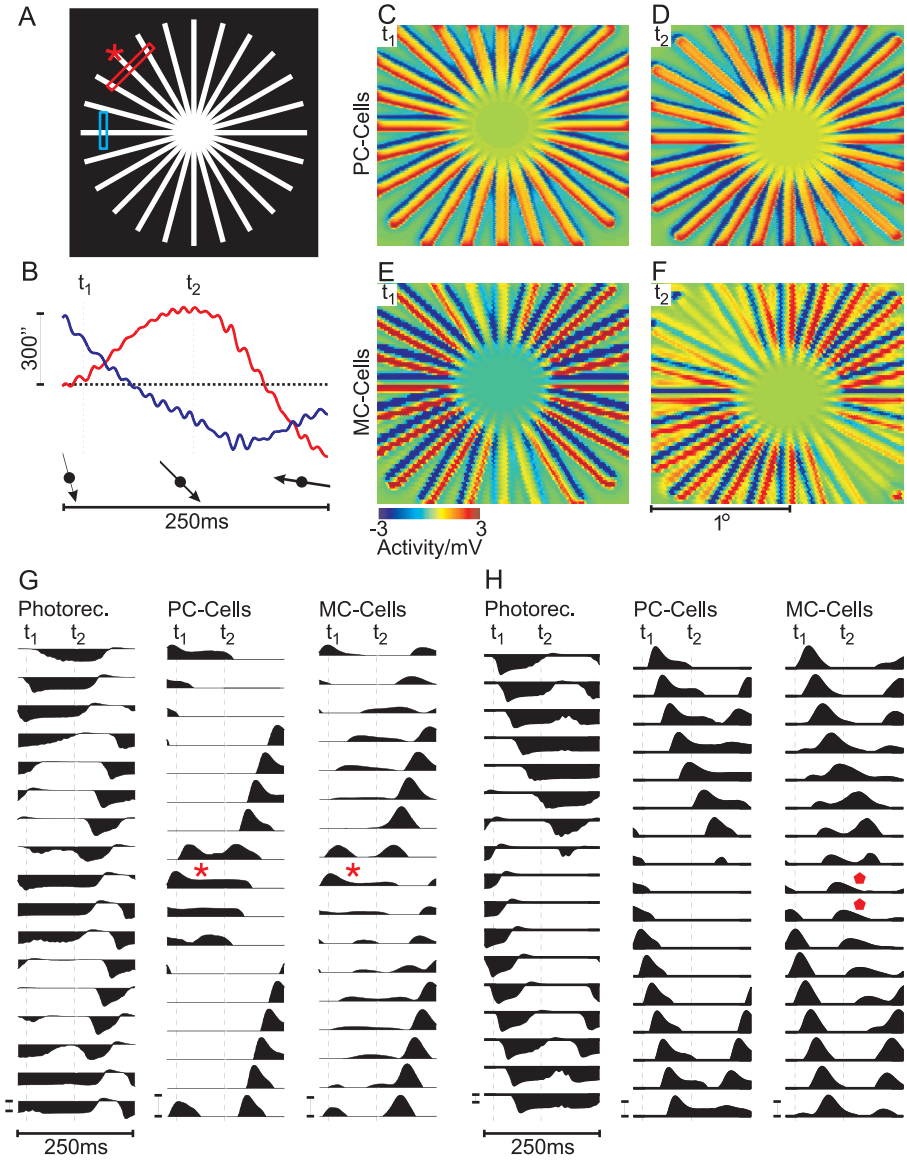

FIGURE 8.4: Population activity of retinal ganglion cells during presentation of a star-shaped stimulus. (A) Schematic drawing of the stimulus. The bars indicate where the single cell activity in panels G (red) and H (blue) was recorded. (B) Simulated horizontal (red) and vertical (blue) eye movements, t_1 and t_2 indicate where the snapshots in C,D and E,F were taken. The relative combined motion direction is indicated by arrows. (C-F) Spatial activity of the population of PC-cells (C and D) and MC-cells (E and F), taken at t_1 and t_2, as indicated in (B). The membrane potential is colour-coded from -3 to $+3$ mV. (G) Activity of single photoreceptors, PC- and MC-cells at a location where axial fading is visible at time t_2 (red bar in A). Time points t_1 and t_2 are indicated by vertical lines. The asterisks indicates where fading occurs in PC- and MC-cells. This location is also marked by an asterisk in (A). (H) as (G), but illustrating the line splitting. Responses were taken from the region marked by a blue bar in (A). Diamonds indicate where splitting is visible. Both in (G) and (H), ganglion cell responses were clipped below resting potential to enhance visibility of the effects. Calibration bars indicate 3 mV membrane potential.

is about 50% compared to the peak activity. In MC-cells, the responses in these sectors are reduced almost to resting potential.

The question arises how eye-movements and fading-direction are related. In the transition from the first snapshot at t_1 to the second at t_2, eye-movement direction has changed from approximately vertical to bottom-right as indicated by the small arrows in panel B. Hence in both situations fading occurs in sectors parallel to the eye-movement direction. In general it can be observed that this type of on-axis fading occurs as soon as the axial eye-motion vector remains the same for more than 40 ms (see films).

The diagrams in panel G of this figure show the activity of the modeled photoreceptors, PC-cells and MC-cells for 17 cells taken from the cross-section marked by the red bar in the schematic panel A. The receptive fields of the cells in the middle row (Fig. 8.4G, asterisks) are those that are stimulated by the marked line of the star-stimulus (asterisk in Fig. 8.4A). Motion of this line in the interval from t_1 to t_2 is approximately axial, thus the spatial stimulation of the corresponding receptive fields does not change much for this time. As a consequence it was found that the transient response mostly decays during this time, an effect which is much weaker in PC-cells. This leads to the observed strong activity drop in the corresponding MC-cell sector in panel D.

The drop in activity is smaller for the PC-cell sector (Fig. 8.4B), because PC-cells are less transient than MC-cells. It is also partly due to the fact that PC-cell receptive fields are smaller than those of the topographically corresponding MC-cells. As a consequence the small amplitude of fast eye movements such as the microtremor is often sufficient to lead to off- axis shifts of the fading stimulus line relative to the PC-cell receptive fields. This can lead to an additional drive of the PC-cells, effectively preventing them from any stronger adaptation.

8.2.3 The Influence of Retinal Nonlinearities on MC-Cell Responses

In addition to sectorial fading a second, subtle effect was discovered by analysing the responses from the model. Figure 8.4 shows this type of effect in the MC-cell colour panels. The snapshot taken at t_2 (Fig. 8.4F) shows that some lines display a spatially separated activity towards the periphery and the activity profile appears to be split at these locations. Instead of the regular pattern, where red (or yellow) depolarising lines alternate with blue hyperpolarising lines, one finds here pairs of depolarising lines next to each other. This effect only occurs in the MC-cell population, PC-cell activity never

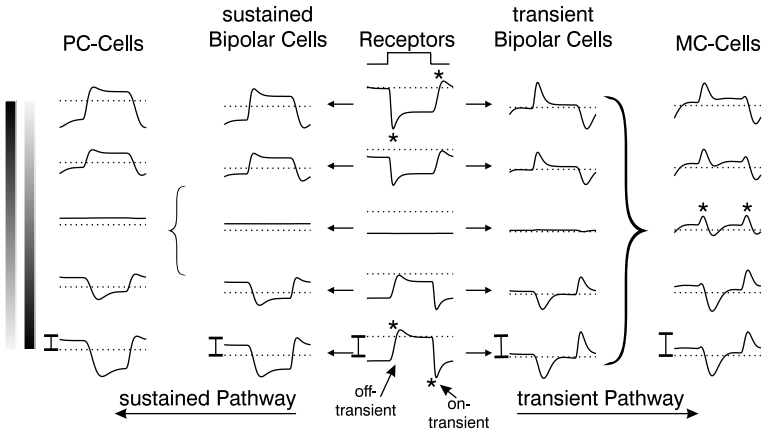

FIGURE 8.5: Illustration of frequency-doubling responses in MC-cells during contrast reversal of a grating. The stimulus is indicated on the left (a grating at 11 cycles/degree). Simulated responses (200ms) of photoreceptors, sustained and transient bipolar cells and PC- and MC-cells are shown at five different spatial phases relative to the stimulus. For cells in the center, the net stimulation does not change during contrast reversal, but the MC-cell response shows phasic depolarisations at each reversal (asterisks). In photoreceptors one finds that a hyperpolarising response to light onset produces a shaper and higher on-transient than the equivalent transient to light offset (off-transient), which is less strong and temporally more long lasting (asterisks). This asymmetry is amplified in transient bipolar cells via amacrine cells leading to a strong differential characteristic of the targeted MC-cells. Due to their smaller receptive fields and weaker asymmetries in bipolar cell responses, frequency-doubling is not visible in PC-cells.

shows this line-splitting[3].

A comparison of the membrane-potential traces details this observation. Figure 8.4H shows membrane-potential traces taken from the cross-section marked by the blue bar in panel A. Photoreceptors and PC-cells show two moving, spatially separated activity peaks, which correspond to two lines of the star stimulus. The same peaks are found in the MC-cells. In between both real peaks, the MC-cells in the middle rows of this panel (H) show a smaller additional activity peak (marked by the diamonds), which does not correspond to the location of any stimulus line.

The model suggests that the splitting effect directly arises from the nonlinear properties of MC-cells which also leads to frequency-doubling for contrast reversed sine gratings (see Chapter 5, Fig. 8.5 illustrates frequency-doubling for simulated MC-cells).

What happens during fixation of the star stimulus? In this case fixational eye-movements often displace two stimulus lines across opposite parts of an MC-cell receptive field. Hence, such a situation creates competing on- and off-transients within the MC-receptive

[3]See also the films available at `http://www.cn.stir.ac.uk/~mhh1/Illusion`, Figs. S1 and S2.

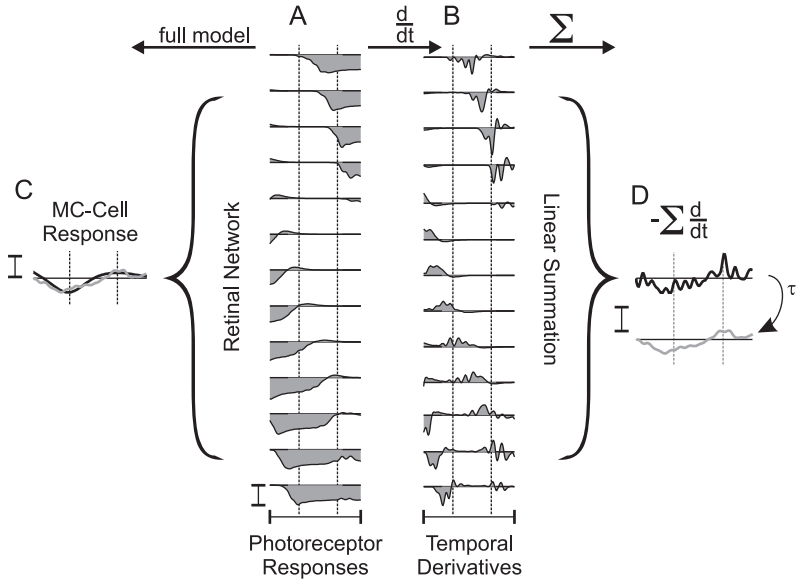

FIGURE 8.6: Frequency-doubling in MC-cells causes the splitting percept. (A) Simulated responses (150ms) of photoreceptors; (B) their temporal derivatives calculated numerically and (C) MC-cell responses to two lines of the star-shaped stimulus calculated with the full model. All calibration bars indicate 5 mV. The central $7^{'}$ of the receptive field of this cell are depicted by the brackets. The response of the differentiated signals (B) summed across the bracket are shown in (D, blue). The red line in (D) was obtained from low-pass filtering ($\tau = 4ms$) the blue line. It matches the response from the full model (see overlay in C). This shows that the "ghost" activity which leads to the line splitting effect essentially arises from the sum of differentiated photoreceptors responses in a similar way as the frequency-doubling effect as explained in Figure 8.5. Furthermore, it shows that an MC-cell response may to a first approximation (at a fixed contrast) be calculated by differentiating, summing and smoothing of the photoreceptor responses within its receptive field.

field. This is shown in Figure 8.6: The photoreceptor responses in A correspond to a case where one bar leaves and the other enters the MC-receptive field. Panel B shows numerically differentiated photoreceptor responses, hence their transients, which is a simplification that in this form is not computed by the full model. However, this representation is sufficient to explain what happens: Since on- and off-transients are not balanced, the above described amplification and integration across the wide MC-receptive field (panel C) will lead to some remaining "ghost" activity, centred at a retinal location where no physical stimulus is present.

The noisy line on top in panel D was obtained by summing all differentiated photoreceptor responses (B) within the bracket. Its smoothed version is shown in the middle of panel D after applying a low-pass filter. This curve was also superimposed on the MC-cell's activity profile in panel C and matches the full-model's response well. This indicates that in a first approximation line-splitting can be understood from the ampli-

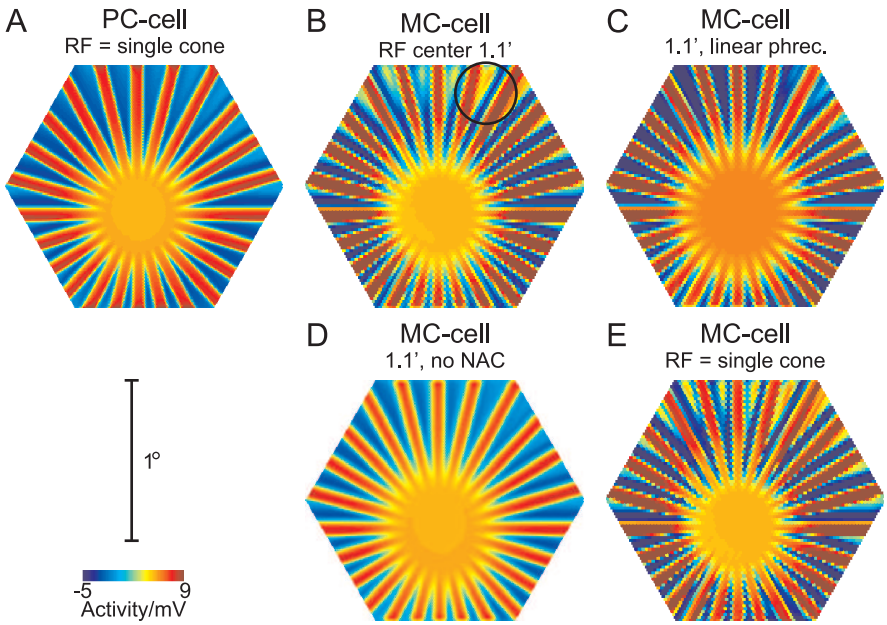

FIGURE 8.7: Effect of modifications of the model on the line-splitting effect. Each panel shows a snapshot of the ganglion cell population response during stimulation with the star-shaped stimulus at saturating photoreceptor luminance (100% contrast, diameter $91'$, bar width $2.4''$). A, B, responses for the full PC- and MC-cell model, respectively. The circle in B indicates a location where line-splitting occurs. C, MC-cell responses after replacing the original photoreceptor model with a linear model. D, MC-cell response with an inactivated nested amacrine circuit. E, Response for MC-cells, when the receptive field centre consists of a single cone.

fication and summing of differentiated photoreceptor responses. Consequentially, no line-splitting occurs in the model as soon as the activity of the nested amacrine circuit, which leads to the amplification, is blocked or when a linear photoreceptor model, which does not produce transients, is used (data not shown).

8.2.4 Differential Effects of Different Sources of Nonlinearities for Line-Splitting

To investigate the role of the different factors contributing to the nonlinear behaviour of simulated MC-cells to the line-splitting effect, Figure 8.7 shows snapshots of the ganglion cell population response for the original model and after certain modifications. Parts A and B show responses of unmodified PC- and MC-cells, respectively. The stimulus was presented at a higher luminance then in Figure 8.4, and in this particular example, eye movements led mainly to a “rotational” movement of the stimulus with little on-axis movement. Accordingly, the line-fading effect weak, but line-splitting is visible in the MC-cell response (circle in B).

Part C shows the MC-cell response after replacing the original photoreceptor model with a "linearised" variant, which consists of a cascaded low-pass filter and a Michaelis-Menten saturation characteristic (see also Section 5.2.1). In this case line-splitting is strongly reduced, indicating that photoreceptor response asymmetries play an important role in generating the nonlinear response. This reduction of nonlinear behaviour is similar to the effect of a linear photoreceptor on the frequency-doubling response for contrast-reversed gratings, as suggested in Chapter 5.

Part D shows an example where the nested amacrine circuit, which leads to transient responses in MC-cells, was inactivated. This modification leads to a complete abolishment of the line-splitting effect. In addition, the response amplitudes of the ganglion cells are weaker than for the full model, which results from the lack of amplification of onset-transients. Hence, in this model, the combination of inhibition and disinhibition caused by the nested amacrine circuit (see Chapter 5 for details) is the main factor that leads to the line-splitting effect.

The separation of the spokes of the star stimulus used here increases with increasing eccentricity, and the splitting effect is visible for a separation of $> 10' - 15'$. This is by far more than the total receptive field diameter of a simulated MC-cell (about $10'$ in this case), therefore MC-cells can not directly integrate asymmetric responses. Instead, the apparent splitting of the lines of the stimulus is caused by the wide-field amacrine cells, which contribute to the response of a given ganglion cell beyond its anatomical receptive field. A similar influence on responses to contrast-reversed gratings in nonlinear ganglion cells is also visible at low spatial frequencies (see Fig. 5.7 in Chapter 5).

This effect is further illustrated in Figure 8.7E, where the responses of MC-cells receiving excitatory input from only a single photoreceptor are shown, but where the size of the amacrine cell receptive fields was unchanged. The splitting effect is in this case even more pronounced than for a larger receptive field, because the smaller receptive fields cause less spatial blurring of the stimulus.

In conclusion, the simulation results suggest that the main source of the line-splitting effect are nonlinearities in the inner retina, which form a part of the extra-classical receptive field of MC-cells. This result leads to the prediction that in an electrophysiological experiment, the line-splitting effect should be largely abolished in the presence of antagonists that block inhibition in the inner retina. Equally, it is expected that TTX-sensitive long-range inhibition in the inner retina by spiking amacrine cells, which has been shown to contribute to the frequency-doubling response in nonlinear ganglion cells (Demb et al., 1999) but was not included in this model, may contribute to line-splitting in a similar way.

8.2.5 Psychophysical Correlate of the Line-Splitting Effect

The model results indicate that a perceptual correlate of the line-splitting effect should be rather subtle and fast-changing. Hence, it was not expected that these response patterns could have a strong influence on visual perception. In spite of this, observers in the qualitative assessment reported a percept which seems to correspond to the line-splitting effect as obtained from the model.

During the observation experiment, 66% percent of the 35 subjects reported in addition to the fading-effect that lines seem to split or that they become denser, as if lines have been "added in between close to the center". Hence this illusion is less clear than the fading effect, which was confirmed by all observers. Observers also consistently reported that the percept is more short-lived than the line-fading. It was further noticed that the MacKay illusion (Fig. 8.8B) induces a stronger splitting effect than the star shape we used. For this illusion, most observers (86%) reported that thin white lines suddenly split some of the wedges for a short moment in the middle. That the splitting effect is more pronounced for the McKay illusion may be related to the scaling of the distance between the wedges of the stimulus, which better matches the scaling of ganglion cell receptive fields with increasing retinal eccentricity.

In general this illusion is more transient than the fading percept, which is in accordance to the activity patterns observed in the model. However, so far it was not possible to find a way to quantify it psychophysically. That it originates from the MC-cell system is supported by the observation that viewing a luminance balanced red-green star does not induce the splitting percept. Most commonly a strong fading of the whole star starting from the center was reported by observers.

8.3 Summary and Discussion

In this chapter, the origin of two visual percepts, both arising as a consequence of fixational eye movements, has been traced back to specific properties of magnocellular ganglion cells. The results show that both, the perceived sectorial fading of a star and the splitting of individual lines of the stimulus during precise fixation, are caused by the retinal circuit that leads to transient responses and frequency-doubling in MC-cells.

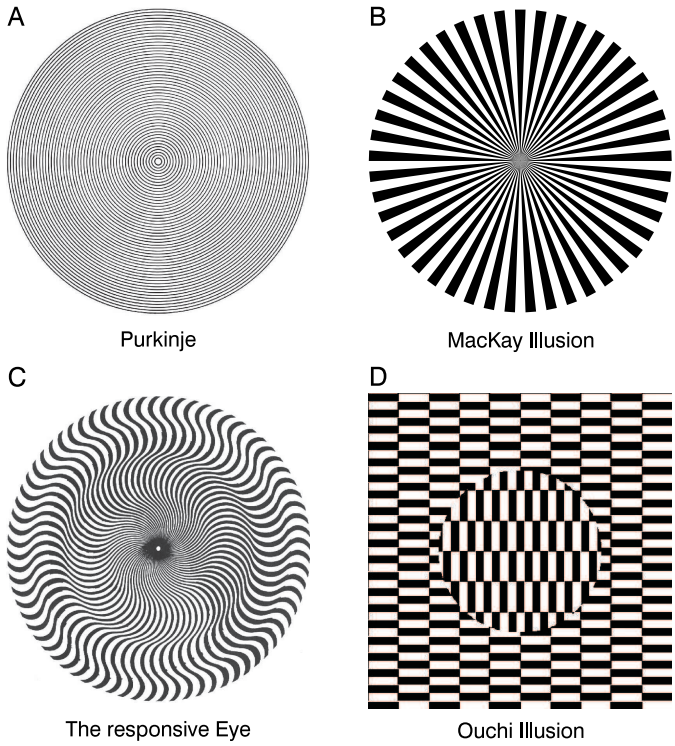

FIGURE 8.8: Examples of stimuli that elicit motion-induced illusions. (A) *Purkinje Illusion* (Wade, 2003). (B) The *MacKay Illusion* (Pirenne et al., 1958). (C) *The Responsive Eye* by Bridget Riley (Wade, 2003). (D) Ouchi Illusion (Spillmann and Werner, 1990).

8.3.1 Relations to Existing Psychophysical Observations

Several impressive visual illusions exist which are elicited by retinal image motion due to eye- or head-movements (Fig. 8.8), some of which were first described by Purkinje and Helmholtz (reviewed by Wade, 2003). These aesthetically appealing pictures, which have even influenced the arts ("Op-Art", Fig. 8.8 C), have been used to deduce possible neuronal mechanisms which underlie their perception. While fixating, observers report for many such illusions unstable flickering or apparent motion percepts, which can affect the image as a whole or, more often, just parts of it.

The star-shaped stimulus investigated here bears some similarities with the MacKay illusion (Pirenne et al., 1958) (Fig. 8.8B). For this stimulus investigated by MacKay, observers perceive a circular movement in the periphery and a shimmering in its centre (Pirenne et al., 1958). The peripheral motion percept has similarities to that experienced for the star stimulus, but in the MacKay illusion the individual segments do not temporarily disappear as do the lines of the star. This difference is probably a result of the increasing diameter of the rays in the MacKay stimulus, which prevents the line-fading effect. Line-fading can only occur when the motion of the stimulus has a very

small orthogonal component, and because they are not parallell, one of the two edges of the rays in the MacKay stimulus will always have an orthogonal component which activates retinal ganglion cells, and therefore remain visible. This however is different for the central part of the stimulus, where the rays are thin. Here, the rays can fade temporarily, and therefore the "shimmering" as described by Pirenne et al. (1958) may, as for the star-shaped stimulus discussed here, also be a consequence of the aperture problem (Zanker, 2004).

The aperture problem has been discussed in conjunction with the illusions shown in Figure 8.8 previously and models have been made to explain the famous Ouchi illusion (Fig. 8.8 D; Mather, 2000; Fermüller et al., 2000) and others by means of cortical motion detectors (Zanker, 2004; Zanker and Walker, 2004). The present results augment this theory by suggesting that some aspects of these illusions can already be found in the retinal population activity. It is conceivable that the apparent motion elicited by these illusions requires at some point the activation of cortical motion detectors. This study however suggests that these illusory percepts are not a direct consequence of the interaction of fixational eye movements and specific properties of cortical motion detectors. Instead, it was shown that the influence of fixational eye movements on response nonlinearities of retinal ganglion cells may play a significant role in the generation of activity patterns that resemble the perceptual correlate instead of the physical stimulus properties.

Chapter 9

Discussion

The central aim of this study was to investigate the origin of retinal nonlinearities and their possible functional implications. Using a computational model, nonlinearities in retinal ganglion cells were investigated under a number of different conditions. The results, as presented separately in Chapters 5-8, suggest distinct effects of these nonlinearities, which will be summarised in the following. This is followed by a general discussion of the limitations of the modelling approach, which summarises and augments the points mentioned in the individual chapters. Then the results will be consolidated and interpreted in the context of visual perception, and possible future steps will be proposed which could advance the understanding of the role of nonlinearities in visual perception.

9.1 Main Results

In this study, a computational model was developed which could account for frequency-doubling responses in Y-like ganglion cells in the cat retina, and the differences between X- and Y-cells. Using this model, different factors were investigated that contribute to frequency-doubling, and their relative contribution was assessed. It was shown that frequency-doubling originates in the temporal imbalanced photoreceptor response, and is amplified by a circuit of amacrine cells that also generates transient responses.

This model was then applied to study the effects of ganglion cell nonlinearities on visual perception in the presence of fixational eye movements. Two stimuli were used: a hyperacuity stimulus and a star stimulus consisting of radiating lines, which causes motion-induced visual illusions.

It was shown that eye movements can improve hyperacuity, in particular for reduced stimulus contrast and that this effect is based on the previously characterised nonlinearities. Furhermore, eye movements were shown to reduce aliasing due to undersampling in the retinal periphery, which otherwise would increase hyperacuity thresholds. This latter effect however does not rely on nonlinearities.

The simulated ganglion cell activity in response to the star stimulus suggested a retinal origin for for two visual illusions which are elicited by fixational eye movements. Both illusions are caused by the typical nonlinearities of Y-like ganglion cells: (i) Due to their transient nature, the activity of Y-like cells quickly adapts when the stimulation of their receptive field remains constant. This causes a fading of lines in segments of the star, and the location of the fading depends directly on the direction of fixational eye movements. (ii) Individual lines of the star appear to split into two lines. This effect is caused by spatiotemporal summation of unbalanced photoreceptor responses, as shown for frequency-doubling responses in Y-cells.

9.2 Limitations of the Model

In order to achieve a level of realism that allows for plausible predictions for the observed effects of retinal nonlinearities, it was attempted to include all relevant details on the basis of the available experimental data. However, full biological realism is difficult to achieve in a model, as it is impossible to include every known fine detail of retinal anatomy and physiology. At the same time, some details may only be of very minor importance to explain the effects investigated here.

Therefore, specific assumptions and simplifications were made in order to ensure a high degree of realism. This was sometimes difficult as the available experimental data is not always conclusive or contradictory. Also, many details of the model are based on experimental evidence from different species. For instance, the implementation of the nested amacrine circuit, which leads to transient responses in Y- and MC-cells, was inspired by data from the tiger salamander retina (Roska et al., 1998).

A further important restriction of the chosen modelling approach is that its complexity prevents a rigorous mathematical analysis. This complicates the adaptation to experimental data, because the consequences of modifying a model parameter are sometimes difficult to predict.

In the following, the most important assumptions and simplifications will be summarised and discussed:

1. The photoreceptor model used here is a qualitative description of the processes of phototransduction, and many details of this process were not included (see Chapter 5, Section 5.3.1). While the model can reproduce the available data on macaque cones for brief stimuli very well, it is unclear whether this description also holds for prolonged stimuli. The properties of the photoreceptor response are crucial for some of the results of this work, hence further experimental data is needed to fully validate this model.

2. The model disregards possible feedback-pathways from horizontal cells to cones and other possible interactions in the outer plexiform layer. The ribbon synapses at the photoreceptor axon terminals are complex structures, and their specific mechanisms may have important implications for the transmission of photoreceptor activity (see Chapter 4, Section 4.6.1). It is in particular unclear whether these mechanisms contribute to nonlinear responses in cones or bipolar cells. A very recent theoretical study however confirms the notion to assign the main source of nonlinearities to photoreceptors, with little influence of postsynaptic processes (van Hateren, 2005). Furthermore, the results presented here are generally in very good agreement with experimental data. Therefore, the simplifications made in this study seem justified.

3. Generally, neural activity was modelled using the passive membrane equation, and synaptic transmission was either assumed linear or a static nonlinearity was used. This implementation neglects activity-dependent mechanisms such as depression, facilitation or augmentation, which would modify synaptic transmission in an activity-dependent way (Zucker and Regehr, 2002). Again, an important question is whether these mechanisms could affect the linearity of the neural responses. While this can not be excluded, the good fits of the model responses to experimental data indicate that their effects on response nonlinearities are possibly only of minor importance.

4. The model only implements a subset of all known types of retinal neurons. But as this study considers only On-center PC/X and MC/Y ganglion cells and photopic vision, those cell types known not to contribute to ganglion cell responses under these conditions can be safely excluded (e.g. those neurons mediating rod-dominated vision, or Off-center cells, which are unlikely to contribute to the On-center pathway; Zaghloul et al., 2003). On the other hand, it is well known that inhibition from amacrine cell types, further to those included into this model, contributes to ganglion cell responses (e.g. spiking amacrine cells, which modulate ganglion cell responses for stimuli beyond their receptive field; Demb et al., 1999, or dopaminergic or cholinergic amacrine cells; **?**).

While this constrains the generality of the model, it was shown that the nonlinear response in Y-like cells is not affected by cholinergic amacrine cells, and that it is not abolished by blocking GABA and glycine receptors (Demb et al., 2001, as partially reproduced in Chapter 5, Section 5.2.8). Therefore, it can be assumed that the present model can account at least for the main features of the nonlinear ganglion cell response and is sufficiently realistic in the context of the questions addressed here.

9.3 Implications of Nonlinear Processing for Visual Perception

Nonlinearities in Y- and MC-cells lead to (i) transient responses and (ii) frequency-doubling in response to contrast reversed gratings. As outlined above, the investigation of these nonlinearities under different stimulus conditions, and in conjunction with fixational eye movements, revealed a number of effects which may be relevant for visual perception. In the following, possible implications of these findings will be discussed.

9.3.1 Transient Responses

In Chapter 6 it was shown that fixational eye movements lead to qualitatively different response patterns in ganglion cells as compared to static stimuli. In the proximity of a contrast transition, the responses of PC- and MC-ganglion cells are dominated by transient bursts of activity. This effect is particularly strong in MC-cells. It was argued that these transient responses could amplify responses to weak stimuli and thereby enhance their detectability, as illustrated for hyperacuity stimuli at reduced contrast in Chapter 7.

This hypothesis is supported by the experimental finding that transient depolarisations, elicited by fixational eye and head movements, lead to synchronous spike bursts in response to correlated spatial structures (Greschner et al., 2002). Furthermore, microsaccades have been shown to generate strong burst in V1 neurons (Martinez-Conde et al., 2000). The basis of these effects may be that neurons at higher processing stages, which integrate retinal activity, are more likely to respond if they receive multiple spikes within a brief temporal interval. For instance, Kara and Reid (2003) found an increased probability for a response in the cat visual cortex when two retinal spikes arrived within less than 10ms. Thus, neurons at higher processing stages integrating retinal activity are likely to respond stronger in the presence of fixational eye movements, which could

lead to an improved detectability for weak stimuli (Hennig et al., 2002; Rucci and Desbordes, 2003).

These effects can also be interpreted in the context of *stochastic resonance* (Wiesenfeld and Moss, 1995; Gammaitoni et al., 1998). Stochastic resonance is the phenomenon when a weak signal is amplified in a nonlinear system due to the presence of noise. Amplification results from the resonance of frequencies in the noise with those also present in the signal. A transformation of the noisy signal by a nonlinearity, e.g. a spiking threshold, can then lead to a selective amplification of the resonant noise components.

In the case considered in this study, noise is provided by random eye movements and nonlinearities are provided by the photoreceptor, amacrine cells (for MC-cells) and spiking thresholds (for ganglion cells and neurons further upstream). In addition, eye movements lead to spatially correlated responses, which reflect spatial correlations in the stimulus. Combined, these effects lead to an amplification of the signal in ganglion cell responses. Hence, the responses produced by fixational eye movements have interesting properties which, in conjunction with nonlinearities, can have important implications for visual perception.

Furhermore, the strong cortical activity caused by transient retinal responses can be interpreted as responses with a high degree of *saliency*. Perceptual saliency has been proposed as an attribute of cortical activity to explain shifts of visual attention (reviewed by Wörgötter et al., 1999), and is high at stimulus locations with inhomogeneities (Lee et al., 2002). As shown, fixational eye movements could lead to strong responses at these locations (e.g. at a contrast transition) and could therefore signal stimulus regions with a high perceptual saliency. This may explain why the percept of the star stimulus investigated in Chapter 8 appeared biased by the transient activity of MC-cells, in spite of the fact that their responses carry false information. PC-cell responses, which convey the correct information, are less transient and hence less *salient*, and consequently contributed less to the percept.

9.3.2 Frequency-Doubling

Frequency-doubled responses to contrast reversed gratings are a very distinct feature of nonlinear ganglion cells (Chapter 5 and Fig. 8.5 in Chapter 8). As shown in Chapter 5, frequency-doubling is only visible in the temporal response of individual Y-like cells. The spatial population response on the other hand encodes the original spatial frequency

the stimulus (see Fig. 5.3 in Chapter 5). This is of relevance because a recently developed clinical test for glaucoma applies the frequency-doubling illusion and is based on the assumption that it is mediated by nonlinear, Y-like MC-cells (Maddess and Severt, 1999).

Hence it appears the proposed line splitting effect, as described in Chapter 8, is the first perceptual correlate of the frequency-doubling nonlinearity in MC-ganglion cell receptive fields. The splitting effect illustrates that the MC-cell nonlinearity operates on a smaller spatial scale than the classical receptive field. Early experimental studies of frequency-doubling in Y-cells in the cat, which share properties with MC-cells, have therefore led to the notion of "nonlinear receptive field subunits" (Enroth-Cugell and Robson, 1966; Hochstein and Shapley, 1976a; Victor, 1988).

The finding that frequency-doubling could influence visual perception raises the question whether these nonlinear subunits could also play a role in the processing of spatial visual information, possibly by improving spatial motion analysis. It has, for instance, been demonstrated that MC-cells can provide cues to detect second-order motion (Demb et al., 2001). It may therefore be interesting to further investigate the influence of the MC-cell nonlinearities in stimulus conditions prevalent in natural scenes. This may be especially important for the retinal periphery, where large receptive fields lead to a low spatial resolution. Here, nonlinearities in Y-like cells could lead to an improved detection or spatial resolution enhancement for moving stimuli.

9.4 Functional Segregation and Upstream Processing

Functional segregation of visual information begins in the retina and appears to be partially conserved in higher visual areas, such as the primary visual cortex. In the following, it will be discussed how the differences between linear and nonlinear ganglion cells could affect cortical processing.

9.4.1 Neural Integration

It is commonly agreed that the finely grained activity, which comes from the retina, is integrated at higher levels of the processing hierarchy. Only by this a correct stimulus interpretation becomes possible, as illustrated in Chapter 8 for the aperture problem. The results presented there suggest that this principle can be violated and that stimulus conditions exist, where the retinal activity pattern appears to directly match the visual

percept. They further suggests that higher processing stages may have contributed only little to the processing and that specific properties of early visual responses may be conserved and have a direct perceptual correlate. Furthermore, it may be suggested that the integrative properties of higher visual areas cannot in all cases compensate against the transient nature of their main inputs from the retinal MC-cell stream. It is also interesting to note that fixational eye-movements, which are normally assumed to improve vision (Ditchburn and Ginsborg, 1953; Riggs et al., 1953; Hennig et al., 2002; Greschner et al., 2002; Rucci and Desbordes, 2003; Olveczky et al., 2003), are in these cases the source of the false percepts. Hence it appears that cortical processing may in some cases be highly biased by retinal processing. Further modelling studies could be a useful tool to address this problem more generally by testing models of cortical circuits using realistic afferent input.

9.4.2 The Ventral and Dorsal Pathways

Both the results for the hyperacuity stimulus and the star-stimulus, suggest a dominant role for MC-cells and hence the dorsal pathway, in visual perception. This is puzzling since the model shows that the star stimulus is more accurately represented by the activity of the PC-cell population, which form the ventral pathway. Furthermore, their dynamic properties appear to prevent PC-cells from mediating information about fine spatial detail despite their high density in the fovea.

So what is the role of the PC-cells, and why are their receptive fields linear? Often it is argued that the linearity of PC-cells, their sustained responses and high density in the fovea could make them more suitable for the spatial analysis of form (Merigan and Maunsell, 1993). Linearity is in principle desirable for this task, because nonlinearities could lead to distortions and subsequently to false percepts. Recent psychophysical evidence however indicates that the analysis of spatial patterns is strongly based on retinal image motion (Nishida, 2004) - motion that could also be provided by fixational eye movements. In this case, cortical image analysis could benefit from the faster and temporally more precise dynamics of MC-cell responses. This hypothesis is consistent with the finding presented in Chapter 7 that the temporally precise MC-cell responses in the presence of retinal image motion could translate into a spatially precise stimulus representation.

For the role of PC-cells and the ventral stream in primates, a more consistent hypothesis is that it is the basis for a highly developed colour vision. Ingling and Martinez-Uriegas (1983) found that primate red-green opponent PC-cells in the LGN signal the difference

between center and surround responses at low spatial frequencies, but their sum at high spatial frequencies. The same applies to cat X-cells (Ingling and Martinez-Uriegas, 1985). Hence, these cells combine luminance and chromaticity of a stimulus. This requires a certain degree of response linearity, because otherwise undesirable nonlinear interactions between stimulus luminance and chromaticity would occur which would interfere with colour vision. This requirement is of particular importance for diurnal primates with trichromatic vision, which may explain the extremely high degree of linearity of PC-cells.

9.5 Conclusion

The results of this theoretical study suggest that nonlinear processing in the retina can have important implications for visual perception. Additionally, it was found that an interaction of nonlinearities with fixational eye movements can lead to improved encoding of visual stimuli. These findings are based on computational modelling of retinal activity and comparisons of the model behaviour with experimental data. A direct experimental confirmation of the effects is still missing, but the simulations provide clear predictions for possible future experiments.

The observation that retinal processing influences visual perception is quite obvious, the results however demonstrate that this influence can be rather subtle and difficult to anticipate even with a good knowledge of retinal image processing. This also complicates the investigation of processes in higher visual areas, as their behaviour will be influenced by the distinct characteristics of linear and nonlinear ganglion cells providing afferent input. To solve this problem, the model developed in this study could provide a good starting point for models of parts of the higher visual system by providing them with an adequately structured input.

Bibliography

Adams DL, Horton JC (2003) A precise retinotopic map of primate striate cortex generated from the representation of angioscotomas. *J Neurosci* 23:3771 – 3789.

Ammermüller J, Kolb H (1995) The organization of the turtle inner retina. I. ON- and OFF-center pathways. *J Comp Neurol* 358:1–34.

Anderson JS, Carandini M, Ferster D (2000) Orientation tuning of input conductance, excitation, and inhibition in cat primary visual cortex. *J Neurophysiol* 84:909–926.

Anderson JS, Lampl I, Gillespie DC, Ferster D (2000) The contribution of noise to contrast invariance of orientation tuning in cat visual cortex. *Science* 290:1968–1972.

Appelle S (1972) Perception and discrimination as a function of stimulus orientation: the ”oblique effect” in man and animals. *Psychol Bull* 78:266–278.

Averill HL, Weymouth FW (1925) Visual perception and the retinal mosaic. II. The influence of eye-movements on the displacement threshold. *J Comp Psychol* 5:147–176.

Awatramani GB, Slaughter MM (2000) Origin of transient and sustained responses in ganglion cells of the retina. *J Neurosci* 20:7087–7095.

Bader CR, Bertrand D (1984) Effect of changes in intra- and extracellular sodium on the inward (anomalous) rectification in salamander photoreceptors. *J Physiol* 347:611–31.

Bair W, O'Keefe L (1998) The influence of fixational eye movements on the response of neurons in area MT of the macaque. *Vis Neurosci* 15:779–786.

Barlow HB (1952) Eye movements during fixation. *J Physiol* 116:290–306.

Barlow HB, Levick WR (1969) Three factors limiting the reliable detection of light by retinal ganglion cells of the cat. *J Physiol* 200:1–24.

Barlow H (1953) Summation and inhibition in the frog's retina. *J Physiol* 119:69–88.

Baylor DA, Fuortes MG, O'Bryan PM (1971) Receptive fields of cones in the retina of the turtle. *J Physiol* 214:265–294.

Baylor DA, Nunn BJ, Schnapf JL (1984) The photocurrent, noise and spectral sensitivity of rods of the monkey macaca fascicularis. *J Physiol* 357:575–607.

Beard BL, Levi DM, Klein SA (1997) Vernier acuity with non-simultaneous targets: the cortical magnification factor estimated by psychophysics. *Vision Res* 37:325–346.

Benardete EA, Kaplan E (1997) The receptive field of the primate P retinal ganglion cell, I: Linear dynamics. *Vis Neurosci* 14:169–185.

Benardete EA, Kaplan E (1999) Dynamics of primate P retinal ganglion cells: responses to chromatic and achromatic stimuli. *J Physiol* 519 Pt 3:775–790.

Benardete EA, Kaplan E, Knight BW (1992) Contrast gain control in the primate retina: P cells are not X-like, some M cells are. *Vis Neurosci* 8:483–486.

Bilotta J, Abramov I (1989) Orientation and direction tuning of goldfish ganglion cells. *Vis Neurosci* 2:3–13.

Bloomfield SA, Dacheux RF (2001) Rod vision: pathways and processing in the mammalian retina. *Prog Retin Eye Res* 20:351–384.

Bolger C, Bojanic S, Sheahan NF, Coakley D, Malone JF (1999) Dominant frequency content of ocular microtremor from normal subjects. *Vision Res* 39:1911–1915.

Boycott BB, Wässle H (1974) The morphological types of ganglion cells of the domestic cat's retina. *J Physiol* 240:397–419.

Boycott BB, Wässle H (1991) Morphological classification of bipolar cells in the primate retina. *Eur J Neurosci* 3:1069–1088.

Brown SP, Masland RH (2001) Spatial scale and cellular substrate of contrast adaptation by retinal ganglion cells. *Nat Neurosci* 4:44–51.

Burkhardt DA (1972) Effects of picrotoxin and strychnine upon electrical activity of the proximal retina. *Brain Res* 43:246–249.

Burkhardt DA (1993) Synaptic feedback, depolarization, and color opponency in cone photoreceptors. *Vis Neurosci* 10:981–989.

Burns ME, Lamb TD (2003) Visual transduction by rod and cone photoreceptors. In Calupa LM, Werner JS, editors, *The Visual Neurosciences*, pp. 215–233. MIT Press, Cambridge, MA.

Caldwell J, Daw N (1978) New properties of rabbit retinal ganglion cells. *J Physiol* 276:257–276.

Callaway EM (1998) Local circuits in primary visual cortex of the macaque monkey. *Annu Rev Neurosci* 21:47–74.

Carandini M, Ferster D (2000) Membrane potential and firing rate in cat primary visual cortex. *J Neurosci* 20:470–484.

Carandini M, Heeger DJ, Movshon JA (1997) Linearity and normalization in simple cells of the macaque primary visual cortex. *J Neurosci* 17:8621–8644.

Carcieri SM, Jacobs AL, Nirenberg S (2003) Classification of retinal ganglion cells: a statistical approach. *J Neurophysiol* 90:1704–1713.

Chichilnisky EJ, Kalmar RS (2002) Functional asymmetries in ON and OFF ganglion cells of primate retina. *J Neurosci* 22:2737–2747.

Cleland BG, Harding TH, Tulunay-Keesey U (1979) Visual resolution and receptive field size: examination of two kinds of cat retinal ganglion cell. *Science* 205:1015–1017.

Cleland BG, Levick WR (1974) Brisk and sluggish concentrically organized ganglion cells in the cat's retina. *J Physiol* 240:421–456.

Clowes MB (1962) A note on colour discrimination under conditions of retinal image constraint. *Optom Wkly* 9:65–68.

Cohen E, Sterling P (1991) Microcircuitry related to the receptive field center of the On-Beta ganglion cell. *J Neurophysiol* 65:352–359.

Cohen E, Sterling P (1992) Parallel circuits from cones to the on-beta ganglion cell. *Eur J Neurosci* 4:506–520.

Cohen ED (1998) Interactions of inhibition and excitation in the light-evoked currents of X type retinal ganglion cells. *J Neurophysiol* 80:2975–2990.

Cohen ED (2000) Light-evoked excitatory synaptic currents of X-type retinal ganglion cells. *J Neurophysiol* 83:3217–3229.

Cohen ED, Miller RF (1994) The role of NMDA and non-NMDA excitatory amino acid receptors in the functional organization of primate retinal ganglion cells. *Vis Neurosci* 11:317–332.

Croner LJ, Purpura K, Kaplan E (1993) Response variability in retinal ganglion cells of primates. *Proc Natl Acad Sci U S A* 90:8128–8130.

Curcio CA, Sloan KRJ, Packer O, Hendrickson AE, Kalina RE (1987) Distribution of cones in human and monkey retina: individual variability and radial asymmetry. *Science* 236:579–582.

Dacey D, Packer OS, Diller L, Brainard D, Peterson B, Lee BB (2000) Center surround receptive field structure of cone bipolar cells in primate retina. *Vision Res* 40:1801–1811.

Dacey DM (1993) The mosaic of midget ganglion cells in the human retina. *J Neurosci* 13:5334–5355.

Dacey DM (1996) Circuitry for color coding in the primate retina. *Proc Natl Acad Sci U S A* 93:582–588.

Dacey D, Petersen M (1992) Dendritic field size and morphology of midget and parasol ganglion cells in the human retina. *Proc Natl Acad Sci U S A* 89:9666–9670.

de Monasterio F (1978) Properties of concentrically organized X and Y ganglion cells of macaque retina. *J Neurophysiol* 41:1394–1417.

De Valois RL, De Valois KK (1988) *Spatial Vision.* Oxford University Press, New York.

Demb JB, Haarsma L, Freed MA, Sterling P (1999) Functional circuitry of the retinal ganglion cell's nonlinear receptive field. *J Neurosci* 19:9756–9767.

Demb JB, Sterling P, Freed MA (2004) How retinal ganglion cells prevent synaptic noise from reaching the spike output. *J Neurophysiol* 92:2510–2519.

Demb JB, Zaghloul K, Haarsma L, Sterling P (2001) Bipolar cells contribute to nonlinear spatial summation in the brisk-transient (Y) ganglion cell in mammalian retina. *J Neurosci* 21:7447–7454.

Demb JB, Zaghloul K, Sterling P (2001) Cellular basis for the response to second-order motion cues in Y retinal ganglion cells. *Neuron* 32:711–721.

Demontis GC, Longoni B, Barcaro U, Cervetto L (1999) Properties and functional roles of hyperpolarization-gated currents in guinea-pig retinal rods. *J Physiol* 515:813–828.

Derrington AM, Lennie P (1984) Spatial and temporal contrast sensitivities of neurones in lateral geniculate nucleus of macaque. *J Physiol* 357:219–240.

DeVries SH (2000) Bipolar cells use kainate and AMPA receptors to filter visual information into separate channels. *Neuron* 28:847–856.

DeVries SH, Qi X, Smith R, Makous W, Sterling P (2002) Electrical coupling between mammalian cones. *Curr Biol* 12:1900–1907.

DeVries SH, Schwartz EA (1999) Kainate receptors mediate synaptic transmission between cones and 'Off' bipolar cells in a mammalian retina. *Nature* 397:157–160.

Dhingra N, Kao Y, Sterling P, Smith R (2003) Contrast threshold of a brisk-transient ganglion cell in vitro. *J Neurophysiol* 89:2360–2369.

Ditchburn RW (1980) The function of small saccades. *Vision Res* 20:271–272.

Ditchburn RW, Ginsborg BL (1953) Involuntary eye movements during fixation. *J Physiol* 119:1–17.

Dow BM, Snyder AZ, Vautin RG, Bauer R (1981) Magnification factor and receptive field size in foveal striate cortex of the monkey. *Exp Brain Res* 44:213–228.

Dowling JE (1968) Synaptic organization of the frog retina: an electron microscopic analysis comparing the retinas of frogs and primates. *Proc R Soc Lond B Biol Sci* 170:205–228.

Dowling JE, Boycott BB (1966) Organization of the primate retina: electron microscopy. *Proc R Soc Lond B Biol Sci* 166:80–111.

Dreher B, Fukada Y, Rodieck RW (1976) Identification, classification and anatomical segregation of cells with X-like and Y-like properties in the lateral geniculate nucleus of old-world primates. *J Physiol* 258:433–452.

Eizenman M, Hallett PE, Frecker RC (1985) Power spectra for ocular drift and tremor. *Vision Res* 25:1635–1640.

Enroth-Cugell C, Robson JG (1966) The contrast sensitivity of retinal ganglion cells of the cat. *J Physiol* 187:517–552.

Enroth-Cugell C, Robson JG, Schweitzer-Tong DE, Watson AB (1983) Spatiotemporal interactions in cat retinal ganglion cells showing linear spatial summation. *J Physiol* 341:279–307.

Euler T, Detwiler PB, Denk W (2002) Directionally selective calcium signals in dendrites of starburst amacrine cells. *Nature* 418:845–852.

Fahle M, Edelman S, Poggio T (1995) Fast perceptual learning in hyperacuity. *Vision Res* 35:3003–3013.

Fahle M, Poggio T (1981) Visual hyperacuity:spatiotemporal interpolation in human vision. *Proc R Soc Lond B Biol Sci* 213:451–477.

Fain GL, Matthews HR, Cornwall MC, Koutalos Y (2001) Adaptation in vertebrate photoreceptors. *Physiol Rev* 81:117–151.

Famiglietti EV, Kolb H (1976) Structural basis for on- and off-center responses in retinal ganglion cells. *Science* 194:193–195.

Feigenspan A, Wässle H, Bormann J (1993) Pharmacology of GABA receptor Cl channels in rat retinal bipolar cells. *Nature* 361:159–161.

Fermüller C, Pless R, Aloimonos Y (2000) The Ouchi illusion as an artifact of biased flow estimation. *Vision Res* 40:77–96.

Ferster D (1988) Spatially opponent excitation and inhibition in simple cells of the cat visual-cortex. *J Neurosci* 8:1172–1180.

Fisher J, Krüger J, Droll W (1975) Quantitative aspects of the shift effect in cat retinal ganglion cells. *Brain Res* 83:391–403.

Flores-Herr N, Protti DA, Wässle H (2001) Synaptic currents generating the inhibitory surround of ganglion cells in the mammalian retina. *J Neurosci* 21:4852–4863.

Freed MA (2000a) Parallel cone bipolar pathways to a ganglion cell uses different rates and amplitudes of quantal excitation. *J Neurosci* 20:3956–3963.

Freed MA (2000b) Rate of quantal excitation to a retinal ganglion cell evoked by sensory input. *J Neurophysiol* 83:2956–2966.

Freed MA, Pflug R, Kolb H, Nelson R (1996) ON-OFF amacrine cells in cat retina. *J Comp Neurol* 364:556–566.

Freed MA, Sterling P (1988) The ON-alpha ganglion cell of the cat retina and its presynaptic cell types. *J Neurosci* 8:2303–2320.

Freed M, Smith R, Sterling P (2003) Timing of quantal release from the retinal bipolar terminal is regulated by a feedback circuit. *Neuron* 38:89–101.

Freeman AW (1991) Spatial characteristics of the contrast gain control in the cat's retina. *Vision Res* 31:775–785.

Fried SI, Münch TA, Werblin FS (2002) Mechanisms and circuitry underlying directional selectivity in the retina. *Nature* 420:411–414.

Frishman AW, Linsenmeier RA (1982) Effects of picrotoxin and strychnine on nonlinear responses of Y-type cat retinal ganglion cells. *J Physiol* 324:347–363.

Gammaitoni L, Hänggi P, Jung P, Marchesoni F (1998) Stochastic resonance. *Reviews of Modern Physics* 70:223–287.

Garcia-Suarez L, Barrett BT, Pacey I (2004) A comparison of the effects of ageing upon vernier and bisection acuity. *Vision Res* 44:1039–1045.

Gaudiano P (1992a) Toward a unified theory of spatiotemporal visual processing - the push-pull shunting model applied to physiological and psychophysical data. *Invest Ophth Vis Sci* 33:1346–1346.

Gaudiano P (1992b) A unified neural network model of spatiotemporal processing in X and Y retinal ganglion-cells. I. analytical results. *Biol Cybern* 67:11–21.

Gaudiano P (1992c) A unified neural network model of spatiotemporal processing in X and Y retinal ganglion-cells. II. temporal adaptation and simulation of experimental data. *Biol Cybern* 67:23–34.

Gaudiano P (1994) Simulations of x and y retinal ganglion cell behavior with a nonlinear push-pull model of spatiotemporal retinal processing. *Vision Res* 34:1767–1784.

Gaudiano P, Przybyszewski AW, van Wezel RJA, van de Grind WA (1998) Spatial asymmetries in cat retinal ganglion cell responses. *Biol Cybern* 79:151–159.

Geen DM, Swets JA (1966) *Signal detection theory and psychophysics.* New York: Wiley.

Gegenfurtner KR (2003) Cortical mechanisms of colour vision. *Nat Rev Neurosci* 4:563–572.

Geisler W (1984) Physical limits of acuity and hyperacuity. *J Opt Soc Am A* 1:775–782.

Gerrits H (1978) Differences in peripheral and foveal effects observed in stabilized vision. *Exp Brain Res* 32:225–244.

Glezer VD, Tsherbach TA, Gauselman VE, Bondarko VM (1980) Linear and non-linear properties of simple and complex receptive fields in area 17 of the cat visual cortex. A model of the field. *Biol Cybern* 37:195–208.

Goodchild AK, Ghosh KK, Martin PR (1996) Comparison of photoreceptor spatial density and ganglion cell morphology in the retina of human, macaque monkey, cat, and the marmoset callithrix jacchus. *J Comp Neurol* 366:55–75.

Greschner M, Bongard M, Rujan P, Ammermüller J (2002) Retinal ganglion cell synchronization by fixational eye movements improves feature estimation. *Nat Neurosci* 5:341–347.

Grünert U, Greferath U, Boycott BB, Wässle H (1993) Parasol (P alpha) ganglioncells of the primate fovea: immunocytochemical staining with antibodies against $GABA_A$-receptors. *Vision Res* 33:1–14.

Gur M, Beylin A, Snodderly D (1997) Response variability of neurons in primary visual cortex (V1) of alert monkeys. *J Neurosci* 17:2914–2920.

Harris JP, Fahle M (1995) The detection and discrimination of spatial offsets. *Vision Res* 35:51–58.

Harris JP, Fahle M (1996) Differences between fovea and periphery in the detection and discrimination of spatial offsets. *Vision Res* 36:3469–3477.

Hartline HK (1938) The response of single optic nerve fibers of the vertebrate eye to illumination of the retina. *Am J Physiol* 121:400–415.

Haverkamp S, Grünert U, Wässle H (2000) The cone pedicle, a complex synapse in the retina. *Neuron* 27:85–95.

Heeger DJ (1991) Non-linear model of neural responses in cat visual cortex In *Computational models of visual processing*, pp. 119–133. MIT Press, Cambridge, MA.

Helmholtz HLF (1896) *Handbuch der Physiologischen Optik.* Leopold Voss, Leipzig, 3 edition.

Hennig MH, Kerscher NJ, Funke K, Wörgötter F (2002) Stochastic resonance in visual cortical neurons: does the eye-tremor actually improve visual acuity? *Neurocomputing* 44:115–120.

Hildreth EC, Koch C (1987) The analysis of visual motion: from computational theory to neuronal mechanisms. *Annu Rev Neurosci* 10:477–533.

Hochstein S, Shapley RM (1976a) Linear and nonlinear spatial subunits in Y cat retinal ganglion cells. *J Physiol* 262:265–284.

Hochstein S, Shapley R (1976b) Quantitative analysis of retinal ganglion cell classifications. *J Physiol* 262:237–264.

Hubel DH, Wiesel TN (1962) Receptive fields, binocular interaction, and functional architecture in the cat's visual cortex. *J Physiol* 160:106–154.

Ingling C, Martinez-Uriegas E (1983) The relationship between spectral sensitivity and spatial sensitivity for the primate r-g X-channel. *Vision Res* 23:1495–1500.

Ingling C, Martinez-Uriegas E (1985) The spatiotemporal properties of the r-g X-cell channel. *Vision Res* 25:33–38.

Kamermans M, Spekreijse H (1999) The feedback pathway from horizontal cells to cones. A mini review with a look ahead. *Vision Res* 39:2449–2468.

Kaneko A (1971) Electrical connexions between horizontal cells in the dogfish retina. *J Physiol* 213:95–105.

Kaneko A, Tachibana M (1986) Effects of gamma-aminobutyric acid on isolated cone photoreceptors of the turtle retina. *J Physiol* 373:443–461.

Kaplan E, Benardete E (2001) The dynamics of primate retinal ganglion cells. *Progress in Brain Research* 134:17–34.

Kaplan E, Shapley RM (1982) X and Y cells in the lateral geniculate nucleus of macaque monkeys. *J Physiol* 330:125–143.

Kara P, Reid R (2003) Efficacy of retinal spikes in driving cortical responses. *J Neurosci* 23:8547–8557.

Kelly D (1966) Frequency doubling in visual responses. *J Opt Soc Am* 56:1628–1633.

Kelly D (1981) Nonlinear visual responses to flickering sinusoidal gratings. *J Opt Soc Am* 71:1051–1055.

Kenyon G, Theiler J, George J, Travis B, Marshak D (2004) Correlated firing improves stimulus discrimination in a retinal model. *Neural Comput* 16:2261–2291.

Kier CK, Buchsbaum G, Sterling P (1995) How retinal microcircuits scale for ganglion cells of different size. *J Neurosci* 15:7673–7683.

Kline M, editor (1962) *H. von Helmholtz, Popular Scientific Lectures.* Dover, New York.

Kolb H (1979) The inner plexiform layer in the retina of the cat: electron microscopic observations. *J Neurocytol* 8:295–329.

Kolb H (1997) Amacrine cells of the mammalian retina: neurocircuitry and functional roles. *Eye* 1:904–923.

Kolb H (2003) How the retina works. *Am Sci* 91:28–35.

Kolb H, Fernandez E, Nelson R (2005) Webvision, http://webvision.med.utah.edu/.

Kolb H, Nelson R (1993) OFF-alpha and OFF-beta ganglion cells in cat retina: II. neural circuitry as revealed by electron microscopy of HRP stains. *J Comp Neurol* 329:85–110.

Kolb H, Nelson R, Mariani A (1981) Amacrine cells, bipolar cells and ganglion cells of the cat retina: a Golgi study. *Vision Res* 21:1081–1114.

Kowler E, Steinman RM (1980) Small saccades serve no useful purpose: reply to a letter by R. W. Ditchburn. *Vision Res* 20:273–276.

Krüger J, Fischer B (1973) Strong periphery effect in cat retinal ganglion cells. Excitatory responses in ON- and OFF-center neurones to single grid displacements. *Exp Brain Res* 18:316–318.

Kuffler SW (1953) Discharge patterns and functional organization of mammalian retina. *J Neurophysiol* 16:37–68.

Laitko U, Hofmann KP (1998) A model for the recovery kinetics of rod phototransduction, based on deactivation on rhodopsin. *Biophys J* 74:803–815.

Lankheet MJ, Frens MA, van de Grind WA (1990) Spatial properties of horizontal cell responses in the cat retina. *Vision Res* 30:1257–1275.

Lankheet MJM, Prickaerts JHHJ, van de Grind WA (1992) Responses of cat horizontal cells to sinusoidal gratings. *Vision Res* 32:997–1008.

Lauritzen TZ, Miller KD (2003) Different roles for simple-cell and complex-cell inhibition in V1. *J Neurosci* 23:10201–10213.

Lee BB, Dacey DM, Smith VC, Pokorny J (1999) Horizontal cells reveal cone type-specific adaptation in primate retina. *Proc Natl Acad Sci U S A* 96:14611–14616.

Lee BB, Kremers J, Yeh T (1998) Receptive fields of primate retinal ganglion cells studied with a novel technique. *Vis Neurosci* 15:161–175.

Lee BB, Pokorny J, Smith VC, Martin PR, Valberg A (1990) Luminance and chromatic modulation sensitivity of macaque ganglion cells and human observers. *J Opt Soc Am A* 7:2223–2236.

Lee BB, Wehrhahn C, Westheimer G, Kremers J (1993) Macaque ganglion cell responses to stimuli that elicit hyperacuity in man: detection of small displacements. *J Neurosci* 13:1001–1009.

Lee BB, Wehrhahn C, Westheimer G, Kremers J (1995) The spatial precision of macaque ganglion cell responses in relation to vernier acuity of human observers. *Vision Res* 35:2743–2758.

Lee T, Yang C, Romero R, Mumford D (2002) Neural activity in early visual cortex reflects behavioral experience and higher-order perceptual saliency. *Nat Neurosci* 5:589–597.

Leventhal AG, Rodieck RW, Dreher B (1981) Retinal ganglion cell classes in the Old World monkey: morphology and central projections. *Science* 213:1139–1142.

Linsenmeier RA, Frishman LJ, Jakiela HG, Enroth-Cugell C (1982) Receptive-field properties of X and Y cells in the cat retina derived from contrast sensitivity measurements. *Vision Res* 22:1173–1183.

Livingstone M, Hubel D (1988) Segregation of form, color, movement, and depth: anatomy, physiology, and perception. *Science* 240:740–749.

MacNeil MA, Heussy JK, Dacheux RF, Raviola E, Masland RH (1999) The shapes and numbers of amacrine cells: matching of photofilled with Golgi-stained cells in the rabbit retina and comparison with other mammalian species. *J Comp Neurol* 413:305–326.

MacNeil MA, Masland RH (1998) Extreme diversity among amacrine cells: implications for function. *Neuron* 20:971–982.

Maddess T, Severt W (1999) Testing for glaucoma with the frequency-doubling illusion in the whole, macular and eccentric visual fields. *Aust N Z J Ophthalmol* 27:194–196.

Malpeli JG, Schiller PH, Colby CL (1981) Response properties of single cells in monkey striate cortex during reversible inactivation of individual lateral geniculate laminae. *J Neurophysiol* 46:1102–1119.

Mangel SC (1991) Analysis of the horizontal cell contribution to the receptive field surround of ganglion cells in the rabbit retina. *J Physiol* 442:211–234.

Marc RE, Liu WLS (2000) Fundamental GABAergic amacrine cell circuitries in the retina: Nested feedback, concatenated inhibition, and axosomatic synapses. *J Comp Neurol* 425:560–582.

Marshall WH, Talbot SA (1942) Recent evidence for neural mechanisms in vision leading to a general theory of sensory acuity. *Biol Symp* 7:117–164.

Martinez-Conde S, Macknik SL, Hubel DH (2000) Microsaccadic eye movements and firing of single cells in the striate cortex of macaque monkeys. *Nat Neurosci* 3:251–258.

Martinez-Conde S, Macknik S, Hubel D (2004) The role of fixational eye movements in visual perception. *Nat Rev Neurosci* 5:229–240.

Masland RH (2001a) Neuronal diversity in the retina. *Curr Opin Neurobiol* 11:431–436.

Masland RH (2001b) The fundamental plan of the retina. *Nat Neurosci* 4:877–886.

Masu M, Iwakabe H, Tagawa Y, Miyoshi T, Yamashita M, Fukuda Y, Sasaki H, Hiroi K, Nakamura Y, Shigemoto R (1995) Specific deficit of the ON response in visual transmission by targeted disruption of the mGluR6 gene. *Cell* 80:757–765.

Mather G (2000) Integration biases in the Ouchi and other visual illusions. *Perception* 29:721–727.

Matsui K, Hosoi N, Tachibana M (1998) Excitatory synaptic transmission in the inner retina: paired recordings of bipolar cells and neurons of the ganglion cell layer. *J Neurosci* 18:4500–4510.

Maunsell JH, Gibson JR (1992) Visual response latencies in striate cortex of the macaque monkey. *J Neurophysiol* 68:1332–1344.

McIlwain JT (1964) Receptive fields of optic tract axons and lateral geniculate cells: peripheral extend and barbiturate sensitivity. *J Neurophysiol* 27:1154–1173.

McKee SP (1991) The physical constraints on visual hyperacuity. In Kulikowski JJ, Walsh V, Murray IJ, editors, *Vision and visual dysfunction*, Vol. 10, pp. 221–233. Macmillan, London.

McMahon MJ, Packer OS, Dacey DM (2004) The classical receptive field surround of primate parasol ganglion cells is mediated primarily by a non-GABAergic pathway. *J Neurosci* 24:3736–3745.

McNaughton PA (1990) Light responses of vertebrate photoreceptors. *Physiol Rev* 70:847–883.

Merigan WH, Maunsell JH (1993) How parallel are the primate visual pathways? *Annu Rev Neurosci* 16:369–402.

Morgan MJ, Watt RJ, McKee SP (1983) Exposure duration affects the sensitivity of vernier acuity to target motion. *Vision Res* 23:541–546.

Murakami I (2004) Correlations between fixation stability and visual motion sensitivity. *Vision Res* 44:751–761.

Müller F, Kaupp UB (1998) Signaltransduktion in Sehzellen. *Naturwissenschaften* 85:49–61.

Nelson R (1977) Cat cones have rod input: a comparison of the response properties of cones and horizontal cell bodies in the retina of the cat. *J Comp Neurol* 172:109–136.

Nelson R (1985) Spectral properties of cat horizontal cells. *Neurosci Res Suppl* 2:167–183.

Nelson R, Famiglietti EV, Kolb H (1978) Intracellular staining reveals different levels of stratification for on- and off-center ganglion cells in cat retina. *J Neurophysiol* 41:472–483.

Nelson R, Kolb H (1983) Synaptic patterns and response properties of bipolar and ganglion cells in the cat retina. *Vision Res* 23:1183–1195.

Nikonov S, Lamb TD, Pugh EN (2000) The role of steady phosphodiesterase activity in the kinetics and sensitivity of the light-adapted salamander rod photoresponse. *J Gen Physiol* 116:795–824.

Nirenberg S, Meister M (1997) The light response of retinal ganglion cells is truncated by a displaced amacrine circuit. *Neuron* 18:637–650.

Nishida S (2004) Motion-based analysis of spatial patterns by the human visual system. *Curr Biol* 14:830–839.

Norton TT, Casagrande VA (1982) Laminar organization of receptive-field properties in lateral geniculate nucleus of bush baby (Galago crassicaudatus). *J Neurophysiol* 47:715–741.

O'Brien BJ, Richardson RC, Berson DM (2003) Inhibitory network properties shaping the light evoked responses of cat alpha retinal ganglion cells. *Vis Neurosci* 20:351–361.

Olveczky BP, Baccus SA, Meister M (2003) Segregation of object and background motion in the retina. *Nature* 423:401–408.

Osterberg G (1935) Topography of the layer of rods and cones in the human retina. *Acta Ophthal* 6:1–103.

Pack CC, Born RT (2001) Temporal dynamics of a neural solution to the aperture problem in visual area MT of macaque brain. *Nature* 409:1040–1042.

Packer O, Williams DR (1992) Blurring by fixational eye movements. *Vision Res* 32:1931–1939.

Passaglia CL, Enroth-Cugell C, Troy JB (2001) Effects of remote stimulation on the mean firing rate of cat retinal ganglion cells. *J Neurosci* 21:5794–5803.

Peichl L, Wässle H (1979) Size, scatter and coverage of ganglion cell receptive field centres in the cat retina. *J Physiol* 291:117–141.

Perry VH, Oehler R, Cowey A (1984) Retinal ganglion cells that project to the dorsal lateral geniculate nucleus in the macaque monkey. *Neuroscience* 12:1101–1123.

Pirenne MH, Compbell FW, Robson JG, MacKay DM (1958) Moving visual images produced by regular stationary patterns. *Nature* 181:362–363.

Pollen DA, Ronner SF (1982) Spatial computation performed by simple and complex cells in the visual-cortex of the cat. *Vision Res* 22:101–118.

Priebe NJ, Mechler F, Carandini M, Ferster D (2004) The contribution of spike threshold to the dichotomy of cortical simple and complex cells. *Nat Neurosci* 7:1113–1122.

Purpura K, Kaplan E, Shapley R (1988) Background light and the contrast gain of primate P and M retinal ganglion cells. *Proc Natl Acad Sci U S A* 85:4534–4537.

Ratliff F, Riggs LA (1950) Involuntary motions of the eye during monocular fixation. *J Exp Psychol* 40:687–701.

Reid RC, Alonso JM (1996) The processing and encoding of information in the visual cortex. *Curr Opin Neurobiol* 6:475–480.

Riggs LA, Ratliff F (1951) Visual acuity and the normal tremor of the eyes. *Science* 114:17–18.

Riggs LA, Ratliff F, Cornsweet JC, Cornsweet TN (1953) The disappearance of steadily fixated visual test objects. *J Opt Soc Am* 43:495–501.

Robinson DW, Chalupa LM (1997) The intrinsic temporal properties of alpha and beta retinal ganglion cells are equivalent. *Curr Biol* 7:366–374.

Rodieck RW, Stone J (1965) Analysis of receptive fields of cat retinal ganglion cells. *J Neurophysiol* 28:833–849.

Rodieck RW, Watanabe M (1993) Survey of the morphology of macaque retinal ganglion cells that project to the pretectum, superior colliculus, and parvicellular laminae of the lateral geniculate nucleus. *J Comp Neurol* 338:289–303.

Roska B, Nemeth E, Werblin FS (1998) Response to change is facilitated by a three-neuron disinhibitory pathway in the tiger salamander. *J Neurosci* 18:3451–3459.

Roska B, Werblin F (2001) Vertical interactions across ten parallel, stacked representations in the mammalian retina. *Nature* 410:583–587.

Rucci M, Desbordes G (2003) Contributions of fixational eye movements to the discrimination of briefly presented stimuli. *J Vis* 3:852–864.

Ruderman DL, Bialek W (1992) Seeing beyond the nyquist limit. *Neural Comp* 4:682–690.

Rüttiger L, Lee BB, Sun H (2002) Transient cells can be neurometrically sustained: the positional accuracy or retinal signals to moving targets. *J Vis* 2:232–242.

Rüttiger L, Lee BB (2000) Chromatic and luminance contributions to a hyperacuity task. *Vision Res* 40:817–832.

Sato Y, Yamamoto M, Nakahama H (1976) Variability of interspike intervals of cat's on-center optic tract fibres activated by steady light spot: a comparative study on X- and Y-fibres. *Exp Brain Res* 24:285–298.

Satoh H, Kaneda M, Kaneko A (2001) Intracellular chloride concentration is higher in rod bipolar cells than in cone bipolar cells of the mouse retina. *Neurosci Lett* 310:161–164.

Schiller PH, Logothetis NK (1990) The color-opponent and broad-band channels of the primate visual system. *Trends Neurosci* 13:392–398.

Schnapf JL, Nunn BJ, Meister M, Baylor DA (1990) Visual transduction in cones of the monkey macaca fascicularis. *J Physiol* 427:681–713.

Schneeweis DM, Schnapf JL (1999) The photovoltage of macaque cone photoreceptors: adaptation, noise and kinetics. *J Neurosci* 19:1203–1216.

Schwartz EA (1982) Calcium-independent release of GABA from isolated horizontal cells of the toad retina. *J Physiol* 323:211–227.

Shapley R, Victor J (1986) Hyperacuity in cat retinal ganglion cells. *Science* 231:999–1002.

Shapley RM, Victor JD (1978) The effect of contrast in the transfer properties of cat retinal ganglion cells. *J Physiol* 285:275–298.

Shulz D, Debanne D, Fr'agnac Y (1993) Cortical convergence of ON- and OFF-pathways and functional adaptation of receptive field organization in cat area 17. *Prog Brain Res* 95:191–205.

Silveira LC, Perry VH (1991) The topography of magnocellular projecting ganglion cells (M-ganglion cells) in the primate retina. *Neuroscience* 40:217–237.

Sinclair JR, Jacobs AL, Nirenberg S (2004) Selective ablation of a class of amacrine cells alters spatial processing in the retina. *J Neurosci* 24:1459–1467.

Sjöstrand J, Olsson V, Popovic Z, Conradi N (1999) Quantitative estimations of foveal and extra-foveal retinal circuitry in humans. *Vision Res* 39:2987–2998.

Smirnakis SM, Berry MJ, Warland DK, Bialek W, Meister M (1997) Adaptation of retinal processing to image contrast and spatial scale. *Nature* 386:69–73.

Smith RG, Sterling P (1990) Cone receptive field in cat retina computed from microcircuitry. *Vis Neurosci* 5:453–461.

Smith VC, Pokorny J, Lee BB, Dacey DM (2001) Primate horizontal cell dynamics: an analysis of sensitivity regulation in the outer retina. *J Neurophysiol* 85:545–558.

Snellman J, Nawy S (2004) cGMP-dependent kinase regulates response sensitivity of the mouse on bipolar cell. *J Neurosci* 24:6621–6628.

Spauschus A, Marsden J, Halliday DM, Rosenberg JR, Brown P (1999) The origin of ocular microtremor in man. *Exp Brain Res* 126.

Spillmann L, Werner JS, editors (1990) *Visual perception: The neurophisiological foundations.* Academic Press, San Diego.

Steinberg RH, Reid M, Lacy PL (1973) The distribution of rods and cones in the retina of the cat (Felis domesticus). *J Comp Neurol* 148:229–248.

Steinman RM, Cunitz RJ, Timberlake G, Herman M (1967) Voluntary control of microsaccades during maintained monocular fixation. *Science* 155:1577–1579.

Steinman RM, Haddad GM, Skavenski AA, Wyman D (1973) Miniature eye movement. *Science* 181:810–819.

Steinman RM, Levinson JZ (1990) The role of eye movement in the detection of contrast and spatial detail. In Kowler E, editor, *Eye movements and their role in visual and cognitive processes*, pp. 115–212. Elsevier Science.

Steinman R (2003) Gaze control under natural conditions. In Calupa LM, Werner JS, editors, *The Visual Neurosciences*, pp. 1339–1356. MIT Press, Cambridge, MA.

Sterling P (2003) How retinal circuits optimize the transfer of visual information. In Calupa LM, Werner JS, editors, *The Visual Neurosciences*, pp. 234–259. MIT Press, Cambridge, MA.

Sterling P, Demb J (2004) Retina. In Shepherd GM, editor, *The Synaptic Organization of the Brain*. Oxford University Press, New York, fifth edition.

Stone C, Pinto L (1993) Response properties of ganglion cells in the isolated mouse retina. *Vis Neurosci* 10:31–39.

Strettoi E, Masland RH (1996) The number of unidentified amacrine cells in the mammalian retina. *Proc Natl Acad Sci U S A* 93:14906–14911.

Swets JA (1996) *Signal Detection Theory & ROC Analysis in Psychology and Diagnostics: Collected Papers.* Lawrence Erlbaum Associates, Inc., Mahwah, NJ.

Teeters J, Jacobs A, Werblin F (1997) How neural interactions form neural responses in the salamander retina. *J Comput Neurosci* 4:5–27.

Teich MC, Prucnal PR, Vannucci G, Breton ME, McGill WJ (1982) Multiplication noise in the human visual system at threshold: 1. Quantum fluctuations and minimum detectable energy. *J Opt Soc Am* 72:419–431.

Thibos LN, Still DL, Bradley A (1996) Characterization of spatial aliasing and contrast sensitivity in peripheral vision. *Vision Res* 36:249–58.

Thibos LN, Walsh DJ, Cheney FE (1987) Vision beyond the resolution limit: aliasing in the periphery. *Vision Res* 27:2193–2197.

Thomson AM, Deuchars J (1994) Temporal and spatial properties of local circuits in neocortex. *Trends in Neurosci* 17:119–126.

Troy JB, Bohnsack DL, Diller LC (1999) Spatial properties of the cat X-cell receptive field as a function of mean light level. *Vis Neurosci* 16:1089–1104.

Troy JB, Enroth-Cugell C (1993) X and Y ganglion cells inform the cat's brain about contrast in the retinal image. *Exp Brain Res* 93:383–390.

Troy JB, Oh JK, Enroth-Cugell C (1993) Effect of ambient illumination on the spatial properties of the center and surround of Y-cell receptive fields. *Vis Neurosci* 10:753–764.

Troy JB, Robson JG (1992) Steady discharges of X and Y retinal ganglion cells of cat under photopic illumination. *Vis Neurosci* 9:535–553.

Usrey WM, Reid RC (2000) Visual physiology of the lateral geniculate nucleus in two species of new world monkey: Saimiri sciureus and Aotus trivirgatis. *J Physiol* 523 Pt 3:755–769.

Vakkur GJ, Bishop PO (1963) The schematic eye in the cat. *Vision Res* 3:357–381.

van Hateren H (2005) A cellular and molecular model of response kinetics and adaptation in primate cones and horizontal cells. *J Vis* 5:331–347.

van Rossum MC, O'Brien BJ, Smith RG (2003) Effects of noise on the spike timing precision of retinal ganglion cells. *J Neurophysiol* 89:2406–2419.

van Rossum MC, Smith RG (1998) Noise removal at the rod synapse of mammalian retina. *Vis Neurosci* 15:809–821.

Vaney DI (1990) The mosaic of amacrine cells in the mammalian retina. *Prog Retinal Res* 9:49–100.

Vardi N, Zhang LL, Payne JA, Sterling P (2000) Evidence that different cation chloride cotransporters in retinal neurons allow opposite responses to GABA. *J Neurosci* 20:7657–7663.

Verweij J, Hornstein EP, Schnapf JL (2003) Surround antagonism in macaque cone photoreceptors. *J Neurosci* 23:10249–10257.

Victor JD (1988) The dynamics of cat retinal Y cell subunit. *J Physiol* 405:289–320.

Volgushev M, Pernberg J, Eysel UT (2000) Comparison of the selectivity of postsynaptic potentials and spike responses in cat visual cortex. *Eur J Neurosci* 12:257–263.

Wachtler T, Wehrhahn C, Lee BB (1996) A simple model of human foveal ganglion cell responses to hyperacuity stimuli. *J Comput Neurosci* 3:73–82.

Wade NJ (2003) Movements in art: from Rosso to Riley. *Perception* 32:1029–1036 Biography.

Wallach H (1935) Über visuell wahrgenommene Bewegungrichtung. *Psychol Forsch* 20:325–380.

Wässle H, Boycott BB (1991) Functional architecture of the mammalian retina. *Physiol Rev* 71:447–479.

Wässle H, Boycott BB, Peichl L (1978) Receptor contacts of horizontal cells in the retina of the domestic cat. *Proc R Soc Lond B Biol Sci* 203:247–67.

Watt RJ, Morgan MJ (1983) The recognition and representation of edge blur: Evidence for spatial primitives in human vision. *Vision Res* 23:1465–1477.

Werblin FS, Dowling JE (1969) Organization of the retina of the mudpuppy, Necturus maculosus. II. Intracellular recording. *J Neurophysiol* 32:339–355.

Westheimer G (1979) The spatial sense of the eye. Proctor lecture. *Invest Ophthalmol Vis Sci* 18:893–912.

Westheimer G (1986) *Handbook of Perception and Human Performance*, Vol. 1, chapter The eye as an optical instrument. John Wiley & Sons, New York.

Westheimer G, Campbell FW (1962) Light distribution in the image formed by the living human eye. *J Opt Soc Am* 52:1040–1045.

Westheimer G, McKee SP (1975) Visual acuity in the presence of retinal-image motion. *J Opt Soc Am* 65:847–850.

Westheimer G, McKee SP (1977) Integration regions for visual hyperacuity. *Vision Res* 17:89–93.

Westheimer G, Pettet M (1990) Contrast and duration of exposure differentially affect vernier and stereoscopic acuity. *Proc Biol Sci* 241:42–46.

Whitaker D, Rovamo J, MacVeigh D, Mäkelä P (1992) Spatial scaling of vernier acuity tasks. *Vision Res* 32:1481–1491.

White AJ, Sun H, Swanson WH, Lee BB (2002) An examination of physiological mechanisms underlying the frequency-doubling illusion. *Invest Ophthalmol Vis Sci* 43:3590–3599.

Wiesenfeld K, Moss F (1995) Stochastic resonance and the benefits of noise: from ice ages to crayfish and SQUIDs. *Nature* 373:33–36.

Wilding TJ, Huettner JE (1997) Activation and desensitization of hippocampal kainate receptors. *J Neurosci* 17:2713–2721.

Williams DR (1985) Aliasing in human foveal vision. *Vision Res* 25:195–205.

Williams DR, Brainard DH, McMahon MJ, Navarro R (1994) Double-pass and interferometric measures of the optical quality of the eye. *J Opt Soc Am A Opt Image Sci Vis* 11:3123–3135.

Williams D, Artal P, Navarro R, McMahon M, Brainard D (1996) Off-axis optical quality and retinal sampling in the human eye. *Vision Res* 36:1103–1114.

Wilson M (2003) Retinal synapses. In Calupa LM, Werner JS, editors, *The Visual Neurosciences*, pp. 279–303. MIT Press, Cambridge, MA.

Wörgötter F, Suder K, Funke K (1999) The dynamic spatio-temporal behavior of visual responses in thalamus and cortex. *Restor Neurol Neurosci* 15:137–152.

Wu SM, Gao F, Maple BR (2000) Functional architecture of synapses in the inner retina: Segregation of visual signals by stratification of bipolar cell axon terminals. *J Neurosci* 20:4462–4470.

Wörgötter F, Nelle E, Li B, Wang L, Diao Y (1998) A possible basic cortical microcircuit called ”cascaded inhibition”. *Exp Brain Res* 122:318–332.

Yagi T, Ohshima S, Funahashi Y (1997) The role of retinal bipolar cell in early vision: an implication with analogue networks and regularization theory. *Biol Cybern* 77:163–171.

Yap YL, Levi DM, Klein SA (1987) Peripheral hyperacuity: three-dot bisection scales to a single factor from 0 to 10 degrees. *J Opt Soc Am A* 4:1554–1561.

Zaghloul KA, Boahen K, Demb JB (2003) Different circuits for ON and OFF retinal ganglion cells cause different contrast sensitivities. *J Neurosci* 23:2645–2654.

Zaghloul K, Boahen K, Demb J (2005) Contrast adaptation in subthreshold and spiking responses of mammalian Y-type retinal ganglion cells. *J Neurosci* 25:860–868.

Zanker JM (2004) Looking at Op Art from a computational viewpoint. *Spat Vis* 17:75–94.

Zanker JM, Walker R (2004) A new look at Op art: towards a simple explanation of illusory motion. *Naturwissenschaften* 91:149–156.

Zucker RS, Regehr WG (2002) Short-term synaptic plasticity. *Annu Rev Physiol* 64:355–405.